Tb/s Superchannels for Optical Communications

Amandeep Kaur
B.TECH, M.TECH
114220531

Thesis submitted for the degree of Doctor of Philosophy



NATIONAL UNIVERSITY OF IRELAND, CORK

SCHOOL OF ENGINEERING

DEPARTMENT OF ENGINEERING SCIENCE

TYNDALL NATIONAL INSTITUTE

PHOTONICS SYSTEMS GROUP

September 2020

Head of Department: Dr Fatima Gunning

Supervisor: Dr Fatima Gunning

Research supported by Science Foundation Ireland (13/CDA/2103)

Contents

List of Figures iv
List of Tables viii
List of Acronyms xi
Acknowledgements xiv
Abstract xv

1 Introduction **1**
1.1 Motivation 1
1.2 Objective and Main Contribution 3
1.3 Thesis Structure 5

2 Towards 100 Gb/s and Beyond **7**
2.1 Trends in Optical Communication Systems 7
2.2 Evolution of Spectral Efficient System 10
2.3 Multiplexing Schemes for Superchannels 11
2.3.1 Orthogonal Frequency Division Multiplexing 13
2.3.1.1 Orthogonality Condition in OFDM 13
2.3.2 Coherent-WDM 15
2.3.3 All Optical-Orthogonal Frequency Division Multiplexing 16
2.3.4 Nyquist-WDM 17
2.3.4.1 Nyquist Criterion and limit 17
2.3.4.2 Nyquist-WDM and OFDM Relationship 17
2.4 Spectral Shaping in Superchannels 20
2.4.1 Digital Spectral Shaping 21
2.4.1.1 Roll-off Factor 22
2.4.2 Optical Spectral Shaping 24
2.4.2.1 Mach-Zehnder Delay Interferometer 25
2.4.2.2 Fiber Bragg Grating 26
2.4.2.3 Arrayed Waveguide Grating (AWG) 27
2.5 VPItransmissionMaker™ 29
2.5.1 Graphical User Interface 29
2.6 Intersymbol Interference (ISI) 30
2.7 Interchannel Interference (ICI) 31
2.8 System Measures and Penalties 32
2.8.1 Bit Error Rate 32
2.8.2 Optical Signal-to-Noise-Ratio 32
2.8.3 Receiver Sensitivity 34
2.8.4 Eye Diagram 35
2.8.5 Constellation diagram 36

3 Optical Spectral Shaping **38**
3.1 Finisar WaveShaper® (WSS) 38
3.1.1 WSS Operation Principle 39
3.1.2 Programming 41
3.2 Designing Filter Profiles 41

3.2.1 Gaussian filter . . . 42
3.2.2 Butterworth . . . 43
3.2.3 Raised Cosine . . . 44
3.3 Characterisation of WSS . . . 45
3.4 Impact of Analogue Pre-filtering in Spectral Roll-off factor Reduction . . . 48
3.4.1 Spectral Amplitude Dip Approach . . . 48
3.4.1.1 Filter Penalty Assessment in Single-Channel Transmission System . . . 49
3.4.2 Adaptive Spectral Shaping Approach . . . 53

4 Generation and Detection of Nyquist-WDM Superchannel 56
4.1 Optical Frequency Comb Generation . . . 56
4.1.1 Theoretical Analysis . . . 58
4.1.2 Result Analysis . . . 60
4.2 Independent subcarrier modulation . . . 62
4.2.1 De-multiplexing using Delay line Mach-Zehnder Interferometer . . . 63
4.2.2 Phase Monitoring of subcarriers . . . 65
4.3 Employing high order modulation formats . . . 67
4.3.1 Electro-absorption Modulator . . . 68
4.3.2 Mach–Zehnder Modulator . . . 69
4.3.3 Intensity Modulation Format- NRZ-OOK . . . 71
4.3.4 Quadrature Phase Shift keying . . . 73
4.3.5 Quadrature Amplitude Modulation . . . 75
4.3.6 Spectral characteristics comparison of modulation formats 76
4.4 Detection of Nyquist-WDM . . . 77
4.4.1 Direct Detection . . . 77
4.4.2 Coherent Detection . . . 79

5 Enabling Nyquist-WDM Transmission with Adaptive Spectral Shaping 81
5.1 NRZ-OOK based Nyquist-WDM Superchannel . . . 81
5.1.1 Performance Evaluation at 10 Gb/s . . . 83
5.1.2 Optical Adaptive Spectral Shaping . . . 88
5.1.3 Performance Evaluation at 28 Gb/s . . . 90
5.2 QPSK based Nyquist-WDM Superchannel . . . 94
5.2.1 Schematic setup for QPSK Superchannel . . . 95
5.2.2 Performance Evaluation at 10 Gb/s . . . 96
5.2.3 Performance Evaluation at 28 Gb/s . . . 100
5.3 16-QAM based Nyquist-WDM Superchannel . . . 104
5.3.1 Schematic setup for 16-QAM Superchannel . . . 105
5.3.2 Performance Evaluation at 10 Gb/s . . . 106
5.3.3 Performance Evaluation at 28 Gb/s . . . 110

6 Conclusion 115
6.1 Summary . . . 115

6.2 Main contributions 118
6.3 Future Work 119

A VPI Images **121**

B Publications **125**

References **141**

List of Figures

1.1 Constellation diagram of various modulation formats. 2

2.1 Schematic of WDM transmission system. 8
2.2 Wavelength grid specified by ITU-T G.694.2 (ViaLite Communications 2019). 9
2.3 ITU-T fixed-grid. 10
2.4 Flexible grid. 11
2.5 (a) Traditional WDM system (b) Superchannel system. 11
2.6 OFDM in Frequency domain. 14
2.7 Frequency and time representation of OFDM and Nyquist-WDM. 19
2.8 Time-Frequency Filtering. 22
2.9 Roll-off-factor characteristics of pulse shaping filter. 23
2.10 Mach-Zehnder delay interferometer architecture. 25
2.11 Working principle of the FBG. 26
2.12 Working principle of an AWG. 27
2.13 VPI Graphical User Interface. 30
2.14 Illustration of ISI in a optical communication system. 31
2.15 Illustration of ICI in an optical communication system. 31
2.16 Theoretical Receiver power sensitivity comparison for different modulation formats based on 10 Gb/s system with five channels. 35
2.17 Illustration of an eye diagram. 35

3.1 Schematic of optical design of LCoS-based Programmable Optical Processor (Finisar Corporation 2014). 39
3.2 Gaussian filter output spectrum at different values of B_{FWHM}/r with desired and measured response 43
3.3 Butterworth filter output spectrum at different values of B_{FWHM}/r with desired and measured response. 44
3.4 Representation of RC pulse at different values of β. 45
3.5 Experimental setup for the characterisation of WSS. 46
3.6 Raised Cosine output spectrum at different values of B_{FWHM}/r with desired and measured response. 47
3.7 Roll-off factor as function of filter bandwidth. 47
3.8 Representation of Amplitude Dip in Raised Cosine filter. 48
3.9 Roll-off factor reduction by amplitude dip. 49
3.10 Schematic design of a single-channel transmission with proposed filter. 50
3.11 RC filter with B_{FWHM}/r= 1 at different data rates. 51
3.12 RC filter with different B_{FWHM}/r at 10 Gb/s. 52
3.13 Receiver Sensitivity with different optical filter profiles at B_{FWHM}/r=1 at 10 Gb/s. 52
3.14 Working principle of LMS algorithm. 53
3.15 Filter shape comparison with and without LMS. 54
3.16 Reduction of roll-off factor for different values of B_{FWHM}/r. . . 54

4.1 Schematic of Optical Frequency Comb Generation. 57
4.2 Time–frequency correspondence for sinc-shaped pulses. 58
4.3 Simulated optical frequency comb spectrum with channel spacing of 10 GHz. 61
4.4 Optimised comb flatness versus drive (V_{RF}) and bias (V_{DC}) voltage. 61
4.5 SMSR versus drive (V_{RF}) and bias (V_{DC}) voltage. 62
4.6 Implementation of optical FFT using cascaded stages of MZDI . 65
4.7 Eye diagram after multiplexing of five optical channels with non-optimal phases. 66
4.8 Optical waveform before combining five channels to form a superchannel. 66
4.9 Eye diagram after multiplexing of five channels with optimal phases. 67
4.10 Mach-Zehnder Modulator architecture. 69
4.11 Power Transfer Characteristics of Mach-Zehnder Modulator. . . 71
4.12 Transmitter Schematic for optical NRZ-OOK. 72
4.13 (a) Optical spectra and (b) Direct-detected eye diagram of NRZ-OOK system. 72
4.14 Transmitter Schematic for optical QPSK. 73
4.15 Optical Spectra of QPSK signal at 10 Gb/s. 74
4.16 (a) Constellation diagram and (b) Direct-detected eye-diagram of QPSK system at 10 Gb/s. 74
4.17 Transmitter Schematic for optical 16-QAM. 75
4.18 Optical spectrum of 16-QAM signal at 10 Gb/s with OSA resolution of 0.02 nm. 76
4.19 (a) Constellation diagram and (b) Direct-detected optical eye diagram of 16-QAM. 76
4.20 Optical spectral comparison of different modulation formats. . . 77
4.21 Direct detection of an optical signal. 78
4.22 Configuration of Phase-diversity Coherent Receiver. 79

5.1 Schematic of NRZ-OOK based Nyquist-WDM system. 82
5.2 Five Channel NRZ-OOK system performance in the absence of spectral shaping. 84
5.3 Received power at BER of 10^{-3} for Ch3: (a) without shaping and (b) after shaping with an RC filter and RC-LMS filter of different bandwidth. 85
5.4 Received eye diagram of the Ch3 without filtering after back to back transmission at 10 Gb/s. 86
5.5 Received eye diagram of the Ch3 after shaping with an RC filter and RC-LMS filter of different B_{FWHM}/r after back-to-back transmission at 10 Gb/s. 87
5.6 Optical Spectrum of: (a) Ch3 and (b) NRZ-OOK superchannel before and after spectral shaping with RC filter of B_{FWHM}/r=1 at 10 Gb/s. 88

5.7 Eye diagram of the Ch3: (a) without and (b) with dispersion compensation after 100 km transmission. 89
5.8 Received eye diagram of the Ch3 after shaping with an RC filter and RC-LMS filter of different B_{FWHM}/r after 100 km. 91
5.9 Received power at BER of 10^{-3} for Ch3: (a) without shaping and (b) after shaping with a RC filter and RC-LMS filter of different bandwidth. 92
5.10 Received eye diagram of the Ch3 after shaping with a RC filter and RC-LMS filter of different B_{FWHM}/r after back-to-back transmission at 28 Gb/s. 93
5.11 Received eye diagram of the Ch3 after shaping with an RC filter and RC-LMS filter of different B_{FWHM}/r after 100 km at 28 Gb/s. 94
5.12 Schematic of QPSK based Nyquist-WDM system 95
5.13 Five Channel QPSK system performance in the absence of spectral shaping. 96
5.14 Received power at BER of 10^{-3} for Ch3: (a) without shaping and (b) after shaping with a RC filter and RC-LMS filter of different bandwidth for QPSK-Nyquist-WDM superchannel at 10 Gb/s. . 97
5.15 Optical spectrum before and after spectral shaping with RC filter having B_{FWHM}/r=1 at 10 Gb/s. 97
5.16 QPSK Constellation diagram of Ch3 without spectral shaping after back-to-back transmission. 98
5.17 QPSK Constellation diagram of the Ch3 after shaping with an RC filter of different B_{FWHM}/r after back to back transmission at 10 Gb/s. 99
5.18 Constellation diagram of the Ch3: (a) without and (b) with dispersion compensation after 100 km transmission at 10 Gb/s. . . 100
5.19 Constellation diagram of the Ch3 after shaping with an RC filter of different B_{FWHM}/r after 100 km transmission at 10 Gb/s. . . 101
5.20 Received power at BER of 10^{-3} for Ch3: (a) without shaping and (b) after shaping with a RC filter and RC-LMS filter of different for QPSK-Nyquist-WDM superchannel at 28 Gb/s. 102
5.21 QPSK Constellation diagram of the Ch3 after shaping with a RC filter of different B_{FWHM}/r after back to back transmission at 28 Gb/s. 103
5.22 QPSK Constellation diagram of the Ch3 after shaping with a RC filter of different B_{FWHM}/r after 100 km transmission at 28 Gb/s. 104
5.23 Five channel spectrally shaped 16-QAM Nyquist-WDM transmission system. 105
5.24 Optical spectrum of 16-QAM before and after spectral shaping with RC filter having B_{FWHM}/r=1 at 10 Gb/s. 106
5.25 Received power at BER of 10^{-3} for Ch3: (a) without shaping and (b) after shaping with a RC filter and RC-LMS filter of different B_{FWHM}/r for 16-QAM based Nyquist-WDM superchannel at 10 Gb/s. 107

5.26 16-QAM Constellation diagram of the Ch3 after shaping with a RC filter of different B_{FWHM}/r back-to-back transmission at 10 Gb/s. 108
5.27 16-QAM Constellation diagram of the Ch3 after shaping with a RC filter of different B_{FWHM}/r after 100 km transmission at 10 Gb/s. 109
5.28 Received power at BER of 10^{-3} for Ch3: (a) without shaping and (b) after shaping with a RC filter and RC-LMS filter of different bandwidth for 16-QAM based Nyquist-WDM superchannel at 28 Gb/s. 110
5.29 16-QAM Constellation diagram of the Ch3 after shaping with a RC filter of different B_{FWHM}/r after back-to-back transmission at 28 Gb/s. 111
5.30 16-QAM Constellation diagram of the Ch3 after shaping with an RC filter of different B_{FWHM}/r after 100 km transmission at 28 Gb/s. 112

6.1 Proposed Experimental Set for Nyquist-WDM Superchannel . . 120

A.1 Simualtion parameter editor window of a VPI laser module. . . 121
A.2 Data visualization and analysis using VPIphotonicsAnalyzer™. . 122
A.3 Global parameters for 10 Gb/s Nyquist-WDM system. 123
A.4 Global parameters for 28 Gb/s Nyquist-WDM system. 123
A.5 Parameters for the CW laser. 124
A.6 Parameters for the Mach Zehnder Modulator. 124

List of Tables

3.1 Parameters for NRZ-OOK based single-channel transmission system. 50

5.1 Parameters for NRZ-OOK based superchannel. 83
5.2 Improvement in optical received power with RC-LMS filter using different modulation formats in back-to-back scenario. 113
5.3 Improvement in optical received power with RC-LMS filter using different modulation formats after 100 km transmission. 114

I, Amandeep Kaur, certify that this thesis is my own work and has not been submitted for another degree, either at University College Cork or elsewhere. All external references and sources are clearly acknowledged and identified within the contents. I have read and understood the regulations of University College Cork concerning plagiarism.

Amandeep Kaur

To my family

List of Acronyms

ADC Analogue to Digital Convertor

AMZI Asymmetrical Mach-Zehnder Interferometer

AO-OFDM All-optical Orthogonal Frequency Division Multiplexing

ASE Amplified Spontaneous Emission

ASK Amplitude Shift Keying

AU Arbitrary Units

AWG Arrayed Waveguide Grating

B2B Back-to-Back

BER Bit Error Rate

CDC Colourless Directionless Contentionless

CP Cyclic Prefix

CW Continuous Wave

DAC Digital to Analogue Converter

DFT Discrete Fourier Transform

DI Delay-line Interferometer

DSP Digital Signal Processing

DWDM Dense Wavelength Division Multiplexing

EAM Electro-Absorption Modulator

EDFA Erbium Doped Fibre Amplifier

ENOB Effective Number of Bits

E/O Electro-Optic

FBG Fiber Bragg Grating

FFT Fast Fourier Transform

FEC Forward Error Correction

FIR Finite Impulse Response

FWHM	Full Width Half Maximum
Gb/s	Gigabits per second
GHz	GigaHertz
ICI	Interchannel Interference
IDFT	Inverse Discrete Fourier Transform
IFFT	Inverse Fast Fourier Transform
ISI	Intersymbol Interference
IM/DD	Intensity Modulation with Direct Detection
ITU	International Telecommunication Union
ITU-T	ITU Telecommunication Standardization Sector
IQ	In-phase Quadrature
LCoS	Liquid Crystal on Silicon
LMS	Least Mean Square
MSE	Mean Squared Error
MZM	Mach-Zehnder Modulator
MZI	Mach-Zehnder Interferometer
MZDI	Mach-Zehnder Delay line Interferometer
NRZ-OOK	Non-Return-to-Zero with On-Off Keying
OBPF	Optical Band Pass Filter
O/E	Optical-to-Electronic
OFDM	Orthogonal Frequency Division Multiplexing
OFC	Optical Frequency Comb
OOK	On-Off Keying
OSA	Optical Spectrum Analyser
OSNR	Optical Signal to Noise Ratio
PC	Polarisation Controller
PIC	Photonics Integrated Circuit

PD	Photodetector
PPG	Pulse Pattern Generator
PRBS	Pseudo Random Bit Sequence
QAM	Quadrature Amplitude Modulation
QPSK	Quadrature Phase Shift Keying
RF	Radio Frequency
ROADM	Reconfigurable Optical Add/Drop Multiplexer
RZ	Return-to-Zero
SE	Spectral Efficiency
SNR	Signal-to-Noise-Ratio
SMF	Single Mode Fibre
SMSR	Side Mode Suppression Ratio
SOA	Semiconductor Optical Amplifie
Tb/s	Terabits per second
WDM	Wavelength Division Multiplexing
WSS	Wavelength Selective Switch

Acknowledgements

Words are often less to someone's sincere regards. An understanding of work like this is never an outcome of a single person. I take this opportunity to express my profound gratitude and respect to those who helped me through the duration of this thesis.

I want to express my sincere gratitude to my supervisor, Dr Fatima Gunning, for her endless encouragement, support and supervision. Her positive outlook and friendly behaviour always created a pleasant atmosphere, and my time spent with her has helped me to grow in many ways. Without her constant help and guidance, this thesis would not have been taken this shape. She has taught me more than I could ever give her credit for here.

I want to thank my progress review committee Dr Stefan Shulz and Dr Giuseppe Talli for their time, encouragement and insightful suggestions during my yearly progress reviews.

A heartfelt thanks to Niamh Kavanagh, Eoin Russell and all my team members for their assistance and encouragement. Working with such a supportive team has been an enjoyable experience. I am also thankful to Cleitus Antony, Mark Power and all of my colleagues at Tyndall National Institute for their help and support during my PhD. It has been a great delight to be a member of the Photonics System Group.

I also thank the Science Foundation of Ireland (SFI) and Irish Photonic Integration Centre (IPIC) for funding my research under grants (13/CDA/2103) and (12/RC/2276).

There is no way to express how much it meant to me to have been a member of Lunch@Tyndall group. The friendship and support from my brilliant friends and colleagues Natalia Canas-Estrada, Yulia Verbishchuk, Eimear O'Mullane, Tim Fass, Hasan Baghbaderani and Kenny Alvarez will always be remembered.

I cannot forget friends who went through hard times together, cheered me on, and celebrated each accomplishment. A special thanks to all my friends Sarita Das, Saroj Kanta Patra, Heena Hussain and Swatchith Lal for giving me the memories, which I will cherish for the rest of my life. Thanks to all friends, I met in Cork who gave me so much needed social reunions and parties.

Last but not least, my greatest thanks to my parents- Jagtar Singh and Jaswinder Kaur, for their endless love, encouragement and support. They always believed in me and without them, none of this would indeed be possible. I also want to express my love for my brothers- Buta Singh, Varinder Singh and my sisters-in-law- Taran and Kajal who always supported me in my every decision. I am also thankful to my uncle Dr Baljit Singh, aunt Sandeep and my cousins Sargun and Virat, who made me feel at home in Ireland.

Abstract

The exponential growth of data traffic has motivated the researchers to find the transmission technologies which can offer high capacity transmission with high spectral efficiency (SE) at economical cost. The next-generation optical transmission systems are expected to operate at 400 Gb/s or 1 Tb/s per line rate, whereas today's recent commercial system operates at 100 Gb/s. The traditional ways to increase the data rate, by increasing the symbol rate and encoding more bits per symbol, face several challenges that make their practical implementations difficult. Increasing the symbol rate to generate 400 Gb/s or 1 Tb/s requires a very high speed optical and electronic components, some of which are not yet commercially available. Superchannel is the emerging technology having the potential to enable Tb/s transmission. In superchannels, optical carriers can be spaced tighter than the standard ITU-T WDM grid, thus allowing higher spectral efficiency (SE). Superchannel approaches, such as all-optical orthogonal frequency division multiplexing (AO-OFDM) and Nyquist wavelength-division multiplexing (Nyquist-WDM) are based on a concept where signal overlapping is allowed either in time or frequency domain as long as the orthogonality between subcarriers is preserved. Nyquist-WDM superchannel is generated by spectrally shaping each subcarrier to occupy a bandwidth equal to the symbol rate. The channel capacity and optical reach of the Nyquist-WDM superchannel can be adjusted to the traffic demand by changing the symbol rate, bits per symbol, and the number of subcarriers. In Nyquist-WDM, spectral shaping has been previously performed in the electrical and digital domains, and it has been demonstrated that digital filters require ultra-high-speed digital-to-analogue converters (DACs) and high-speed digital-signal-processing (DSP) for the precise shaping of the optical signal which can be possibly implemented only with high complexity and cost. To overcome the challenges, the objective of this thesis is to investigate novel spectral shaping techniques which can reduce the complexity of current state-of-the-art DSP by utilising the now commercially available optical filters such as a wavelength selective switch (WSS). However, the currently available WSS has a limited resolution of $\sim$10 GHz. In this thesis, we propose for the first time; two novel filter input optimisation approaches for enhancing the output response of the WSS. This thesis also details the simulation implementation of five-channel Nyquist WDM superchannel system to test and validate the proposed spectral shaping technique with higher modulations formats at different data rates. We show that by implementing

optical spectral shaping utilising a WSS and a simple adaptive algorithm, it is possible to reduce the complexity of state-of-the-art by 19.8 %.

Chapter 1

Introduction

This chapter briefly describes the evolution of optical communications networks as well as the need for a higher capacity, and how superchannels can potentially fulfil the need for higher capacity. The challenges faced by the next generation of optical systems and proposed solutions are also highlighted in terms of motivation and objectives of this thesis. The work contributed by the author is detailed in the structure of this thesis.

1.1 Motivation

In this internet-era, everybody desires to have access to information at their fingertips all the time, everywhere and in whatever format they need it. The information is provided to us through our global mesh of communication networks, whose current implementations cannot support the foreseeable bandwidth demand. Fibre-optic technology is the ultimate saviour because of its potentially limitless capabilities like data rates (nearly 50 terabits per second (Tb/s)), low signal attenuation (as low as 0.2 dB/km), low cost and power requirement (Mukherjee 1997). Our challenge is that the growing need for fast broadband connectivity globally requires a reliable, affordable, and scalable state-of-the-art communications infrastructure network. With this capacity crunch looming, the short-term solution for service providers is to lay down additional cables to meet the demand for internet. The additional cost for laying down the extra infrastructure is expected to be translated to the end consumers, leading to a higher cost of internet services. It is crucial to make the most out of the scarce network resources such as the fibre bandwidth and allow accommodating the ever-increasing traffic demands. Therefore, service

providers need transmission systems which should provide larger network capacity, and become more flexible to support the growing number of users without compromising on optical reach. The amount of information that a system can transmit for a given bandwidth is referred to as the capacity of the system and is first defined by Claude Shannon as given in equation 1.1 (Shannon 1948).

$$C = B \log_2 \left(1 + \frac{S}{N}\right) \tag{1.1}$$

where C is the capacity measured in bits/s, B is the bandwidth in Hz, S is the signal power in watts, and N is the noise power in watts. The capacity of a given channel is then dependent on the available bandwidth as well as the signal-to-noise ratio (SNR) of the transmitted signal. For an optical fibre, however, Shannon's theorem is limited by another important factor: as the signal power is increased, eventually non-linearities are dominant, and the capacity of a given channel within the fibre is then reduced. This is popularly known as the "non-linear Shannon limit" (Mitra & Stark 2001) (Essiambre et al. 2010). Moreover, the migration from traditionally used modulation formats like NRZ-OOK to formats with more bits per symbol leads to a reduction of the symbol rate and narrower spectral widths. The constellation diagrams of currently most popular modulation formats are shown in Fig. 1.1. Employing higher-order modulation formats like quadrature phase-shift keying

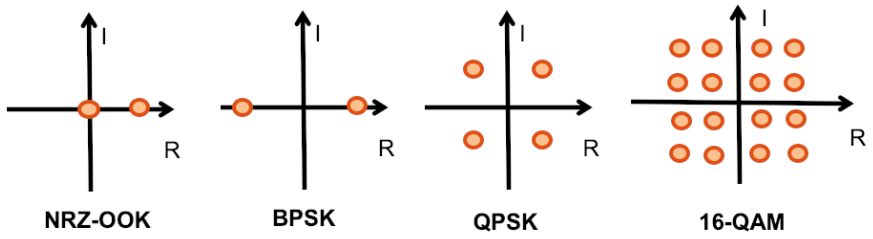


Figure 1.1: Constellation diagram of various modulation formats.

(QPSK) and quadrature amplitude modulation (QAM) (Bosco et al. 2017) can provide significantly more capacity with raising the minimum limits of the SNR to keep the required signal at the acceptable level of the bit error rate (BER). Alternatively, channels can be placed closer than the standard 50GHz ITU-T wavelength division multiplexing (WDM) grid (ITU-T 2012). Hence, the concept of superchannels has been introduced, in which optical carriers can be spaced tighter than the ITU-T WDM grid (Li et al. 1998) (Sanjoh et al. 2002) (Ellis & Gunning 2005*b*). The use of higher-order modulation formats and advanced multiplexing techniques like Nyquist wavelength division

multiplexing (Nyquist-WDM) (Gavioli et al. 2010) (Hillerkuss et al. 2012) along with coherent detection, makes the superchannel systems to be spectral efficient. Spectral efficiency (SE) is the information rate that can be transmitted over a given bandwidth and can be expressed as equation 1.2.

$$SE = \frac{BitRate}{Bandwidth} \quad \frac{(\mathrm{bit/s})}{\mathrm{Hz}} \tag{1.2}$$

It indicates how efficiently the available fibre bandwidth is being utilised. The evolution of higher-order modulation to Nyquist-WDM is explained in detail in Chapter2.

Nyquist-WDM is a superchannel technology that shapes the wavelength spectrum of each subcarrier close to its symbol rate (Nyquist bandwidth) either in the digital domain through the use of high-precision DAC filtering or in the optical domain by using commercially available programmable optical filter such as Finisar WaveShaper® (Finisar Corporation 2012) (Imran et al. 2018) . Optical spectral shaping is attractive for high data rates, as optical filters with higher bandwidths can attain a near rectangular transfer function. On the other hand, digital filters at higher data rates are challenging from the electronics point of view when considering solutions beyond test laboratories and hero experiments towards practical implementations with potential integrated or co-packaged devices. Nevertheless, it takes much effort and complexity to realise rectangular spectra in either way. The digital and optical spectral shaping methods are explained in detail with their advantages and limitations in Chapter 2. The main focus of this thesis is to design the low-complexity and potentially cost-effective solutions using novel spectral shaping techniques for spectral efficient optical networks.

1.2 Objective and Main Contribution

The work reported in this thesis is motivated by the need to develop optical communication systems capable of providing future network capacity growth. For terabit transmission, Nyquist-WDM technique is expected to achieve the same performance but with less receiver bandwidth needed as compared with its counterpart, all-optical orthogonal frequency division multiplexing (AO-OFDM) (Sanjoh et al. 2002) (Lowery et al. 2017). Nyquist-WDM applies bandwidth-constrained pre-filtering approach at each transmitted subcarrier at channel spacing equal to the symbol rate. Nyquist filter either in the digital or

optical domain is usually implemented at the transmitter. The main drawback when performing spectral shaping in the digital domain is the finite sampling speed of state-of-the-art DACs, which limits the achievable symbol rate. Also, costly DACs are required with significantly high power consumption (Xie & Chongjin 2016). As optical filtering can avoid the limitation of electronics bandwidth, it may become the preferred approach if the desired filter shape can be easily achieved. Optical filters with a very steep profile are required to approximate the desired rectangular spectrum, which is critical to design and build using state-of-the-art technology. Programmable liquid crystal on silicon (LCoS) filters like the Finisar WaveShaper® is a potential candidate; however, due to the limited number of pixels available on the current generation of LCoS based devices, its resolution is limited to ∼10 GHz (Yang et al. 2016), but have the potential for further integration with other optical devices (Corbett et al. 2019). Finisar WaveShaper® is also known as wavelength selective switch (WSS), therefore the term "WSS" will be used for it in this thesis. The main objective of the thesis is to investigate the novel spectral shaping techniques, which can reduce the complexity of current state-of-the-art in Nyquist–WDM.

To achieve the given objective, the following methodologies are used:

- Investigation of low-complexity novel optical spectral shaping at the transmitter side.
- Develop a full Nyquist-WDM superchannel system schematic using VPItransmissionMaker™ (VPIphotonics GmbH 2015) simulations to validate the proposed spectral shaping techniques.
- Enabling Nyquist-WDM superchannel transmission with higher-order modulations formats at different data rates with proposed novel spectral shaping techniques.

As discussed above, the current generation WSS has limited resolution; therefore, it is practically impossible to obtain zero roll-off modulated spectra. However, implementing signal processing with full control of amplitude and phase to the input response of WSS can help to approximate the filter transfer function closer to the desired shape. The optimisation of the input response of WSS can further open up the possibility of high performance with low complexity. In this thesis, two novel filter input optimisation approaches are proposed for enhancing the output response of the WSS.

- Spectral Amplitude Dip Approach

- Adaptive Spectral Shaping Approach

In **Spectral Amplitude Dip Approach**, the raised-cosine (RC) filter profiles are created, each differing in attenuation against signal power from 0 to 5 % but only at the centre of the filter. This difference in attenuation at the centre of filter against signal power refers to the amplitude dip. With the introduction of amplitude dip, the response of WSS becomes closer to the square function required, which results in an improvement in the steepness of the WSS. The improvement in WSS output response is verified with results in Chapter 3 by implementing in single-channel transmission system.

In **Adaptive Spectral Shaping Approach**, the spectral roll-off factor is reduced by the optimising the input response of the WSS to minimise the mean squared error (MSE) between the desired filter profile and the actual measured output filter profile by using a feedback-based optimisation method known as least mean square (LMS) algorithm. The details and working principle of LMS are defined in Chapter 3. To validate the performance of the filter with the proposed algorithm, the impact of narrow-band spectral shaping at the transmitter is investigated in five-channel Nyquist-WDM superchannel system using different modulation formats at different data rates in Chapter 5.

1.3 Thesis Structure

To accomplish the established research objectives, this thesis is organised into six chapters.

In **Chapter 2**, the need for higher capacity is highlighted with the fundamentals of a technological breakthrough like the deployment of WDM systems. The different spectral efficient technologies like AO-OFDM, Coherent wavelength division multiplexing (Coherent-WDM) and Nyquist-WDM are presented and compared. The state-of-the-art of the different digital and optical spectral shaping techniques are reviewed. This chapter also highlights the limitations of such techniques which pave the way for exploring novel ideas to overcome the challenges raised by complexity and cost of the current state-of-the-art methods.

Chapter 3, focus on the optical spectral shaping with the help of programmable optical filter. This chapter explains the working principle of the WSS, followed by designing different filter profiles. The limitations of the

WSS's accuracy and resolution is studied in terms of roll-off factor, and two novel methods are proposed to reduce the spectral roll-off factor by the optimising the input response of the WSS. In the last part, the impact of spectral shaping at the transmitter side of the single-channel system is investigated with different filter profiles to validate the practicality of WSS generated filter.

In **Chapter 4**, all major building blocks required for the generation and detection of Nyquist-WDM superchannel are discussed. The comb generation is first explained, and simulation results of a five-tone optical frequency comb are presented. de-multiplexing of the optical frequency comb with all-optical fast Fourier transform (0FFT) demultiplexer is elaborated, and simulation results are presented to describe the impact of the phase monitoring on the superchannel-transmitters. The individual modulation of subcarriers using a Mach-Zehnder modulator (MZM) device is discussed and different modulation formats like NRZ-OOK, QPSK and 16-QAM are generated and compared for most spectral efficient modulation format. After that, the need for spectral shaping is highlighted. In last part, the direct and coherent detection techniques are described with their merits and demerits.

Chapter 5, focuses on the implementation of Nyquist-WDM superchannel based on different modulation format like (NRZ-OOK, QPSK and 16-QAM) at data rates of 10 Gb/s and 28 Gb/s with our proposed, a low-complexity spectral shaping technique. The impact of narrow-band spectral shaping at the transmitter side is investigated and the performance penalties originating from effective channel bandwidth reduction are also evaluated.

Chapter 6, concludes the thesis with a summary of the important achievements and also potential research directions for future works are proposed.

Chapter 2

Towards 100 Gb/s and Beyond

In this chapter, the groundbreaking technological trends in the field of optical communication are discussed. Towards higher capacity and longer distances, as well as lower cost, the fibre-optic communication systems evolve over several distinct generations, each of which is marked by representative techniques and progresses that contribute to the evolution. The need to scale higher-capacity is also elaborated with different spectrally efficient technologies like AO-OFDM, Coherent-WDM and Nyquist-WDM. In following sections, the need for spectral shaping is highlighted with the state-of-the-art technologies and the main challenges faced so far.

2.1 Trends in Optical Communication Systems

Alexander Graham Bell used the optical signal to carry voice through the atmosphere with the help of Photophone in the 1880s but was disappointed by the loss of signal in the air (Bell 1880). The invention of optical fibre cable was attributed to Koa and Hockham (1965) (Kao & Hockham 1966). However, the idea of "total reflection of light at the common surface of two media of different refractive indices" -water and air -was first demonstrated by John Tyndall in 1854 (Tyndall 1854) before it was adapted for communications. The introduction of fibre in the transmission layer, replacing copper, increased the available bandwidth many folds. The invention of semiconductor lasers played a crucial role in making the attempts of optical signal transmission a reality. The rapid progress over a period from 1975 to the current date can be grouped into several generations. Each new generation brought fundamental changes that helped to improve the performance of the next system. The first

generation lightwave systems were commercially deployed in 1983 and operated in the first wavelength window of 800 nm over multimode optical fibre (MMF) at transmission bit rates of up to 45 Mb/s (Ivan Kaminow & Willner 2002) (Sanferrare 1987). The second generation of lightwave transmission systems became available in the early 1980s (Kogelnik 1985) with the shift of operating wavelengths to the second window of 1300 nm. The repeater spacing of the second-generation lightwave systems was limited by the fibre losses at the operating wavelength of 1.3 μm (typically 0.5 dB/km). The fibre losses became minimum near 1.55 μm, and a 0.2 dB/km loss were realised in 1979 in this spectral region (Miya et al. 1979). In the 1980s, the coherent systems were under development, and their potential benefits were demonstrated in many system experiments (Linke & Gnauck 1988). However, commercial introduction of such systems was postponed with the advent of fibre amplifiers with the idea of doping the optical fibre itself with rare-earths by David Payne at Southampton University in 1987 (Payne & Laming 1991) (Agrawal 2011). The third generation optical communication systems operating at 2.5 Gb/s became available commercially in 1990, and their bit rate was soon extended to 10 Gb/s (Agrawal 2016).

The fourth generation of lightwave systems has started a revolution with the advent of the wavelength division multiplexing (WDM) technique. In WDM, information is carried in any format using individual wavelengths and then multiplexed and transmitted over the optical fibre, as shown in Fig. 2.1. The addition and removal of the desired channel are performed using optical add-drop multiplexers (OADMs), which can be realised using Bragg gratings

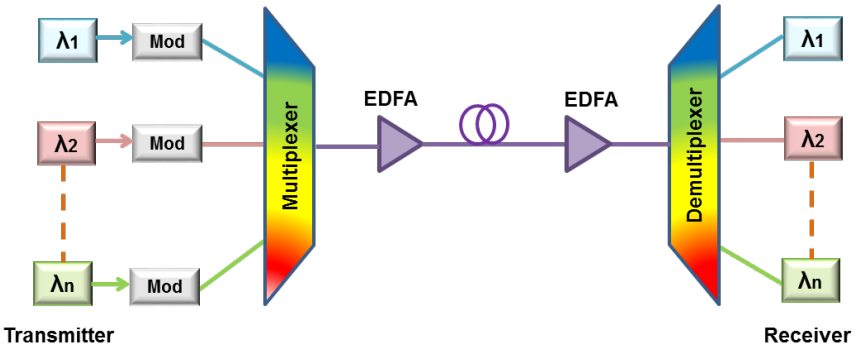


Figure 2.1: Schematic of WDM transmission system.

(Zhou et al. 2011) and liquid-crystal-on-silicon (LCoS) based filters (Frisken et al. 2011). The optical signal is demultiplexed into individual channels and distributed to the intended destination at the receiver side. Traditional WDM

systems are divided into coarse WDM and dense WDM (DWDM). Both formats are based on the same concept of using multiple carriers at different wavelengths propagating through a single fibre but differ in the spacing and number of channels. According to current international telecommunication union (ITU) standards, coarse WDM utilises channels ranging from 1271 nm to 1611 nm with a wavelength spacing of 20 nm (ITU-T 2003), as shown in Fig. 2.2. DWDM refers to the compact multiplexing of optical signals in the

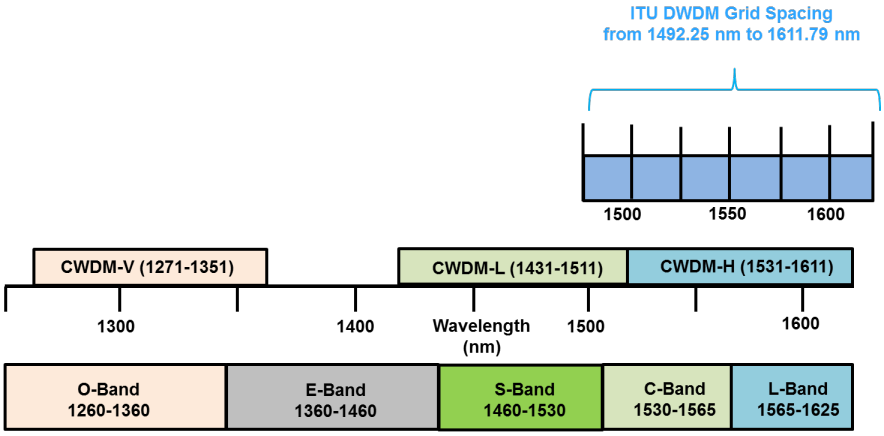


Figure 2.2: Wavelength grid specified by ITU-T G.694.2 (ViaLite Communications 2019).

conventional (C) band (1530 nm to 1565 nm) to take advantage of Erbium-Doped Fibre Amplifier (EDFA) for long-range data transmission. The fifth-generation DWDM system are generally composed of either 40 channels at 100 GHz spacing or 80 channels at 50 GHz spacing (ITU-T 2012). The addition of Raman amplification has increased the number of wavelengths into the L-band (1565 nm-1625 nm), effectively doubling the number of useable channels. The focus of this generation of systems has been to utilise the bandwidth of fibre efficiently with dense wavelength division multiplexing (DWDM) by reviving the coherent detection schemes. The commercial availability of coherent receivers has motivated researchers to employ advanced modulation formats in which information is encoded using both the amplitude and phase of an optical carrier. The integration of digital signal processing (DSP) in optical communication systems has marked another significant progress with the development of high-speed electronics. DSP algorithms are designed to mitigate transmission impairments, recover polarisation multiplexed signals, and subsequently encoded information. Coherent detection and DSP has led to the deployment in late 2000s-early 2010s of 100 Gb/s line rates transponders. The next logical step from 100

Gb/s is towards spectral-efficient systems with a capacity of 400 Gb/s and terabits per second (Tb/s) which are discussed in detail in the next section.

2.2 Evolution of Spectral Efficient System

Optical fibre amplifiers are needed to compensate for the loss of an optical fibre to transmit optical signals over a long distance (>100 km). The bandwidth of an optical fibre amplifier is somewhat limited; therefore, a tight wavelength spacing is needed to accommodate a large number of channels. DWDM takes advantage of the operating window 1525–1565 nm (C band), or 1570–1610 nm (L band) of the EDFA to extend the operating range of the system to over 1500 km (Bhasin et al. 2016). The standard DWDM networks employ rigid connections with a fixed bit rate using fixed-grid of frequencies defined by the ITU-T in Recommendation G.694.1 (ITU-T 2012). The frequency of a given optical channel is defined by a central reference frequency of 193.1 THz or the equivalent 1552.52 nm of wavelength. The difference between the centre frequencies of adjacent optical channels is usually 50 or 100 GHz. In this fixed-grid, the various channels are allocated with the same channel spacing even while carrying signals of different bandwidths, as shown in Fig. 2.3. It can be observed that 10 Gb/s and 40 Gb/s

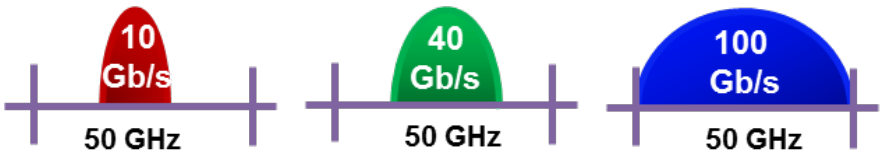


Figure 2.3: ITU-T fixed-grid.

only occupy a small fraction of the total 50 GHz of the channel, while 100 Gb/s signals use almost all the available spectrum. In the first case, a large part of the spectrum is unused, resulting in a waste of spectrum, thereby poor spectral efficiency. To fully utilise the available bandwidth, a new flexible frequencies grid is introduced as a substitute to the fixed-grid traditionally used with DWDM. The flexible grid networks do not use a predetermined channel bandwidth and guard bands between channels. It allows channels with different transmission rates, modulation techniques and dimensions in the same grid. Each channel can be optimised to the bandwidth requirements, transmission rate and a modulation technique, as shown in Fig. 2.4. One of the significant innovations brought by flexible networks is the concept of

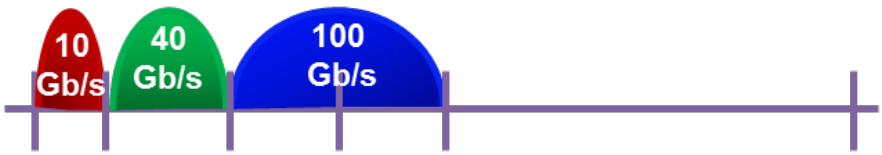


Figure 2.4: Flexible grid.

superchannels. Superchannels are formed by multiple combined optical carriers encoded with high order modulation formats and spectrally close-spaced as shown in Fig. 2.5 thereby, fulfilling the bandwidth demands with transmissions of >100 Gb/s per channel while keeping pace with the spectral efficiency. The traditional long-haul DWDM systems are based on 50 GHz channel spacing, and superchannel implementations can remove the guard band between carriers currently defined by ITU-T wavelength grids, enabling tighter spacing of carriers. Superchannel systems combined with

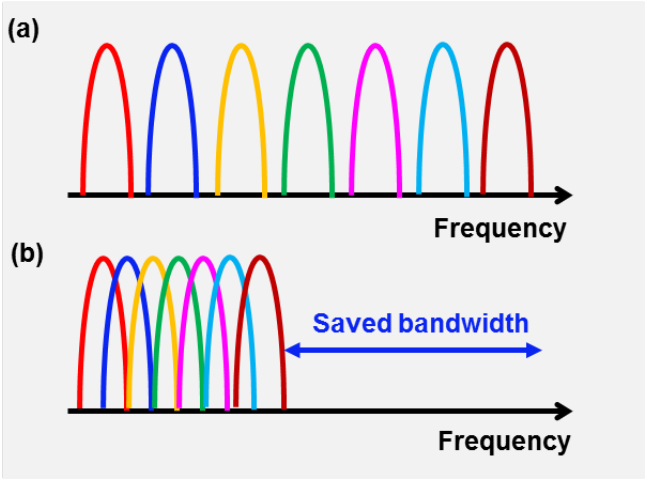


Figure 2.5: (a) Traditional WDM system (b) Superchannel system.

multi-level modulation are considered promising candidates to achieve Tb/s in terms of practical implementation and performance (Schmogrow et al. 2012) (Roberts et al. 2015) . In the next section, multiplexing techniques for generating spectral efficient superchannel are explored.

2.3 Multiplexing Schemes for Superchannels

Orthogonal frequency division multiplexing (OFDM) was proposed as a mathematical possibility in 1957 with “Kineplex”, a multi-carrier high frequency (HF) modem designed by Mosier and Clabaugh (Doelz et al. 1957). The first proposal to use OFDM as an alternative to the existing frequency

division multiplexing (FDM) for transmission appeared in 1966 by Bell Laboratories (Chang 1966) and first US patent was obtained on OFDM in 1970 (Chang 1970). Weinstein and Ebert proposed a modified version of the OFDM system in which a bank of sinusoidal modulators was replaced by the discrete Fourier transform (DFT), reducing the complexity of the system design while maintaining the orthogonality of the subcarriers (Weinstein & Ebert 1971). The cyclic prefix (CP) was proposed in 1980 for the improvement of mitigation of intersymbol interference (ISI) (Peled & Ruiz 1980). The pilot tone technique was introduced in 1985 for compensating channel induced interference and noise, and OFDM began to be considered for practical wireless applications (Cimini 1985). In 1987, the use of OFDM was considered for radio broadcasting, and the importance of combining forward error correction (FEC) with OFDM was noted (Alard & Lassalle 1987). The demonstration of AO-OFDM in single-mode fibre was first seen in 2002, where the concepts from wireless communications were transferred to the optical domain with the aid of an optical discrete Fourier transform based symmetric Mach-Zehnder interferometers (AZMI) (Sanjoh et al. 2002). A new technique called "Coherent WDM" was developed by Ellis and Gunning to increase the spectral density of NRZ binary coded signals in a single polarisation from 0.4 to 1 Tb/s/Hz (Ellis & Garcia Gunning 2005). In Coherent WDM technique, the bit rate was set equal to the channel spacing, and the phase between adjacent subcarriers could be carefully adjusted without ideal matched filters, at the transmitter to preserve orthogonality. There were many other inventions in the generation of AO-OFDM, including the achievement of AO-OFDM fast Fourier transform (AO-OFDM-FFT) with the implementation of tree-topology technique of Mach-Zehnder delay interferometer (MZDI) (Hillerkuss et al. 2010). The de-multiplexing method used by Ellis and Gunning was simple and cost-effective among all other techniques (Ellis & Gunning 2005*b*) (Ellis & Gunning 2005*a*). Following this, Sheih proposed an optical equivalent of the radio frequency OFDM called Coherent-OFDM (CO-OFDM) taking advantage of coherent detection and digital signal processing which enables the use of the matched filters to combat dispersion in fibre media system (Shieh & Athaudage 2006). Later, the concept of superchannel has been introduced to achieve high spectral efficiency. The different approaches of forming spectrally-efficient multi-carrier superchannels are explained in later sections.

2.3.1 Orthogonal Frequency Division Multiplexing

An OFDM is a multi-carrier modulation technique, where a data stream is encoded onto many orthogonal subcarriers that are transmitted together using a single-channel (Antonio Teixeira 2012). The word orthogonal indicates that there is a precise mathematical relationship between the frequencies of carriers in the system. The subcarriers are packed close together in the frequency domain to achieve the highest spectral efficiency, and the orthogonality of the subcarriers is required. In this scheme, all the subcarriers may overlap, but at the frequency of the n^{th} subcarrier, the power of all other subcarriers is zero. This orthogonality is achieved if the frequencies of the subcarriers are equidistant in frequency domain leading to the frequency of the k^{th} subcarrier.

$$\mathrm{f_k} = \mathrm{f_0} + \mathrm{k} \times \Delta\mathrm{f} \tag{2.1}$$

where f_0 is the lowest frequency of the OFDM spectra, Δf is the subcarrier spacing, and k is the index of subcarriers. The superposition of the independently modulated subcarriers is typically performed by the inverse discrete Fourier transform (IDFT), where the input channels are spaced equivalently as shown in equation 2.1. Each subcarrier is modulated with a modulation scheme such as QPSK and 16-QAM at a low symbol rate. For demodulation of the orthogonal subcarriers, a matched filter bank is required. The DFT can replace the analogue demodulator realisation exhibiting desired functionality. In practice, the DFT and IDFT are realised by the fast Fourier transform (FFT) algorithm and its inverse (IFFT), presenting a practical realisation for computation of complex values in a digital domain. The number of sampling points in the time domain, as well as the number of grid points in the frequency domain, are a power of 2.

2.3.1.1 Orthogonality Condition in OFDM

Orthogonality is considered as a property that allows multiple information signals to be transmitted perfectly on the same channel and allow detection without interference. In OFDM, the orthogonality in the frequency domain is achieved by allocating the separate information symbols onto different orthogonal subcarriers. The mathematical representation of the OFDM subcarrier is shown in equation 2.2 (Abd el Samie et al. 2014).

$$s_K(t) = \begin{cases} \sin(2\pi k f_o t), & 0 < t < T, k = 1, 2, \ldots, N \\ 0, & \text{otherwise} \end{cases} \tag{2.2}$$

where f_o is the subcarrier spacing, N is the number of subcarriers, and T is the symbol period. The signals are considered orthogonal if they are mutually independent of each other by satisfying the following condition mentioned in equation 2.3 (Lawrey 2001).

$$\int_0^T s_i(t)s_j(t)dt = \begin{cases} c, i = j \\ 0, i \neq j \end{cases} \tag{2.3}$$

In the frequency domain each OFDM subcarrier has a sinc, (sin(x)/x), spectrum. The sinc shape has a narrow main lobe, with many side-lobes that decay slowly with the magnitude of the frequency difference away from the centre. The spectrum of OFDM signal comprising of five subcarriers is simulated in MATLAB®, as shown in Fig. 2.6. Each carrier has a peak at the

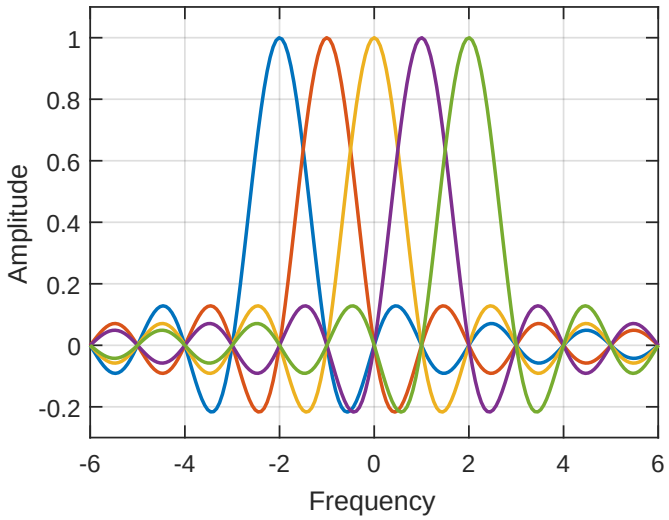


Figure 2.6: OFDM in Frequency domain.

centre frequency and nulls evenly spaced with a frequency gap equal to the carrier spacing. The orthogonality is a result of the peak of each subcarrier corresponding to the nulls of all other subcarriers as shown in equation 2.4 (Zhang et al. 2013).

$$\begin{aligned} \frac{1}{T}\int_0^T e^{j2\pi f_k t}e^{-j2\pi f_k t}dt &= \frac{1}{T}\int_0^T e^{j2\pi\frac{k}{T}t}e^{-j2\pi\frac{i}{T}t}dt \\ &= \frac{1}{T}\int_0^T e^{j2\pi\frac{(k-i)}{T}t}dt \\ &= \begin{cases} 1, & \forall \text{ int} \quad k = i \\ 0, & \text{otherwise} \end{cases} \end{aligned} \tag{2.4}$$

These orthogonal subcarrier sets, with their frequencies spaced at multiples of the inverse of the symbol periods, can be recovered with the matched filters without interchannel interference (ICI), despite strong spectral overlapping.

2.3.2 Coherent-WDM

Coherent-WDM is based on similar concept like OFDM, the latter is used to increase spectral efficiency in the electrical domain. In Coherent-WDM, the subcarriers are modulated, multiplexed and demultiplexed in the optical domain. For Coherent-WDM, it is essential to have optical subcarriers which are spaced by a specific frequency and have a stable phase relationship. If independent lasers are used for each subcarrier, their relative phases can be random and beat incoherently, which can cause crosstalk for closely spaced subcarriers. However, if the phase difference between the channels is controlled or fixed, the interference can become deterministic. A series of closely spaced coherent channels of equal amplitude can produce a periodic pulse train. The variation in the power of this pulse train can be expressed as a function of the number of channels (N) and the spacing frequency (ω). If the period of this train T is an integral multiple of the bit period used, the pulse peak always occurs at the same point within a bit (Ellis & Garcia Gunning 2005) as given in equation 2.5

$$\mathrm{P} \propto \frac{\sin^2\left(\frac{N\omega t}{2}\right)}{\sin^2\left(\frac{\omega t}{2}\right)} \qquad T = \frac{2\pi}{\omega} \tag{2.5}$$

The advanced control of the relative phase of the carriers can be used to increase or decrease an eye-opening using the pulse train. The fundamental principle of coherent WDM is the phase control of the channels. An optical frequency comb is the best approach to achieve coherent optical channels for Coherent-WDM transmitter. A detailed explanation of the optical frequency comb is given in Chapter 4.

2.3.3 All Optical-Orthogonal Frequency Division Multiplexing

The concept of AO-OFDM has been introduced to overcome electronic circuit bandwidth limitations. Even with the advancement high-speed and bandwidth, and low-cost electronic circuits, they still have a bottleneck in achieving very high data rates. In conventional optical OFDM systems, both FFT and IFFT are typically performed in the electronic domain and therefore limit the transmission bit rate. In AO-OFDM, every optical carrier represents a single OFDM subcarrier, the orthogonality condition is satisfied when carrier frequencies are spaced at multiples of the inverse of the symbol periods. Each optical subcarrier is modulated with the desired modulation format whose symbol rate equals the frequency separation between adjacent optical subcarriers to satisfy the orthogonality condition. The multicarrier optical sources which have phase-locked optical carriers are typically used in AO-OFDM systems for phase correlation to mitigate crosstalk between optical channels (Sano et al. 2009) (Chen et al. 2010). Although, a set of continuous-wave (CW) lasers can also generate AO-OFDM carriers as long as the laser frequencies are precisely tuned and locked to satisfy the orthogonality condition (Rhee et al. 2013) (S. Chandrasekhar, Xiang Liu & Peckham 2009). However, the lack of phase correlation between optical carriers might cause additional optical signal-to-noise ratio (OSNR) penalty as the impact of ICI may not be eliminated by digital signal processing at the receiver. In practice, AO-OFDM has been implemented using several techniques, which may differ in transmitter and receiver design but all target to benefit from orthogonality between carriers. A number of IDFT/DFT designs have been reported recently: cascaded delay-line interferometers (DIs) based IDFT/DFT (Hillerkuss et al. 2010), AWG based IDFT/DFT (Huang et al. 2009) (Rhee et al. 2013) and LCoS based IDFT/DFT design (Schroder et al. 2014) for multiplexing optical subcarriers to form optical OFDM signal. The real-time generation of AO-OFDM signals by real-time optical FFT processing of 10.8 Tb/s and 26 Tb/s has been experimentally demonstrated (Hillerkuss et al. 2011). In the methods above, DFT is attained by optical phase shifts and multiple interferences, therefore, system performance is highly dependent on the phase accuracy of optical DFT. The phase error is unavoidable in actual devices because of manufacturing uncertainty (Yuanliang Chu et al. 2002), which is responsible for ICI.

2.3.4 Nyquist-WDM

An alternative superchannel scheme known as Nyquist-WDM has an almost rectangular spectrum with a bandwidth close to the Nyquist limit for ISI free transmission. The subcarriers are aligned with the frequency spacing close to the symbol rate, which is the Nyquist limit, while avoiding spectral overlap of subcarriers. Before moving further, it is very important to understand the concepts like Nyquist limit and Nyquist Criterion.

2.3.4.1 Nyquist Criterion and limit

In communication systems, data can be distorted when symbols interfere with their neighbours, resulting in ISI. This unwanted phenomenon induces errors in signal detection and makes the transmission less reliable. According to the first Nyquist criterion, ISI can be all eliminated if the spectrum of a signal satisfies the condition mentioned in equation 2.6 in time domain (Nyquist 1928).

$$h(nT) = \begin{cases} 1, n = 0 \\ 0, n \neq 0 \end{cases} \tag{2.6}$$

Here T is duration of a symbol. The reason for no ISI is that each pulse is zero at the sampling time of other pulses. The minimum bandwidth needed to fully encode a bandwidth-limited signal is called Nyquist bandwidth. The Nyquist frequency is the minimum rate at which a finite bandwidth signal needs to be sampled to retain all of the information. Nyquist frequency is also known as Nyquist limit and is equal to $1/2T$. A pulse shape satisfying Nyquist Criterion and the bandwidth requirement has the shape of a sinc function, which has a rectangular spectrum extending exactly to the Nyquist frequency. Any filter that has an excess bandwidth with odd symmetry around Nyquist frequency also satisfies the requirement. A family of such filters is known as raised cosine (RC) filters. The details of RC filters are discussed in Chapter 3. In the next part, the relation of Nyquist WDM with OFDM is described, and its comparison with other multiplexing techniques is also discussed.

2.3.4.2 Nyquist-WDM and OFDM Relationship

Nyquist-WDM can be derived from OFDM simply by interchanging time and frequency domain when describing the signal. Generally, an OFDM signal $x(t)$ is an infinite sequence of temporal symbols $x_i(t)$. Each symbol consists of a superposition of N temporal sinusoidal with equidistant carrier frequencies

(f_k). The frequency spacing (F_s) and temporal symbol length (T_s are interrelated to establish orthogonality by the given equation 2.7.

$$\begin{aligned} F_s &= f_{k+1} - f_k \\ &= 1/T_s \end{aligned} \tag{2.7}$$

The OFDM carriers are encoded with complex coefficients c_{ik}, which correspond to the data in the i^{th} symbol on the k^{th} subcarrier with x_k being the waveform. The sum of all subcarriers is transmitted through a transmission link with the spectral impulse response $H(f)$ and demultiplexed with matched filters at receiver. The summed signal is expressed in equation 2.8 and equation 2.9 (Schmogrow et al. 2012).

$$x(t) = \sum_{i=-\infty}^{+\infty} x^{(i)}(t), \quad x^{(i)}(t) = \sum_{k=0}^{N-1} c_{ik} x_k \left(t - iT_s\right) \tag{2.8}$$

$$x_k(t) = \mathrm{rect}\left(\frac{t}{T_s}\right) \mathrm{e}^{\mathrm{j}2\pi f_k t}, \quad |f_{k+1} - f_k| = F_s = \frac{1}{T_s} \tag{2.9}$$

The frequency domain representation of the i^{th} temporal OFDM symbol is obtained by Fourier transform is shown in equation 2.10 (Schmogrow et al. 2012).

$$\begin{aligned} X(f) &= \sum_{i=-\infty}^{+\infty} X^{(i)}(f), \quad X^{(i)}(f) = \sum_{k=0}^{N-1} c_{ik} X_k(f) \mathrm{e}^{-\mathrm{j}2\pi f i T_s} \\ X_k(f) &= T_s \,\mathrm{sinc}\left(\frac{f - f_k}{F_s}\right) \end{aligned} \tag{2.10}$$

Unlike OFDM, the spectrum $Y(f)$ of a Nyquist signal is a finite sequence of N spectral symbols. Each spectral symbol consists of a superposition of infinitely many spectral sinusoidals with equidistant Nyquist pulse position (t_k). The temporal spacing ($T_s = t_{k+1} - t_k = 1/F_s$) and spectral symbol length (F_s) are interrelated to establish orthogonality. The Nyquist subcarriers are again encoded with complex coefficients c_{ik} as shown in equation 2.11 and equation 2.12

$$Y(f) = \sum_{i=0}^{N-1} Y^{(i)}(f), \quad Y^{(i)}(f) = \sum_{k=-\infty}^{+\infty} c_{ik} Y_k \left(f - iF_s\right) \tag{2.11}$$

$$Y_k(f) = T_s \,\mathrm{rect}\left(\frac{f}{F_s}\right) \mathrm{e}^{-j2\pi f t_k}, \quad |t_{k+1} - t_k| = T_s = \frac{1}{F_s} \tag{2.12}$$

The time domain representation of the i^{th} spectral symbol is given by Fourier transform in equation 2.13.

$$y(t) = \sum_{i=0}^{N-1} y^{(i)}(t), \quad y^{(i)}(t) = \sum_{k=-\infty}^{+\infty} c_{ik} y_k(t) \mathrm{e}^{+\mathrm{j}2\pi i F_s t}$$
$$y_k(t) = \mathrm{sinc}\left(\frac{t - t_k}{T_s}\right) \tag{2.13}$$

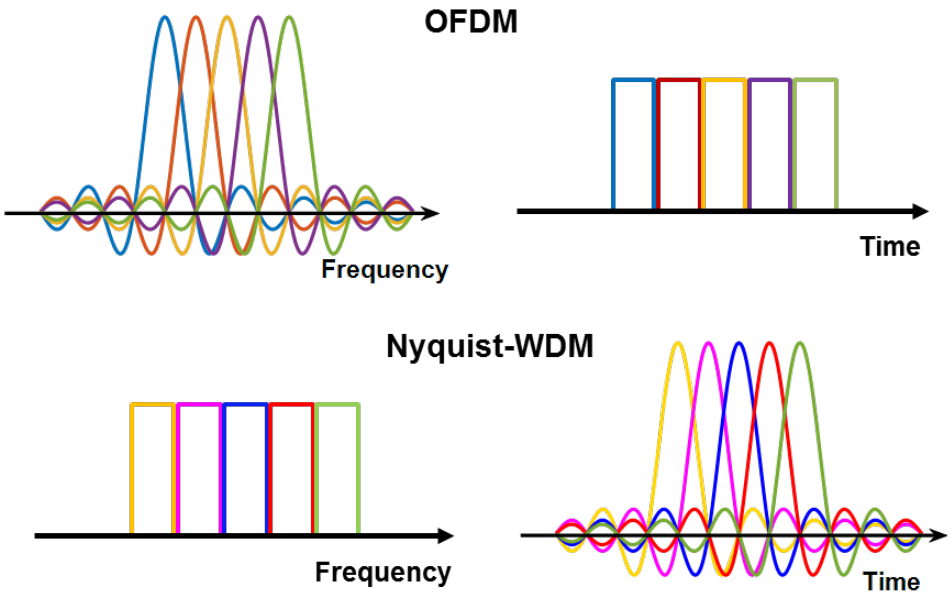


Figure 2.7: Frequency and time representation of OFDM and Nyquist-WDM.

Despite the reciprocity in frequency and time of the two multiplexing techniques seen in Fig. 2.7, Nyquist-WDM with an adequate spectral shaping in frequency, and overlapping in time, has been proven to be a more reliable solution (Djordjevic 2017). Filtering in the frequency domain is more computationally efficient than filtering in the time domain. The convolution of signals in the time domain is equivalent to multiplying their Fourier transforms in the frequency domain. Therefore, it takes less time to do the operations in the frequency domain. In the OFDM scheme, data is transmitted on several subcarriers in parallel with overlapping spectra in the frequency domain; simple bandpass filters cannot separate the subcarriers. The signal processing techniques like optical FFT is required for demultiplexing of the signals. On the other hand, in Nyquist-WDM, the spectrum is rectangular, which confines the modulated carriers to the Nyquist bandwidth of the signal. Hence it is possible to place the subcarriers next to each other without introducing

crosstalk and they can be de-multiplexed with bandpass filters. Moreover, Nyquist-WDM requires a less complex transceiver and a lower peak to average power ratio (PAPR) (Hillerkuss et al. 2012) (Song et al. 2016) (Yu & Zhang 2016).One major limitation of OFDM is the high peak-to-average power ratio of the transmit signal, which occurs due to the summation of many subcarrier modulated signals. A high PAPR requires a wide dynamic range for the power amplifier at the transmitter, or more commonly the power amplifier needs to be backed off to accommodate high peaks. This results in a significant reduction of the transmission power, which leads to very low power efficiency. If at the receiver end, there is a change in frequency of the sub-carriers due to any reason, then the orthogonality among them are lost, and ICI occurs resulting in signal degradation (Myung et al. 2006). With all these advantages over all other multiplexing techniques, Nyquist-WDM is considered as the most promising candidate for generation of the terabits superchannels.

2.4 Spectral Shaping in Superchannels

Spectral shaping techniques play a vital role in the generation of the advanced optical waveforms that optimise the overall performance of the optical communication system to extend the transmission reach, optical multiplexing with highest spectral efficiency and limiting crosstalk distortions. The new regimes in Nyquist-WDM have been enabled by utilising spectral and temporal shaping of the pulses that carry the data. The spectral and temporal signal shaping has been used to mitigate transmission impairments and to enable more efficient usage of available bandwidth. Spectral shaping methods can generate the desired shape of the signal (Schmogrow et al. 2013). Several pulse shapes have been investigated, but rectangular shaped, sinc-shaped, raised-cosine and root-raised-cosine shaped pulses are the dominant pulse shapes (Leuthold & Freude 2013) (Shieh & Djordjevic 2010) (Erkilinc et al. 2014). The orthogonality between adjacent pulses allows the transmission of signals without ICI and ISI. Spectral pre-shaping at transmitter side is an essential function to create nearly rectangular signal spectra that can restrict the signal bandwidth to close to the signal baud rate. The digital and optical methods of spectral shaping are discussed in detail in the next sections.

2.4.1 Digital Spectral Shaping

In Nyquist-WDM, the spectrum for each channel is confined to minimum bandwidth through filtering, generally using digital filters before modulating onto an optical carrier. The advent of high-speed DAC converters and advances in DSP engines now allow the precise shaping of transmitting optical signals to reduce their spectral extent. The key advantage of using digital filters to perform spectral shaping is the ability to control the spectrum of signal precisely. Digital spectral shaping is performed by convolving a data sequence with a digitally generated finite impulse response (FIR) filter which has the desired filter coefficients (taps) to define the impulse response of the filter (Maldonado-Basilio et al. 2010). An FIR filter is realised by a tapped delay line with a finite-duration impulse response, which reads input samples from an analogue to digital (A/D) converter. The digital signals are converted to the analogue regime by DAC (Weng et al. 2018). The DAC can be exhibited as a sample and hold a device, which generates N different levels correspond to the samples of the ideal signal. For each sample of the digital input signal, the DAC chooses the closest discrete representation and output the corresponding signal amplitude. To generate a perfectly rectangular Nyquist-spectrum with a bandwidth equal to the symbol rate (R_s), DAC should operate at a sampling rate of R_s Sa/s, with bandwidth at-least half of R_s, and having a perfectly rectangular transfer function. DAC has a finite resolution depending on the number of quantisation bits used. The presence of both noise and bandwidth limitations effectively reduce the number of equivalent bits. This is often defined in terms of effective number of bits (ENOB) which assumes a random approximation in the quantisation error (Walden 1999). The combination of DAC resolution and ENOB describe the quality of the output signal, including noise from the DAC itself. State-of-the-art DACs are characterised by a maximum sampling speed around 34 GSa/s(Puttnam et al. 2012). The number of resolution bits (N_{DAC}) limits the cardinality of the modulation format. Spectral shaping with digital filters at higher data rates is challenging from the electronics point of view. The higher is the order of the modulation format, the higher is the required value of N_{DAC}. Current generation DACs typically have 8-bit resolution with effective number of bits (ENOB) of 5.5, specified 3dB RF bandwidth of less than 16 GHz, and sampling rates in the order of 65 GSa/s (Rafique et al. 2014) (Fujitsu 2014) (Teledyne LeCroy 2014) (Tektronix 2014). Six-bit DACs and ADCs are sufficient for modulation formats up to 16-QAM. However, higher modulation formats (32-QAM and

above) require higher OSNR, which dictate a minimum converter resolution of 8 bits. Hence, the maximum symbol rates with integrated commercial DACs are still limited to around 30 Gbaud (Ghazisaeidi et al. 2013) (Rasmussen et al. 2013) (Zhang et al. 2014).

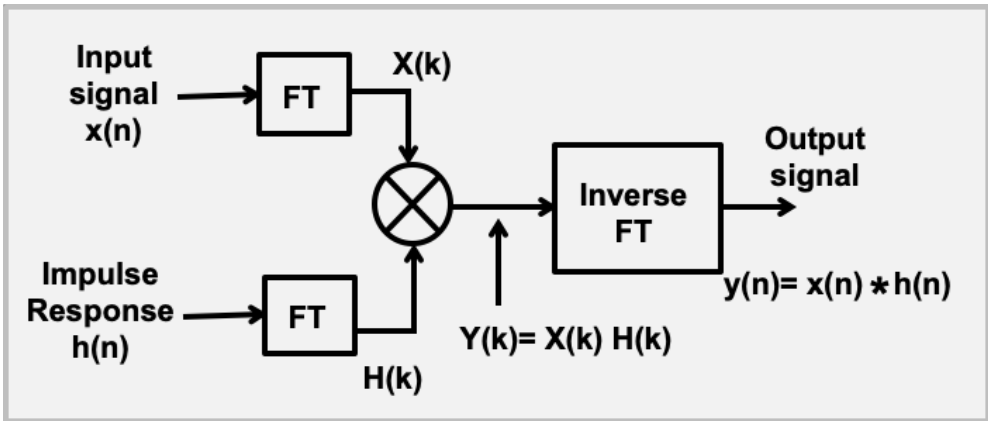


Figure 2.8: Time-Frequency Filtering.

The general idea of filtering is given in Fig. 2.8. The output of the FIR filter is a convolution between the input signal and the FIR's impulse response, as shown in the equation 2.14.

$$y(n) = \sum_{j=0}^{N-1} h(j)x(n-j) \tag{2.14}$$

Here, x is the input signal to the FIR filter, h is the tap coefficient of the FIR filter, and N is the total number of taps. The capability of the FIR filter to adjust the signal's spectrum is limited by the total number of taps. The Nyquist filter is widely used as a spectral shaping filter to improve the spectral efficiency, which is usually a RC filter. RC filters also satisfy the Nyquist ISI criterion that only the sampled symbol contributes to the signal. All other symbols are zero at the sampling points. The roll-off factor for the RC filter determines the spectral response whose value lies between 0 to 1.

2.4.1.1 Roll-off Factor

Roll-off factor gives the measure of the excess bandwidth occupied by any filter as compared to that of theoretical minimum Nyquist bandwidth. From signal theory, it is known that the minimum bandwidth needed to fully encode a bandwidth-limited signal is the Nyquist bandwidth (Nyquist 1928). In real-time communication, the signals usually tend to occupy the bandwidth

more than specified by Nyquist bandwidth. It can also be defined as the

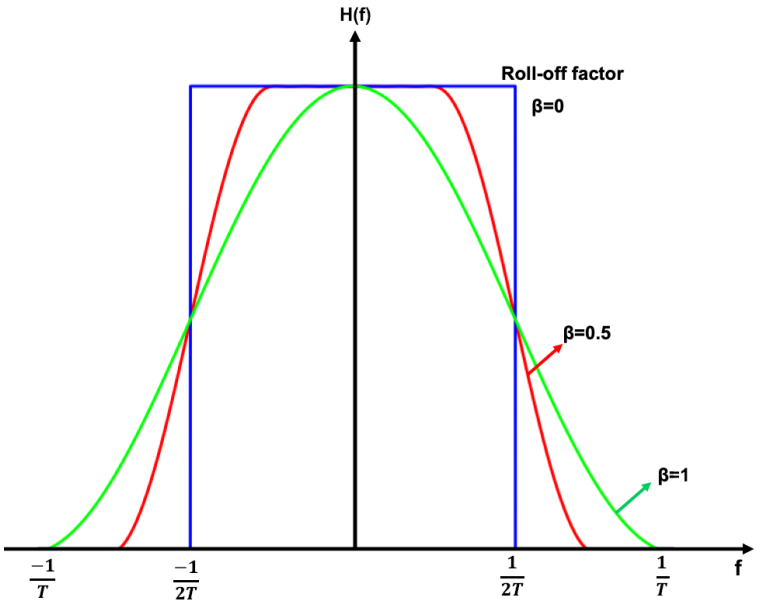


Figure 2.9: Roll-off-factor characteristics of pulse shaping filter.

steepness measure in the transition between the stop-band and pass-band of the filters. While the ideal roll-off factor of these filters should be zero, equivalent to no excess bandwidth beyond the Nyquist limit, its implementation is impractical. Mathematically, for the Nyquist bandwidth of $\frac{1}{2T}$, if the excess bandwidth is Δf then the roll-off factor β is given by equation 2.15.

$$\beta = \frac{\Delta f}{1/2T} \tag{2.15}$$

where T is the symbol period, it is an crucial modulation parameter to determine the signal bandwidth and spectral efficiency. The frequency response of β at different values are shown in Fig. 2.9. It can be observed that, when β=1 and 0.5, the function $H(f)$ cut-off gradually as compared with the ideal Nyquist channel and is therefore easier to implement in practice. The variation in the roll-off factor values causes a change in the characteristics of modulated signal which directly affects the impact of the transmission signal. Higher roll-off means low ISI since it reduces the change rate of the amplitude of output pulse at zero crossings. But it makes the signal bandwidth wider consequently consuming larger spectrum. In short, comparative lower roll-off values means a corresponding decrease in bandwidth usage and increase in symbol rate and overall throughput. Although using DSP, the roll-off factor can be reduced to even less than 0.1, but it requires high-speed DACs, whose

specifications are aggressive for high data rate systems. Some of the hero experiments based on DSP included the use of 600-tap FIR filter to perform digital pre-shaping of QPSK-WDM system with channel spacing of 10 GHz at 20 Gb/s (Igarashi et al. 2011). To reduce the roll-off factor from 10 % down to 0.1 %, the number of filters taps increased from 320 to 1000 (Maher et al. 2015). Nyquist-WDM with channel spacing equal to 1.1×symbol rate was realised using 57-tap digital FIR filter with roll-off factors from 0.1 to 0.2 at 28 Gbaud (Weng et al. 2016). With the implementation of 35 and 81 taps, a roll-off factor of 0.1 and 0.01 was achieved for 16-QAM based Nyquist WDM (Xiang et al. 2015). Due to the time and cost associated with an application-specific integrated circuit (ASIC) for real-time operation, most of these experiments were based on offline processing with MATLAB®. A real-time 30 Gbaud Nyquist signal with four subcarriers was demonstrated with relative length of 56 taps and ADCs having a sampling rate of 32 GSa/s, an electrical 6 dB bandwidth of more than 16 GHz and an frequency-dependent ENOB of 4.5 bits (Baeuerle et al. 2018). For real-time implementations, it is still difficult to design an ASIC with these incredibly large number of taps. And this is why we want to investigate optical filter pre-shaping, to work hand-in-hand with the digital and electrical filters for real-time implementations. Recently, a joint optimisation procedure of optical and digital pre-emphasis filters for the silicon coherent transmitter is demonstrated in single-carrier 400 Gb/s to 600 Gb/s data transmission using an all-silicon IQ modulator (Lin et al. 2019) (Zhalehpour et al. 2019). Following similar footsteps, if our proposed techniques are also used with digital pre-emphasis filters, then this can further improve the spectral shaping experience with limited complexity.

2.4.2 Optical Spectral Shaping

Spectral shaping in the optical domain has been investigated with the implementations MZDI (Hillerkuss et al. 2011), arrayed waveguide gratings (AWG) (Cincotti 2015) (Lowery et al. 2015) (Xie et al. 2016), fiber Bragg gratings (FBG) (Chen et al. 2009) and commercially available programmable optical filter, which is a wavelength selective switch (WSS) (Heismann 2010). In this section, firstly, the basic working principles of optical filters (MZDI, FBG and AWG) are elaborated. Later, their significant contribution to state-of-the art so far is reviewed.

2.4.2.1 Mach-Zehnder Delay Interferometer

The most common use of MZDI is filtering, modulation and demodulation of optical signals. It is an optical device which utilises the effect of interference; the signal in input is divided between the two arms. Each arm applies a phase change to the signal, and at the output the two signals, from different paths are joined together. The relative phase change between the interferometric arms is due to their different lengths thereby, introducing a time delay τ. The basic MZI architecture is shown in Fig.2.10. Since the phase change is

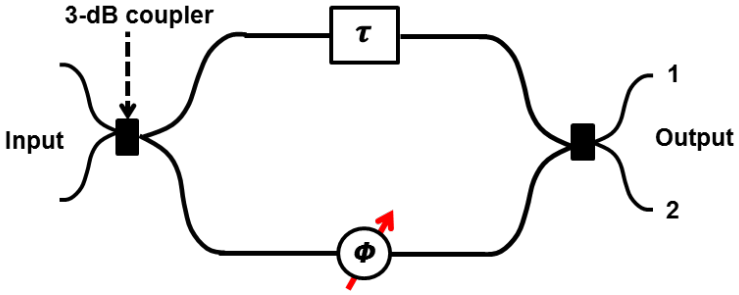


Figure 2.10: Mach-Zehnder delay interferometer architecture.

different for each arm, a transfer function which alternates transmission maxima and minima as a function of wavelength is obtained. This produces a sinusoidal filter which is commonly used to filter out channels from WDM systems and to demodulate phase-encoded data, such as BPSK. The free spectral range (FSR) is the spacing in frequency between successive intensity maxima or minima of an interferometer and is determined by the time delay, where FSR $=\frac{1}{\tau}$. A multi-stage filter can be realised by cascading different MZIs. The MZI filter response is given by equation 2.16 (Nyman et al. 2001)

$$I(f) = I_0 \cos^2\left(f\frac{n_e \Delta L \pi}{c}\right) \tag{2.16}$$

where f is the optical frequency and n_e is the effective refractive index of the delay line. The 3-dB bandwidth of the filter is given by equation 2.17.

$$\Delta f = \frac{c}{2n_g \Delta L} \tag{2.17}$$

n_g representing the group refractive index evaluated at central frequency f_0. The filter characteristics are dependent on the coupling ratio of the 3-dB couplers. The coupling ratio has to be precisely controlled owing to its wavelength dependence. The frequency response function shape of MZI filters

is cos^2. The drawbacks of the MZI concept include the insufficient channel separation, need of additional filtering, the need for an active temperature stabilization and high component costs. Optical spectral shaping by MZDI is not scalable, as N-1, number of MZDIs are required for an N-channel system along with thermal phase shifters that increase the cost and complexity of the device.

2.4.2.2 Fiber Bragg Grating

Fiber Bragg Grating is a type of distributed Bragg reflector constructed in a short segment of optical fibre that reflects particular wavelengths of light and transmits all others as shown in Fig. 2.11. FBG is fabricated by modulating the refractive index of a fibre core by exposing it with high-intensity ultraviolet light (Hill et al. 1993). Based on the Bragg effect, FBGs essentially act like

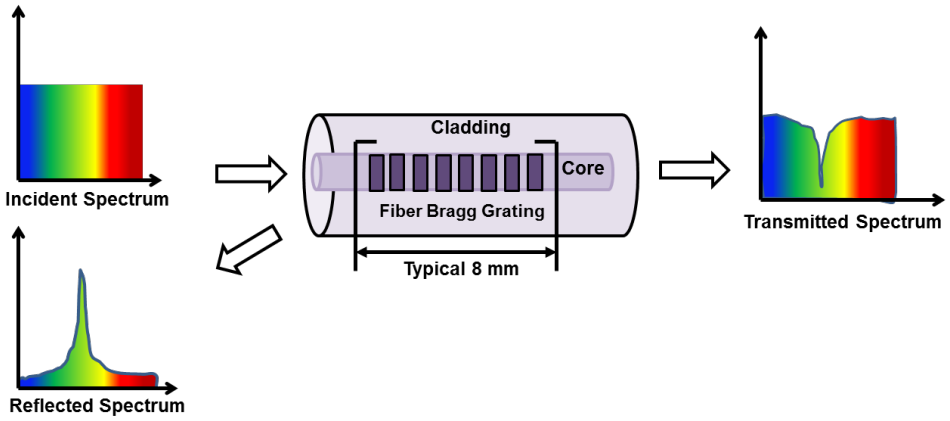


Figure 2.11: Working principle of the FBG.

wavelength-selective mirrors. A grating will reflect light with a wavelength corresponding to twice the grating period multiplied by the effective index of refraction, and this is called the Bragg condition. Bragg grating wavelength λ_B is the central wavelength that is reflected by an FBG and is calculated by using below equation 2.18.

$$\lambda_B = 2n_{\text{eff}}\Lambda \tag{2.18}$$

where Λ is the grating period and n_{eff} is the effective refractive index of light in the fibre. All other wavelengths pass through to the other end since they are not in phase with the grating period. FBGs can tune the filtered wavelength slightly by change of temperature or strain. Hence they are very popular as a sensing platform. FBG can be used as an optical filter, but N different devices are required in the N-channel optical system.

2.4.2.3 Arrayed Waveguide Grating (AWG)

In WDM systems, AWGs are used as multiplexers/demultiplexers, filters and add-drop devices. The AWG concept for the realization of optical filters is basically a generalization of the MZI concept. It consists of multiple input/output (I/O) waveguides, two slab waveguide star couplers (or free propagation region (FPR)) connected by a dispersive waveguide array with the equal length difference between adjacent waveguides (Adam et al. 2008). The principle of operation is based on separating the lightwave channels by phase-shifting them. When a WDM signal with different wavelengths propagate through an FPR, the signal is spatially diverged and later coupled into an array of waveguides. Each waveguide has different length (ΔL), and the signal has phase shift in each waveguide depending on its frequency as shown in Fig. 2.12. By using the concept of constructive and destructive

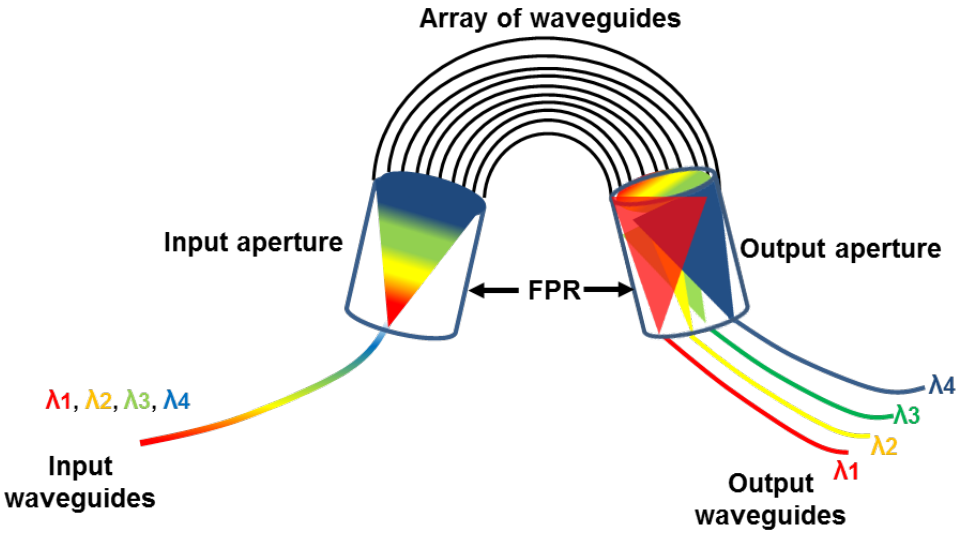


Figure 2.12: Working principle of an AWG.

interference at the image plane, the different wavelengths can be separated into an array of N outputs carrying one channel each. The length difference (ΔL) is expressed in equation 2.19

$$\Delta L = n\frac{\lambda_c}{N_g} \tag{2.19}$$

where n is the order of channel, λ_c is the centre wavelength of all channels and N_g is the effective index of the waveguide mode (Fredrik Ahlbom 2016) in equation 2.19. Since AWG is highly dependent on the phase shifts generated by ΔL and they are not flexible. An AWG with a free spectral range (FSR) of

100 GHz will always have fixed FSR of 100 GHz. One can control the centre wavelength with temperature for some types, but the spacing is not flexible. To achieve flexible bandwidth management, AWG has been replaced by WSS at the transmitter (Fabrega et al. 2016). WSS can be pre-programmed to any arbitrary filter shape and hence is quite flexible. However, due to the limited number of pixels available on the current generation of LCoS based devices, WSS has resolution limitations. The detailed working principle of the WSS is given in Chapter 3. The resolution which is defined as the 10 %-90 % roll-off factor of wavelength routing devices is, however, limited to $\sim$ 7 GHz (Finisar Corporation 2016). Hence, it is practically impossible to obtain zero roll-off modulated spectra. Many researchers have studied the effects induced by optical filters, including simulation of signal impairment originated by cascaded WSSs (Pan & Tibuleac 2017).

Moving further, advances in photonic integration technology have also enabled improvements in the resolution and variety of optical filters to separate Nyquist WDM channels (Goh et al. 2015). Many chip-based passive optical filters and the tapped-delay-line-based interferometric filters architectures are characterised by FIR with multiple optical delays to implement a filter circuit (Xie et al. 2017). A large number of delays and phase tuning elements increases circuit complexity, crosstalk and power consumption. This intrinsic trade-off between performance and complexity poses barriers to the practical photonic integration of such filters for use in Nyquist-WDM systems. While effort is still needed to reach industrial maturity, a resolution-enhanced WSS, a ring-assisted Mach–Zehnder interferometer (RAMZI) chip as a wavelength interleaver is used to pre-process the incoming superchannel before launch into a commercial WSS (Corcoran et al. 2016). Although, the use of ring resonators in RAMZI introduces dispersion to the signal. Low cost colourless, directionless, and contention-less (CDC) technologies based WSS (Yang et al. 2017) is also reported. The applications of these new variations are expected to improve the optical performance and the switching functionalities of the LCoS based WSSs with low cost and complexity.

Alternatively, implementing signal processing with full control of amplitude and phase to the input response of WSS can help to better approximate the filter transfer function. The optimisation of the input response of WSS can further open up the possibility of high performance with low complexity.

2.5 VPItransmissionMaker™

VPItransmissionMaker™ is a powerful simulation tool which provides a platform for end-to-end photonics system design, analysis and optimisation of components, systems and networks. It enables accurate simulation of a wide range of optical transmission designs, giving the possibility to create multiple configurations for a given transmission scenario. This award-winning software is used by more than 100 private companies, including service providers and equipment manufacturers. It is widely used in more than 160 public research and development (R&D) and universities (VPIphotonics GmbH 2015). VPItransmissionMaker™ includes an interface with all of these products, which provides a comprehensive set of additional functionality, including the ability to model and integrate the user's own equipment models. The simulations results presented in the thesis are performed using the VPItransmissionMaker™ 9.2 version, though it will be referred to as VPI during this work.

2.5.1 Graphical User Interface

When starting VPI, the basic screen layout is similar to other simulation programs based on the interconnection of modules to create, design and simulate the operational characteristics of determined systems. In order to understand VPI's simulation environment, its graphic user interface is shown in Fig. 2.13. The highlighted toolbar menu in (1) presents functions such as creating a new scenario, saving, zooming, executing or stopping the simulation. A schematic window is shown in (2) where different modules and components are combined together to design the desired system. In order to add already existing modules, the quick find or search tabs in (3) can be selected to look for them in given resources. The category panel (4) contains all the demonstration simulations offered by VPI. By selecting a category, another panel containing the corresponding demos appears, as shown in (5). Finally, the schematic's package explorer consisting of a folder browse panel (6) and a contents panel (7) is highlighted. The folder panel is used to attach and store any data to be used by the schematic. The contents panel shows the files and documents contained in the currently selected folder in the folder panel. VPI also offers simulation scripting, data import with automatic file format conversion and MATLAB®/Python co-simulation streamline and capture design processes (VPIphotonics GmbH 2014). When executing a

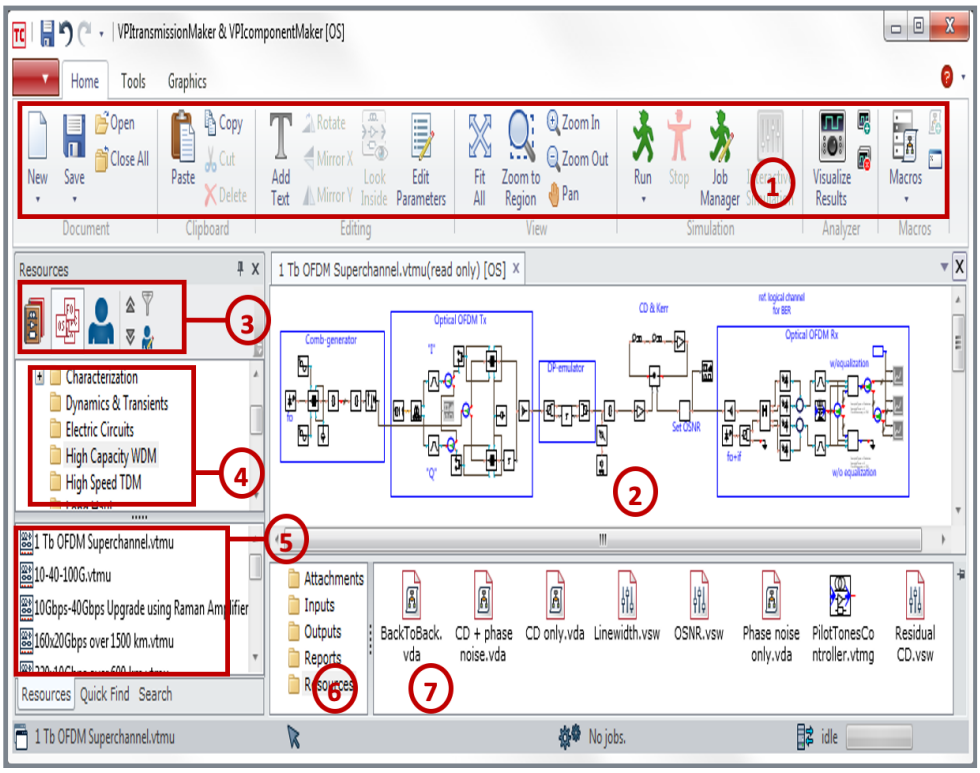


Figure 2.13: VPI Graphical User Interface.

simulation, any module will operate according to certain parameters. The value for these parameters can be changed from the corresponding parameter editor window. The more details of parameter editor window are given in section A in Appendix A. VPI allows maximum freedom in the display, arrangement, export and analysis of simulation results using a universal framework which is known as VPIphotonicsAnalyzer™. The more information about VPIphotonicsAnalyzer™is provided in section A in Appendix A.

2.6 Intersymbol Interference (ISI)

In optical communication, ISI is a form of distortion of a signal in which one symbol interferes with subsequent symbols. This is an unwanted phenomenon as the previous symbols have a similar effect as noise, thus making the communication less reliable. The spreading of the pulse beyond its allotted time interval causes it to interfere with neighbouring pulses (Lathi 1998). An example of intersymbol interference is shown in Fig. 2.14. When the signal waveform passes through a communication system, its shape will be broadened in time because the bandwidth of the system is limited. The bandwidth limitations in the transmitter, fibre, or receiver cause the pulses to

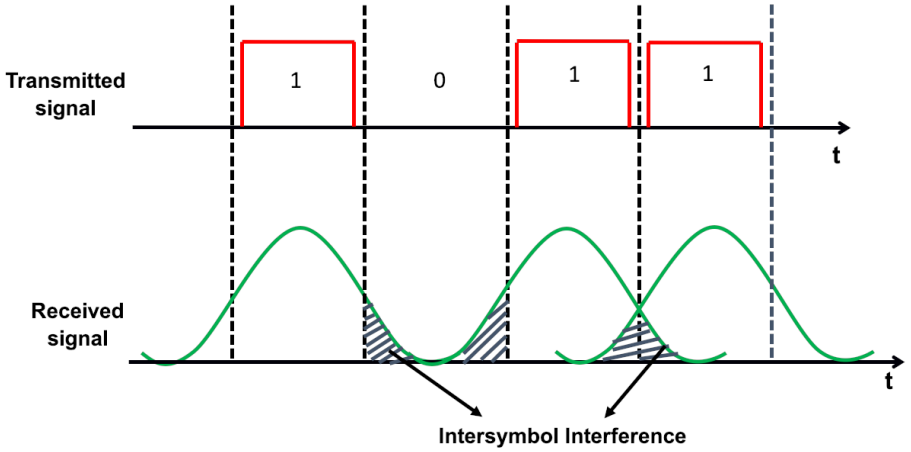


Figure 2.14: Illustration of ISI in a optical communication system.

spread out in time. Each pulse will overlap to the adjacent pulses (Simon Haykin 2010). The presence of ISI in the system introduces errors in the decision device at the receiver output. The ultimate goal of researchers is to minimize ISI by using different spectral shaping filters at transmitter and receiver sides.

2.7 Interchannel Interference (ICI)

Interchannel interference occurs due to overlapping of frequency bands of different subcarriers. ICI effects are inevitable in practical implementations of the transmission system due to the imperfect channel response and tight channel spacing and may cause significant performance degradations.
Fig. 2.15 shows the illustration of ICI between different subcarriers. It is

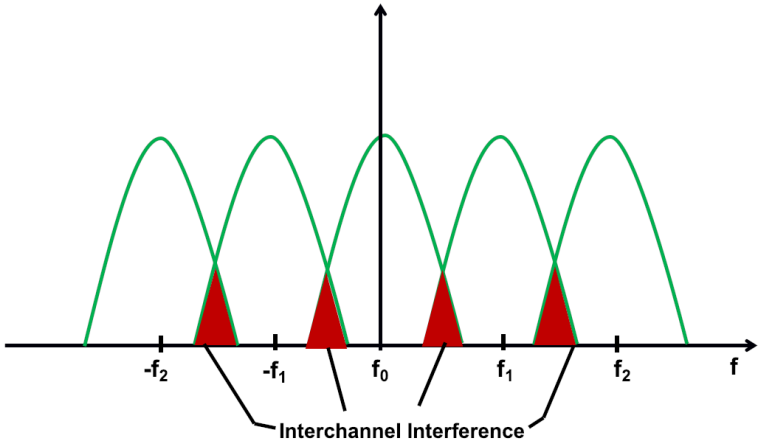


Figure 2.15: Illustration of ICI in an optical communication system.

important to limit the bandwidth of each channel through the implementation of spectral shaping filters to avoid ICI. However, subcarriers can partially overlap without interfering with adjacent sub-carriers only if the orthogonality is preserved between them.

2.8 System Measures and Penalties

The right choice of the system performance measures and evaluation criteria represents one of the key issues for an effective design of future high speed systems. The evaluation criteria should provide a precise determination and separation of dominant system limitations, making them crucial for the system performance improvement. In this section, the parameters which are used to evaluate the performance of our proposed system are mentioned here.

2.8.1 Bit Error Rate

The most common evaluation method is BER for performance estimation based on the counting of errors in received bit streams in transmission systems. BER is defined as the ratio between the number of bit errors received in a certain time interval and the total number of bits transferred during the same time. It can also be defined as the average probability of identifying a bit incorrectly. If p_1 is the probability of incorrectly identifying a 1-bit and p_0 is the probability of incorrectly identifying a 0-bit, and if the two bits are equally likely to be transmitted, then the BER in this case is given by equation 2.20

$$BER = \frac{1}{2}(p_0 + p_1) \tag{2.20}$$

It is important to transmit enough bits through the system to ensure the true probability of having a detection error. The BER target that has to be met by a system depends, on the system applications and typical values for target BER is 1×10^{-3} for systems before employing forward error correction (FEC).

2.8.2 Optical Signal-to-Noise-Ratio

In optical transmission system, OSNR serves as a benchmark for the performance assessment. It is used to quantify the amount of optical noise a receiver can tolerate to maintain transmission at the desired performance level. OSNR limit determines how far an optical signal can travel before

regeneration. WDM networks need to operate above their OSNR limit to ensure error-free operation. The OSNR is the signal-to-noise ratio (SNR) measured in a reference optical bandwidth and is measured in decibels (dB) and is given by equation 2.21.

$$OSNR = 10\log\frac{P_i}{N_i} + 10\log\frac{B_m}{B_{ref}} \tag{2.21}$$

where P_i is the optical signal power in watts and N_i is value of noise power in watts measured in noise equivalent bandwidth (B_m) and (B_{ref}) is the reference optical bandwidth. The value of B_{ref} is mostly considered 12.5 GHz which corresponds to 0.1 nm wavelength (Essiambre et al. 2010). The optical signal can suffer from a variety of impairments like attenuation, fibre non-linearities, crosstalk from adjacent channels during transmission over fibre. The effect of these system impairments on transmission performance can be estimated by the difference between theoretical value and the measured value. This difference is referred to as the OSNR penalty. The most well-known modulation schemes used in this thesis are NRZ-OOK, QPSK and 16-QAM. From the digital communication theory, the BER of each modulation scheme can be expressed as equation 2.22 (Elganimi 2013).

$$\begin{aligned} BER_{NRZ-OOK} &= \frac{1}{2}erfc(\frac{1}{2\sqrt{2}}\sqrt{SNR}) \\ BER_{QPSK} &= erfc(\sqrt{SNR}) \\ BER_{16-QAM} &= \frac{3}{2}erfc(\sqrt{SNR/10}) \end{aligned} \tag{2.22}$$

In optical communication, the term OSNR is used instead of SNR. OSNR is related to SNR by equation 2.23.

$$OSNR_{db} = 10log_{10}[\frac{R_b}{B_{ref}}] + 10log_{10}[SNR] \tag{2.23}$$

where R_b is bit rate = 10 Gb/s and B_{ref} is the reference bandwidth and is commonly taken to be 12.5 GHz (Essiambre et al. 2010), corresponding to a 0.1 nm resolution bandwidth of optical spectrum analyzers. The term SNR is replaced in equation 2.22 by OSNR. In thesis, OSNR is not directly used as performance measure, but it is used to derive the received optical power from its relation with BER.

2.8.3 Receiver Sensitivity

In a fibre-optic transmission system, the receiver has to correctly recover the data carried by the optical carrier. Most of the times, the optical signal that reaches the receiver is very weak after experiencing attenuation of the optical fibre, a high-quality receiver has to be sensitive enough. The criterion of optical receiver qualification depends on the configuration of the optical system and the dominant degradation sources. Receiver sensitivity is defined as the minimum signal optical power level required at the receiver to achieve a certain BER performance. For example, in a specific optical system, for the BER to be less than 10^{-3}, the minimum signal optical power reaching the receiver has to be no less than -35 dBm; therefore the receiver sensitivity is -35 dBm. The definition of receiver sensitivity depends on the targeted BER level and the data rate of the optical signal. It is mainly used for the characterisation of the penalty accumulation over transmission distance and represents a good evaluation method for the comparison of theoretical, simulation and experimental works. The optical received power is expressed in equation 2.24 (Nakazawa 2010).

$$R_X Power(Watt) = OSNR \times NF \times h \times f \times B_{ref} \tag{2.24}$$

where NF is noise figure, h is Planck constant = 6.626 $\times$ 10^{-34} Js and f is frequency of central channel. In optical system, the optical power is usually preferred to be measured in dBm and hence the conversion is done by following function 2.25

$$R_X Power(dBm) = 10log_{10}(R_X Power(Watt)) + 30 \tag{2.25}$$

This is the optical receiver power for a single-channel system. For multi-channel system, the optical received power of N channel system is given by equation 2.26

$$N_{ch} R_X Power(dBm) = R_X Power(dBm) + 10log_{10}(N) \tag{2.26}$$

where N is the number of channels. Fig. 2.16 shows that to obtain a BER of 10^{-3} at 10 Gb/s, a received optical power of -39.95 dBm is required for five channel NRZ-OOK system which is $\sim$1 dBm more than to achieve the same bit rate for a QPSK. QPSK based system has better receiver power sensitivity than 16-QAM by 3.59 dB. These values of received power sensitivity will be used as

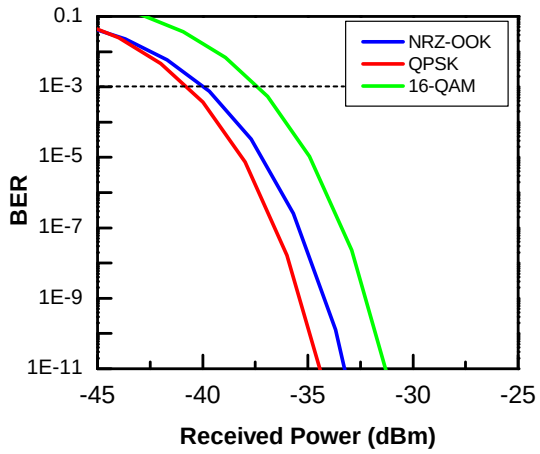


Figure 2.16: Theoretical Receiver power sensitivity comparison for different modulation formats based on 10 Gb/s system with five channels.

reference theoretical values against the simulated five-channel Nyquist-WDM superchannel system in Chapter 5.

2.8.4 Eye Diagram

The eye diagram is another performance indicator used in this thesis, which is formed when consecutive combinations of two or more bits are overlapped on an oscilloscope, resulting in a pattern which resembles an open eye in the ideal case. Eye diagram gives a qualitative analysis of the signal reaching the

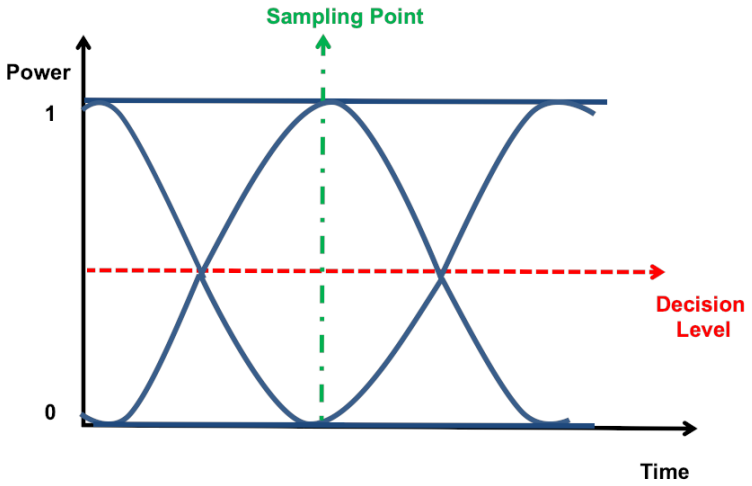


Figure 2.17: Illustration of an eye diagram.

detector and hence informs expectations about the performance of the transmission link. An illustration of an eye diagram for an NRZ-OOK bitstream is represented by the blue lines in Fig. 2.17. The decision threshold and

optimal sampling time can be visualised via the eye diagram. The decision threshold is the power level which corresponds to the centre of the eye-opening, and the optimal sampling time corresponds to the maximum opening of the eye. As such, any reduction in eye-opening indicates an increase in the BER, and the eye diagram provides a visual way of monitoring the performance of the optical communication system. The eye diagram does not show protocol or logic problems. The eye amplitude and eye height are mostly used parameters for the analysis of the eye diagram. As the data receiver logic circuits will ultimately determine whether the data bit is a “0” or “1”, based on the eye amplitude. While eye diagrams provide an accessible and intuitive view of parametric performance, systems ultimately are judged on their ability to pass bits without error. However, BER provides an overall score for how well a system is performing. It should be noted that BER tests logical problems as well as parametric ones- whether the correct bit was sent in the first place. The eye diagram will not reveal whether an incorrect logic state has been sent. Therefore, in this thesis, BER is used as main quantative measure.

2.8.5 Constellation diagram

Constellation diagrams are also used as quality analysis for complex signals that are encoded not only in amplitude but also in phase, and it can depict these signals in both the horizontal and vertical polarisations. In a constellation diagram, information is shown only at specified time intervals. The constellation diagram shows the I-Q positions that correspond to the symbol clock times. These points are commonly referred to as detection decision-points and are interpreted as symbols. Constellation diagrams help to identify amplitude imbalance, quadrature error and phase noise. The constellation diagram gives fast insight into the quality of the transmitted signal as it is possible to see distortions or offsets in the constellation points. It is also useful to quantify the disparity between measured and ideal signals as well by calculating the error vector magnitude (EVM). EVM is the scalar distance between the endpoints of the ideal or reference phasor and the actual generated or received phasor. EVM can be defined in both percentage and dB (Technologies 2020). EVM just provides the distance between two constellation points, and it does not provide logic information like if the correct symbol is transmitted or not in first place. Even, if the symbol is in the wrong place, it can show good EVM, only the BER analysis can determine the certainty of the error. The key performance indicators (BER, eye diagram,

constellation diagram and receiver sensitivity) are used in this thesis to analyse the performance of our proposed single-channel system in Chapter 3 and Nyquist-WDM superchannel system which is explained in Chapter 5.

Summary

Demand for network capacity, driven by media-rich applications, is pushing service providers to deploy optical networks with increased capacity. Two main methods to increase the capacity are to employ more optical bandwidth (which is not feasible) or to utilise the existing bandwidth more efficiently. Employing higher-order modulation formats (64-QAM) can increase the data rate per channel. However, there are both electrical and optical restrictions on spectrally efficient modulation formats. A currently proposed solution for maximising the capacity of optical communications is superchannels. In superchannels WDM channels are placed closer together, potentially at the symbol rate, and more channels can be transmitted through the same bandwidth. The different configurations of superchannels like OFDM, Coherent-WDM and Nyquist-WDM are presented in this chapter with their theoretical background. Nyquist-WDM is found to be the best candidate in terms of its performance and low-complexity of implementation.
Nyquist-WDM systems require more tightly spaced subcarriers, achievable through narrow spectral shaping in the digital domain using FIR filters and in the optical domain by using optical filters. The state-of-the-art of digital and optical filters are reviewed and compared in terms of performance, complexity and flexibility in this chapter. It is concluded that the DSP-based approach is limited by complexity, speed, and power consumption. Therefore, spectral shaping by programmable optical filters like WSS at the transmitter side can be an alternative solution to minimise the complexity and potential cost of the current state-of-the-art. In the next chapter, the characterisation and optimisation of WSS are performed to evaluate the impact and limitations due to the WSS's accuracy and resolution. Also, the practicalities of WSS generated optical filters at the transmitter side via VPI simulations are tested by evaluating the performance in terms of receiver sensitivity and BER.

Chapter 3

Optical Spectral Shaping

Spectral shaping plays a crucial role in high capacity optical networks as it allows carriers to be squeezed closer together to maximise capacity resulting in increased spectral efficiency. To overcome the challenges raised by the complexity and cost of the state-of-the-art of digital filters, programmable optical filters such as a Finisar WaveShaper® can be used for spectral shaping at the transmitter side. The term 'WSS' is used for Finisar WaveShaper®, a device used in this thesis. In this chapter, the analysis of spectral shaping using a WSS is discussed, including limits of current standard commercial devices, and how to overcome these limitations. The impact of narrow-band spectral shaping at the transmitter side in a single-channel system using VPI simulations is also investigated in later sections.

3.1 Finisar WaveShaper® (WSS)

The Finisar WaveShaper® (WSS) is a programmable optical processor that provides a range of programmable optical filtering and switching options in optical communications. The WSS used in this work is Finisar WaveShaper® 1000s which is the single-input-single-output device and has a spectral resolution of 10 GHz. However, the different models of WSS are available like WaveShaper® 4000A and WaveShaper® 16000A which are multi-input-multi-output devices and have spectral resolution of 7 GHz (Corporation 2020). The spectral resolution of WSS is limited by the number of pixels in the LCoS array. The details of LCoS are discussed in subsection 3.1.1. Due to these lower number of pixels, WSS has some limitations which are explained in section 3.3. The number of pixels can be

increased but at the cost of more complexity and cost. As in every instrument, some limitations affect its precision and resolution. The idea behind choosing WSS, even it has some limitations that it is a multi-function device, the same device can be used for the optical filtering and routing by switching channels, which can reduce the cost and complexity of transmission system. However, there is a scope to counteract WSS spectral resolution limitations, which is the challenge addressed in this thesis.

3.1.1 WSS Operation Principle

It is based on solid-state Liquid Crystal on Silicon (LCoS) optical engine and provides excellent control of amplitude and phase including centre wavelength, bandwidth, shape, dispersion over C-band. The working principle of the device is that the incoming light is first passed through polarisation diversity optics which separates and aligns the orthogonal polarisation states (Finisar Corporation 2016), as shown in Fig. 3.1. The diffraction grating

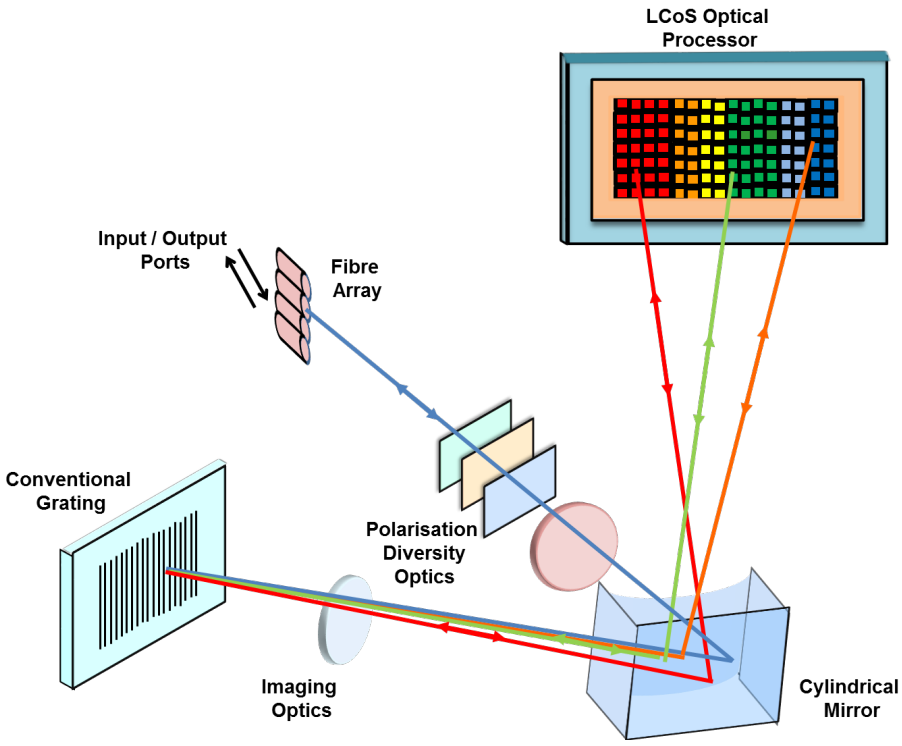


Figure 3.1: Schematic of optical design of LCoS-based Programmable Optical Processor (Finisar Corporation 2014).

angularly disperses the incoming light, so that each wavelength is sent to the different pixel of the LCoS array across the horizontal axis (Schröder et al. 2012). The light diverges vertically so that the signal overlaps a large number

of pixels. The number of pixels in the horizontal direction determines the width of the channel, while the beam deflection can be controlled in a vertical direction by varying the pitch of the grating (Finisar Corporation 2012). The reflected light is traced back through the system to the output port. As the wavelengths are separated on the LCoS after the dispersion from the grating, each wavelength is controlled independently and without interfering with other wavelengths. The phase of the signal is modulated by controlling the voltage-dependent retardation of each pixel. The attenuation control for each pixel is achieved by setting the phase pattern on the LCoS array such that the light is split into two components. One component is sent to the output port, while the other component is directed to a power dump within the Finisar wave processor. By changing the relative power in each of these two beams, the attenuation is precisely controlled, with better than 0.1 dB attenuation resolution (Roelens et al. 2008). The WSS can be used for routing by switching channels as well as for spectral shaping of the optical signals. The WSS available in our laboratory is operated in C band and has an attenuation setting resolution of 0.01 dB and a frequency setting resolution of 1 GHz, which would be sufficient to generate arbitrary, complex filters having a maximum filter bandwidth of 5 THz, which covers the whole C- band. The filter profiles can be generated by using WaveManager software, and it allows users to choose from pre-designed filter shapes with adjustable bandwidth and centre wavelength. A user can also create any arbitrary filter shape that falls within the boundaries and upload it to the WSS. The created filters have a file type of .wsp, which stands for WSS profile. The format of the .wsp file has four parameters: the frequency in THz with a 1 GHz resolution, the attenuation at that frequency, the phase change at the frequency and the output port. As our chosen WSS model only has one port, setting the port to 0 is the equivalent of setting the attenuation to its maximum value. Each line corresponds to 1 GHz of controllable attenuation, phase and port, from 191.250 THz to 196.275 THz. The attenuation setting range is $\pm$ 1.0 dB from 0-10 dB and $\pm$ 10 % from 10-30 dB (Finisar Corporation 2014). The phase is adjustable between π and $-\pi$. There is no specification for the limit to the amount of attenuation change between two adjacent frequency settings, only that the minimum filter bandwidth is 10 GHz.

3.1.2 Programming

The WSS profiles are created with commercial available WaveManager software available from manufacturer, this process requires the user to add the desired .wsp or .ucf in the proper folder and manually select it for uploading to the WSS. Any small change in filter profile requires the manual editing and uploading of the updated profile again. This process is not just time-consuming but also not suitable for uploading a large number of filter profiles consecutively or frequent customising filter profiles. Alternatively, the WSS has a C based application programming interface (API) that allows the same commands to be called without requiring the use of the graphical user interface. This API can be called using MATLAB®, Python and LabVIEW to connect to a WSS device and upload hundred of filter profiles, in a matter of seconds. In this work, MATLAB® is chosen to connect to the WSS.

3.2 Designing Filter Profiles

For a band-limited system, it is highly probable to have distortion or ISI due to bandwidth limitation when transmitted at a high modulation rate. Hence, spectral shaping plays a vital role in transforming the transmitted signal into the shape such that signal remains in the confined bandwidth. The pulse shaping filters are designed to satisfy the Nyquist ISI criterion (explained in Chapter 2). Many spectral shaping filters like sinc shaped filter, rectangular filter, Gaussian, Butterworth and RC filters are in practice. An optical filter can be represented as a filter function, which describes how the signal amplitude changes after filtering. When an input wave with frequency-dependent amplitude $E_{in}(f)$ is filtered, its output amplitude is given by $F(f) \times E_{in}(f)$. Generally, $F(f)$ is a complex number with a modulus describing the change in amplitude and a complex angle describing the change in phase. Alternatively, a filter can also be represented by its attenuation and phase change. Attenuation indicates the change in optical intensity of the signal corresponding that intensity is proportional to the square of wave amplitude. The phase information must also be present in order to fully describe the filter behaviour. The WSS filter profiles are represented in terms of attenuation and phase. The equation 3.1 shows the conversion of filter function into

attenuation $A(f)$ and phase change ϕ_f.

$$\begin{aligned} A(f) &= -20\log_{10}(|F(f)|) \\ \phi(f) &= \arg(F(f)) \end{aligned} \tag{3.1}$$

The factor of 2 arises from squaring $F(f)$ to convert amplitude coefficients to the intensity coefficients. The negative sign corresponds that the attenuation is a measure of loss rather than gain.

3.2.1 Gaussian filter

The Gaussian filter has a smooth transfer function with no zero-crossings. The Gaussian filter has a narrow absolute bandwidth and has sharp cut-off, low overshoot and pulse area preservation properties. The optical transfer function of Gaussian filter is expressed as function 3.2.

$$F(f) = Ae^{-(f-f_0)^2/2\sigma^2} \tag{3.2}$$

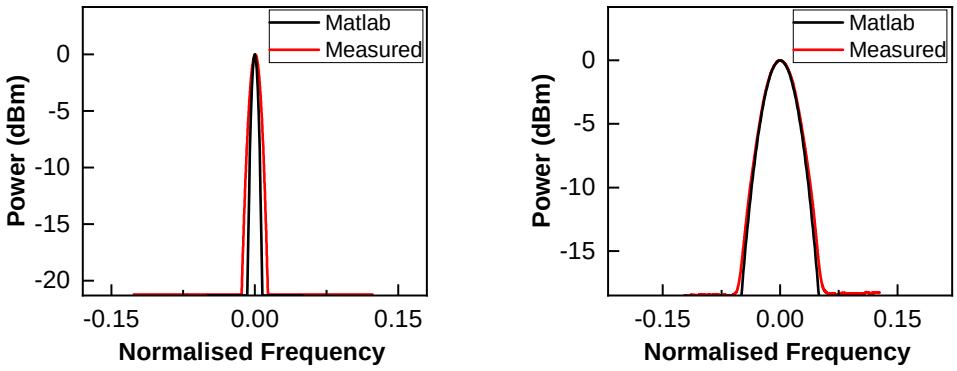
where A is the spectrum amplitude, f_o is the filter center frequency, $(f - f_o)$ is the frequency offset and σ^2 is spectral variance of the Gaussian spectrum. The spectral variance is related to the -3 dB bandwidth (BW_{3dB}) of a Gaussian spectrum by the relation shown in function 3.3

$$\sigma = \frac{BW_{3dB}}{2\sqrt{2\ln 2}} \tag{3.3}$$

As σ increases, the spectral occupancy of the Gaussian filter decreases and the impulse response spreads over adjacent symbols. The impulse response of the Gaussian filter in the continuous-time domain is given by function 3.4.

$$h(t) = \frac{\sqrt{\pi}}{\alpha}\exp\left[-\left(\frac{\pi}{\alpha}t\right)^2\right] \tag{3.4}$$

The Gaussian pulse is neither a Nyquist pulse nor an orthogonal pulse (Cramer et al. 1999). For sufficiently small σ, if high proportion of the pulse energy is included in one symbol time, this pulse can be approximately considered as both Nyquist and orthogonal pulse. Fig. 3.2 shows the measured transfer function of Gaussian filter with -3 dB bandwidth (B_{FWHM}) =10 GHz and 50 GHz. The B_{FWHM} is normalised by the bandwidth resolution (r) of WSS,



(a) B_{FWHM}/r=1 (b) B_{FWHM}/r=5

Figure 3.2: Gaussian filter output spectrum at different values of B_{FWHM}/r with desired and measured response

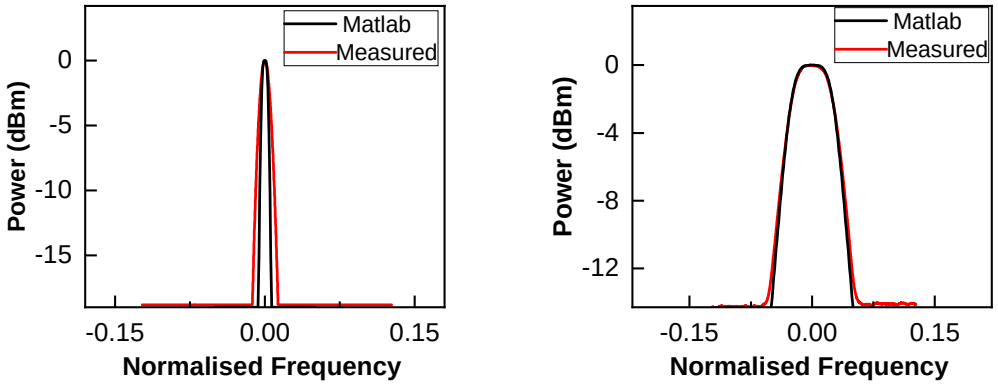
which is 10 GHz for our case. The net effect of convolution with a Gaussian is to smooth out the sharp features of the rectangular function, which makes the output spectrum narrower than the original rectangular profile at the top and wider at the bottom.

3.2.2 Butterworth

Butterworth filters have a magnitude response which is maximally flat near the center frequency and declines monotonically for ω>0. The squared transfer function of optical bandpass Butterworth filter is given by equation 3.5 (Slobodnik et al. 1975).

$$|H_b(f)|^2 = \frac{1}{1 + \left(\frac{2(f-f_c)}{\Delta f_{-3dB}}\right)^{2N}} \tag{3.5}$$

where $H_b(f)$ is the Butterworth filter transmittance, Δf_{-3dB} is filter -3 dB bandwidth, N is filter order, f is the frequency and f_c is the central-frequency of filter. In this work, the order of Butterworth filter is 5 which is a higher-order filter. The advantage of a higher-order filter is that it will have a steeper roll-off slope than a similar lower-order filter. The Fig. 3.3 shows the measured transfer function of Butterworth filter at B_{FWHM}/r =1 and 5 generated with WSS. It can be seen that the actual filter shape generated for B_{FWHM}/r =1 is narrower at the top part of the channel and wider at the bottom. The spectra match reasonably well when B_{FWHM}/r=5 verifying that the generalized WSS structure produces a bandpass filter shape that matches quite well to our predictions at larger bandwidths.



(a) B_{FWHM}/r=1 (b) B_{FWHM}/r=5

Figure 3.3: Butterworth filter output spectrum at different values of B_{FWHM}/r with desired and measured response.

3.2.3 Raised Cosine

RC filters are known for their ability to reduce the ISI of the signal. The name raised cosine stands for non-zero portion of the frequency spectrum with roll-off factor equal to 1 which defines the cosine function raised above the horizontal axis. For the channel with bandwidth B, if $T > \frac{1}{2B}$ then the pulse spectrum for this condition is called the raised cosine spectrum where $1/T$ is the sampling rate of the signal. Rectangular pulses have sharp edges in the time domain indicating the large bandwidth in the frequency domain, therefore, it requires infinite bandwidth. Sinc pulses have an infinite length of time domain sequence. RC pulses are most preferred as they exhibit the balance between the rectangular pulse and the sinc pulses. RC pulses do not have infinite length in both the time and frequency domains. When the passband frequency of these filters is half the data rate, it satisfies the Nyquist criterion (Gentile 2002), where T is the data period and N is any integer. The frequency response of a RC function is given by equation 3.6 (Proakis 1989).

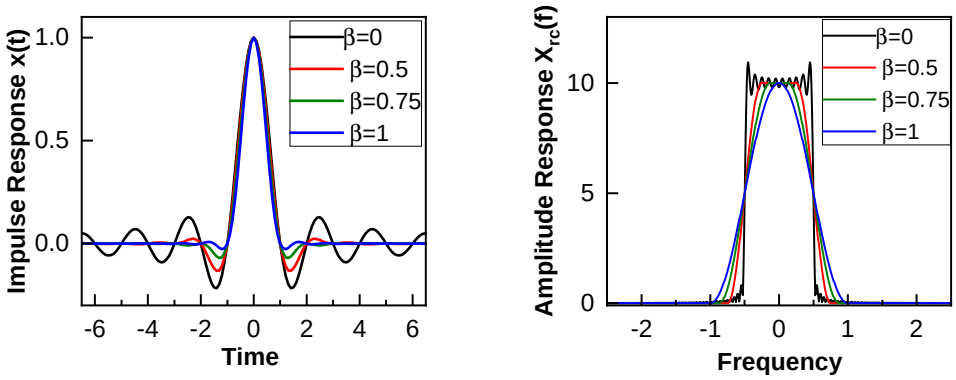
$$X_{rc}(f) = \begin{cases} T & \text{for } 0 \leq |f| \leq \frac{1-\beta}{2T} \\ \frac{T}{2}\left\{1 + \cos\left(\pi T/\beta\left(|f| - \frac{1-\beta}{2T}\right)\right)\right\} & \text{for } \frac{1-\beta}{2T} \leq |f| \leq \frac{1+\beta}{2T} \\ 0 & \text{for } |f| > \frac{1+\beta}{2T} \end{cases} \quad (3.6)$$

β is the roll-off factor and T is the reciprocal of symbol rate. The impulse response of the spectrum for raised cosine function is given by (Proakis 1989)

in equation 3.7.

$$x(t) = \frac{\sin(\pi t/T)}{\pi t/T}\frac{\cos(\pi\beta t/T)}{1-4\beta^2t^2/T^2} = \mathrm{Sinc}(\pi t/T)\frac{\cos(\pi\beta t/T)}{1-4\beta^2t^2/T^2} \tag{3.7}$$

The bandwidth of the pulse and the rate of decay are determined by the value of roll-off factor (β). The value of β is varied from 0 to 1. At β=1, it gives the pure RC spectrum removing the unwanted flat portion. The tails of the signal $x(t)$ is decayed as $1/T$ for roll-off factor greater than zero (Hadkhale 2015). The ideal response of a RC filter has a unity gain in the region of low



(a) Time domain (b) Frequency domain

Figure 3.4: Representation of RC pulse at different values of β.

frequency and total attenuation at the high frequency. In the middle of these two frequencies, responses have a RC function, size of which is determined by the roll-off factor. For best performance, the value of β should be lower to have a sharper spectrum. Roll-off factor, β that varies between 0 and 1 as shown in Fig. 3.4. A roll-off factor close to 0 is attributed to higher quality pulses as the corresponding optical spectrum becomes steeper and therefore, provides better spectral efficiency.

3.3 Characterisation of WSS

In this section, the characterisation of WSS is shown. For this purpose, a desired filter specification is provided as a filter response input to WSS to compare desired and realized filter profile. To carry out this experiment, an EDFA is used to produce amplified spontaneous emission (ASE) signal, which is fed to a WSS to emulate the filter shape as shown in Fig 3.5. A raised cosine

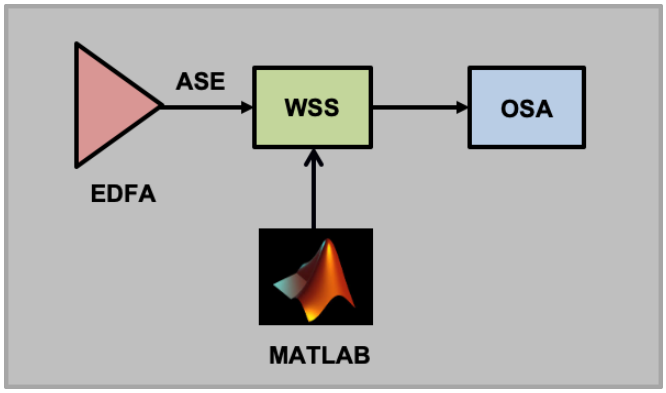
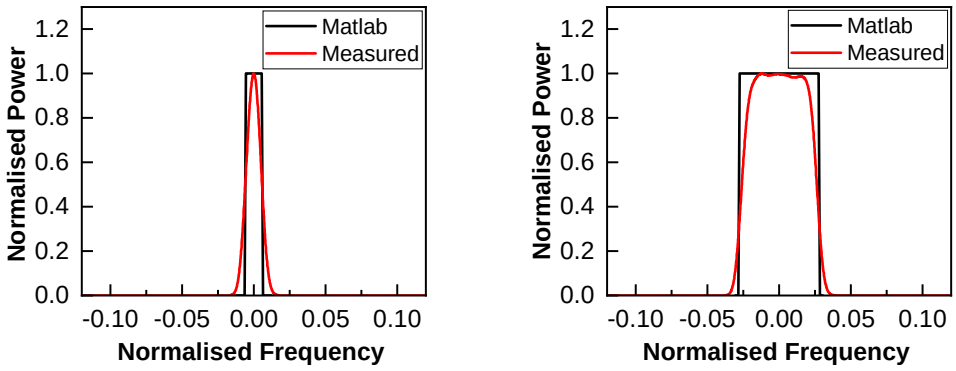


Figure 3.5: Experimental setup for the characterisation of WSS.

(RC) filter shape is realised in MATLAB® and then uploaded into the WSS by using software called WaveManager, and the output is measured with an optical spectrum analyser (OSA). The filter profile has a center frequency of 193.1 THz. The accuracy of the filter representation is measured in terms of roll-off factor. The primary task is to determine the maximum possible steepness of roll-off factor, and knowing that the spec-sheet accuracy of WSS spectral resolution is 10 GHz or attenuation setting accuracy of $\pm$ 1.0 dB from 0-10 dB, $\pm$ 10 % from 10-30 dB. The impact of roll-off factor on the spectral shape, considering RC filters with different -3 dB bandwidth (B_{FWHM}) ranging from 10 GHz to 60 GHz is included in this work (Kaur & Garcia Gunning 2017*a*). To measure roll-off factor experimentally, the output spectrum of uploaded filter profile is analysed using OSA. The markers of OSA are moved to measure B_{FWHM} of filter profile first and the total bandwidth B_T of the filter are measured by same procedure. The roll-off factor (β) is calculated by equation 3.8.

$$\beta = 1 - \frac{B_{FWHM}}{B_T} \tag{3.8}$$

The B_{FWHM} is normalised by the spectral resolution (r) of WSS, which is 10 GHz for our case. It is clear from that WSS does not have a spectral roll-off steep enough to reproduce the same output as the desired one. The reason behind this is that for narrow bandwidth filters, the accuracy and resolution of the WSS plays a role, hence preventing the desirable filter output. In Fig. 3.6 (a) the programmed filter bandwidth is the same as the WSS's bandwidth resolution of 10 GHz. There is a sharp steepness in roll-off factor for $B_{FWHM/r}$=1 and the output produced by WSS is not rectangular. Next, a filter profile with B_{FWHM}/r=5 is uploaded to the WSS and it is found that as the filter bandwidth become broader, the steepness in roll-off factor improves as



(a) B_{FWHM}/r=1 (b) B_{FWHM}/r=5

Figure 3.6: Raised Cosine output spectrum at different values of B_{FWHM}/r with desired and measured response.

shown in Fig. 3.6 (b). To measure the steepness, the roll-off factor is plotted against B_{FWHM}/r as shown in Fig 3.7. The roll-off factor is varied from 0.68

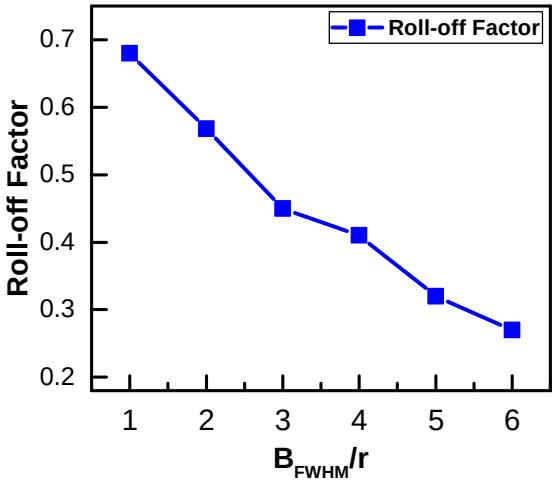


Figure 3.7: Roll-off factor as function of filter bandwidth.

to 0.27 for filter when B_{FWHM}/r is changed from 1 to 6 (Kaur & Garcia Gunning 2017*b*). It can be estimated from the results that for the narrow filters, the roll-off factor is too high, thus hindering the generation of RC filter with sharp transition. Therefore, it is possible to manipulate the programmed filter profile, designing a filter that would counter-effect these observations.

3.4 Impact of Analogue Pre-filtering in Spectral Roll-off factor Reduction

In previous section, it is shown that the current generation WSS has limited spectral resolution; therefore, it is practically impossible to obtain spectra with zero roll-off factor. Implementing signal processing to the input response of WSS can help to approximate the filter transfer function closer to desired shape. In this section, two novel filter input optimisation approaches for enhancing the output response of the WSS are discussed in this section.

3.4.1 Spectral Amplitude Dip Approach

In this approach, the input profile of the filter is optimised so that WSS would be able to produce output as an approximation of the input filter with the steepest slope. The RC filter profiles are created, each differing in attenuation

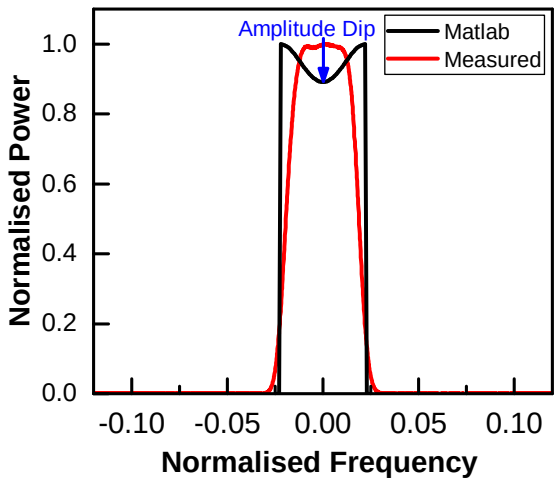


Figure 3.8: Representation of Amplitude Dip in Raised Cosine filter.

against signal power from 0 to 5 % but only at the center of the filter (Kaur & Garcia Gunning 2018). This difference in attenuation at centre of filter against signal power refers to the amplitude dip as shown in Fig 3.8. With the introduction of amplitude dip, the response of WSS becomes closer to the square function required which results in improvement in steepness of the WSS. To study the impact of amplitude dip on the roll-off factor in detail, RC spectral shape is analysed with B_{FWHM}/r=1, 4 and 5. It can be seen from the Fig. 3.9 that, for B_{FWHM}/r=1, the roll-off factor is reduced from 0.69 to 0.61 when amplitude dip changes from 0 to 5 %. Hence, there is 10.1 % reduction

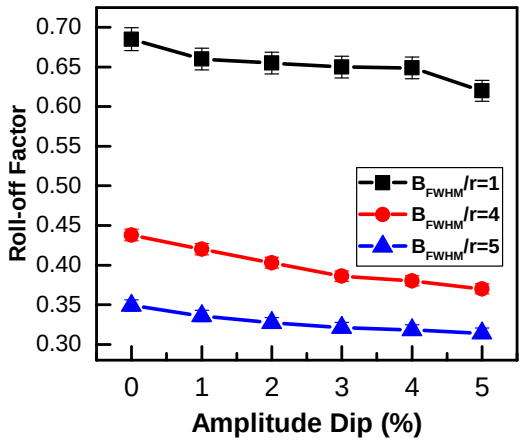


Figure 3.9: Roll-off factor reduction by amplitude dip.

in roll-off factor by this method. Furthermore, for B_{FWHM}/r=4, the roll-off factor is dropped from 0.44 to 0.36, therefore, improving the WSS output response by 8 %. Similarly, at B_{FWHM}/r=5, the roll-off factor is reduced by the factor of 5 %.

3.4.1.1 Filter Penalty Assessment in Single-Channel Transmission System

In order to verify the system's performance of the new filter characteristics, we demonstrated a single-channel transmission system based on 10 Gb/s NRZ-OOK data modulation, using $LiNbO_3$ -based modulator and a pseudo-random bit-sequence (PRBS) sequence of $2^7 - 1$ to evaluate the performance of our proposed WSS generated filter. The short PRBS pattern is chosen here because the long PRBS sequence takes a longer time to complete the entire sequence, which can be a significant issue at lower bit rates. As a result, it is generally recommended that short PRBS patterns be used at lower data rates (10 Gb/s) and long PRBS patterns be used at the higher data rates (Phabrix 2019). The NRZ modulated signal is launched to a WSS filter for pre-spectral shaping. The output response of WSS generated RC, Butterworth and Gaussian filters profiles are uploaded to optical bandpass filter (OBPF) by co-simulation with MATLAB® for spectral shaping. The setup for the filter emulation is implemented on a MATLAB®/VPI co-simulation platform is shown in Fig. 3.10. The parameters of system components are mentioned in Table 3.1. As the signal propagates through the WSS, there can be a significant power penalty resulting from the filter. The filters can also induce optical crosstalk from the neighbouring channels. Therefore, it is important to properly characterise it thoroughly the performance of the filter before

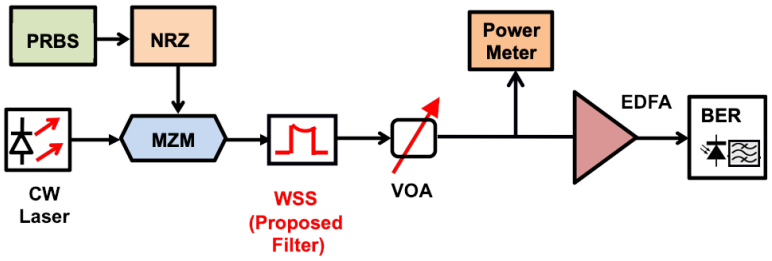


Figure 3.10: Schematic design of a single-channel transmission with proposed filter.

Table 3.1: Parameters for NRZ-OOK based single-channel transmission system.

Parameters	**Value**	**Unit**
Emission Frequency	193.1	THz
Noise Figure	3	dB
Bit Rate	10	Gb/s
Gain	20	dB
Thermal Noise	10^{-12}	A/$\sqrt{Hz}$
Responsivity	0.8	A/W

implementing it in complex superchannels. The spectrally shaped signal is received by the direct-detection optical receiver, which is comprised of the variable optical attenuator (VOA) and the optical power is measured after VOA. The function of VOA is to adjust the optical power in stepwise variable attenuation. The optical power attenuation is varied from 0 dB to 7 dB in seven iterations with a step size of 1 dB. Since it is pre-amplifier receiver, therefore, the upcoming signal is amplified by EDFA having 20 dB gain and maximum output power of 5 dBm, with a noise figure of 3 dB. The purpose of using EDFA is to maintain power at the PIN photodetector constant. The photodetector has a responsivity of 0.8 A/W. The thermal noise of 10^{-12} A/Hz is taken into account. The received signal is then launched to a post-detection electrical low pass 2^{nd} order Bessel filter with a bandwidth of 75 GHz. Bessel filters are often used because of their advantageous properties concerning low overshoot and hence, low pulse broadening. The cut-off frequency of an electrical filter should not be lower than the data rate. The reason for choosing a Bessel filter with a bandwidth of 75 GHz is that very narrow filters cause higher penalties than broad ones (Winzer et al. 2001). The performance of the proposed system is assessed in terms of received power sensitivity and BER in a back-to-back scenario. To characterise the WSS channel shape in an optical transmission system, three common filter profiles are tested: Gaussian, Butterworth and RC. The performance of the RC filter with B_{FWHM}/r at

different data rates is shown in Fig. 3.11. The data rate is varied from r to 6×r

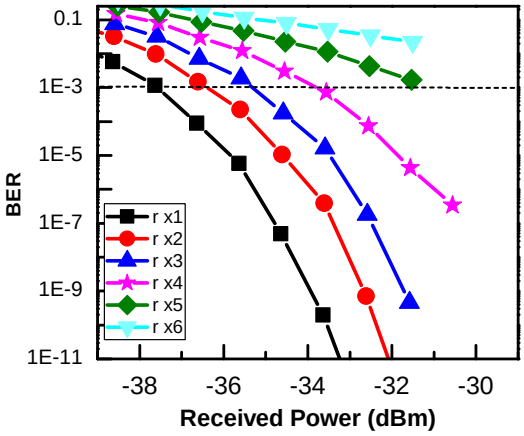


Figure 3.11: RC filter with B_{FWHM}/r= 1 at different data rates.

without changing the filter bandwidth. It can be seen in Fig. 3.11, for a given value of r to achieve target BER of 10^{-9}, the required received power is -34.06 dBm. There is a 1.38 dB and 2.46 dB power penalty in received power when data rate got doubled and tripled respectively to achieve the same BER. While considering, the BER of 10^{-3}, the power penalty is ∼1.5 dB, between r and 3× r, which is acceptable for system performance. A relatively larger BER floor for the case of higher bit rates is observed as compared to lower data rates. As indicated, the transmitter with a low data rate can improve its performance for a fixed channel width. For example, in this simulation, a 10 GHz filter has been used with 10, 20 and 30 Gb/s data. The simulations show that, although a penalty is seen for the first 3 cases, it is small and easily recovered. However, for a sharper and narrower filter in comparison to the data rate, the penalties are much increased as expected. The bandwidth of optical signals depends on their data rate and transmission technique. A 10 Gb/s data stream occupies a minimum of 20 GHz of the optical band when NRZ modulation is used (Dorf 2006). The penalty would increase by increasing the symbol rate but keeping filter bandwidth fixed to 10 GHz, as the higher the symbol rate, the larger the bandwidth it occupies. It is hence of no surprise that symbol rates beyond 3×B_{FWHM}/r suffer significant penalties. Looking at this issue further, we explored the impact of different B_{FWHM}/r on the system performance. It is found that for the lower values of B_{FWHM}/r, the power penalty is high as compared to broad bandwidth filters. A power penalty of 1.85 dB is measured between B_{FWHM}/r=1 and 6, as shown in Fig. 3.12. As the filter becomes narrower, the performance of system deteriorates. The different filter shapes

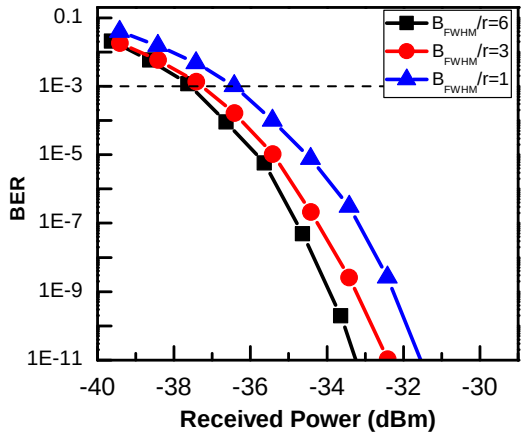


Figure 3.12: RC filter with different B_{FWHM}/r at 10 Gb/s.

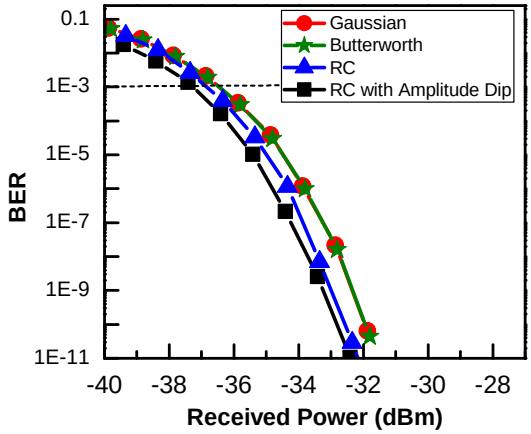


Figure 3.13: Receiver Sensitivity with different optical filter profiles at B_{FWHM}/r=1 at 10 Gb/s.

will have a different impact on signal transmission. In the scope of this work, the performance of different filters has been compared in terms of receiver sensitivity and BER as depicted in Fig. 3.13. When all the filters are aligned perfectly with the laser's central frequency, the RC filter with proposed amplitude dip outperforms among other filters with 1 dB power improvement at target BER of 10^{-9}, but with a reduced penalty at BER of 10^{-3}. These simulations validate our WSS generated filters in the single-channel transmission system, and it is found that the RC filter profile is best among other filter profiles for further optimisation procedures. For further reducing roll-off factor, another optimisation approach called "Adaptive Spectral Shaping" is investigated, which is discussed in the next section.

3.4.2 Adaptive Spectral Shaping Approach

As mentioned in previous sections, the challenge at hand is producing the desired filter shape with WSS. The desired filter specifications can be given as an input filter response to the WSS device, but this does not guarantee that the WSS will realise the desired filter. To overcome this challenge, another approach of reducing the spectral roll-off factor by optimising the input response of the WSS was investigated. The concept of our work relies on the principle of a feedback-based optimisation method known as least mean square error (LMS) algorithm (Simon Haykin and Bernard Widrow 2003). LMS algorithm serves the purpose to reduce the mean square error (MSE) between the desired filter shape and the measured WSS filter shape output by altering the input filter response until the MSE is minimised. LMS can help reshape the output profile closer to the desired shape by a few iterations when configuring the transmitter, in a "set and forget" scenario. Fig. 3.14 shows the basic principle of the LMS algorithm. Here $x(k)$ represents the input filter

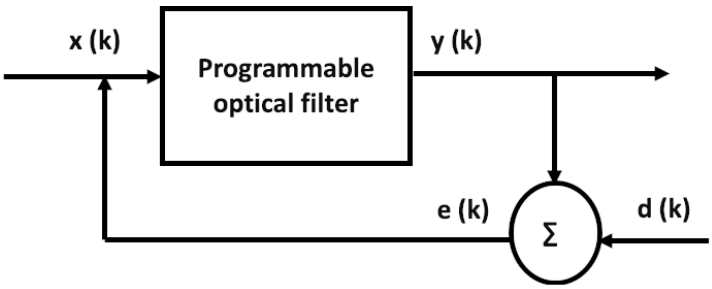


Figure 3.14: Working principle of LMS algorithm.

profile loaded to the programmable optical filter, and $y(k)$ is the output response of the programmable optical filter. $d(k)$ is the desired filter profile, which is the same as $x(k = 1)$ for the 1^{st} iteration only. The difference between the ideal desired profile and measured output response is given by $e(k) = d(k) - y(k)$ where $e(k)$ is the MSE. Note that strictly speaking, in LMS algorithms, a ratio between the desired and measured outcomes is typically taken as the error value. Here, using the dB scale of the measured optical spectrum, this ratio becomes a subtraction/addition. The new filter response $y(k) + e(k)$ is fed back to the filter input, altering the input filter response. This process repeats until the MSE is minimised. Therefore, after uploading the new input into the programmable optical filter, it produces a new output which has a more accurate representation of the desired filter profile. The advantage of this "set and forget" filter is that there is no significant time delay in setting

up the filter with new coefficients. The coefficients are updated quickly as soon as the new filter profile is uploaded to the WSS. Experimentally, to carry out this process, an EDFA is used to produce an amplified spontaneous emission signal, which is fed to a WSS to emulate the filter shape. As a default filter profile, an RC filter shape is realised in MATLAB® and uploaded to the WSS by the API. The roll-off factor dependency on the spectral shape, considering RC filters with B_{FWHM} of 10 GHz, 30 GHz and 60 GHz, is measured. The B_{FWHM} is normalised by the bandwidth resolution r of WSS (10 GHz in our case). Fig. 3.15 shows the spectral results between the ideal filter, the 1^{st} output and

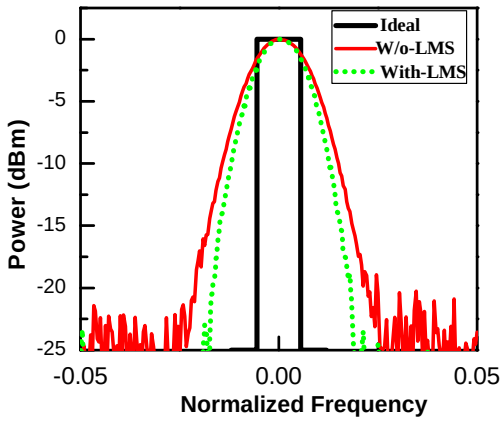


Figure 3.15: Filter shape comparison with and without LMS.

after the first LMS iteration. It clearly shows that the total bandwidth of the filter (B_T) is reduced, dropping the roll-off factor from 0.67 to 0.63 after the first iteration. Therefore, a ∼4.8 % improvement in roll-off factor after one

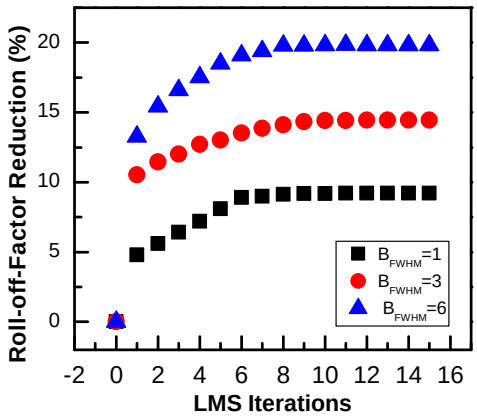


Figure 3.16: Reduction of roll-off factor for different values of B_{FWHM}/r.

iteration alone, and an overall reduction of 9.22 % after 6 iterations for the

case when B_{FWHM}/r=1. Similarly, the overall roll-factor is reduced by 14.3 %, and 19.8 % for B_{FWHM}/r equals to 3 and 6, respectively, after six iterations as seen in Fig. 3.16. The performance and impact of these LMS based filters are investigated in Chapter 5 with simulations in five-channel Nyquist-WDM superchannel system.

Chapter Summary

The accuracy of the output response of WSS is studied, and also the impact of limitations on reducing the spectral roll-off is investigated. In this work, a method of reducing spectral roll-off by introducing amplitude dip in input filter response of WSS is discussed. For a filter with B_{FWHM}/r, the roll-off factor is reduced by a factor of 10.1 % when amplitude dip changes from 0 to 5 %. An optical system to observe the total power penalty caused by different types of WSS generated filters is simulated. From the simulation results, it can be seen that the penalty induced by Gaussian and Butterworth filters is 1 dB larger than that caused by the RC filter. The results are also in agreement that in the case of narrow optical filtering, the induced penalty increases for reduced filter bandwidths. It is concluded that WSS is a flexible programmable optical filter, but its performance is always limited by low spectral resolution. The proposed adaptive optical filter using a WSS can reduce the roll-off factor of up to 19.8 %. This can significantly reduce the complexity of the transmitter DSP to achieve Nyquist-WDM superchannel, and hence enabling a real implementation. Note that the method can also be used to the design of integrated optical filters, particularly allowing for full photonic integration. Breaking this resolution limitation while retaining narrow bandwidth operation would significantly improve the filtering experience with WSS.

Chapter 4

Generation and Detection of Nyquist-WDM Superchannel

Superchannels are considered as key enablers for high capacity next-generation optical transport networks. The superchannel of the desired capacity is the combination of several independent data modulated optical subcarriers mostly generated from the single continuous wave (CW) laser source. A particularly promising approach exploits optical frequency combs for superchannel generation. The combined subcarriers in a superchannel offer the highest spectral efficiency, and it can be achieved by using a higher-order modulation format (like QPSK and 16-QAM) and spectral shaping techniques with coherent detection at the receiver. The generation of superchannels that uses advanced modulation formats and multi-carrier modulation techniques require an optical multi-wavelength transmitter capable of creating multiple, closely frequency spaced and stable optical carriers. This chapter focuses on the implementation of a Nyquist-WDM superchannel in simulations, in order to verify the performance of adding analogue optical filter as part of the spectral shaping of subcarriers, easing the DSP requirements. In this chapter, all building blocks required for the generation of Nyquist-WDM like optical frequency comb are also discussed.

4.1 Optical Frequency Comb Generation

The generation of OFC is a topic of intense interest due to its wide application range in different areas of photonic technology. An OFC is a spectrum of

discrete, equispaced frequencies often generated from a single laser source. A salient feature of OFC is the precise frequency spacing and a high degree of coherence between the comb lines, which makes them ideally suitable in the development of transmitter units for O-OFDM and Nyquist-WDM superchannels. A single comb source can replace hundreds of lasers, which would have to be controlled precisely in their relative and absolute frequencies (Hillerkuss et al. 2013). Several techniques have been investigated to generate OFC, such as re-circulating frequency shifter (RFS) loop (Zhang et al. 2011) (Lin et al. 2014), self-feedback oscillation techniques (Lin et al. 2013), cascading of different types of modulators (Wang et al. 2014) (Sakamoto et al. 2007) (Chen et al. 2013). In RFS, comb generation scheme, there is noise accumulation in each round trip which forces network designers to employ noise suppression techniques. This enhances system complexity and degrades its stability (Zhang et al. 2012). Choosing an optimum comb generation technique clearly involves application dependent performance trade-offs. A simple technique of comb generation, using two cascaded MZMs (Healy et al. 2007) is simulated by using VPI software. This method is chosen as it provides excellent spectrum flatness and side mode suppression ratio (SMSR) with low complexity. The spectrum flatness refers to the amplitude deviation of the optical power distribution of comb lines. Flat-top optical power distribution among comb lines is desirable in communication applications to avoid equalisation and ensure similar performance between channels. The comb generator consists of CW laser, two cascaded MZMs, each being driven by sinusoidal signal and a phase shifter as shown in Fig .4.1. The CW laser beam

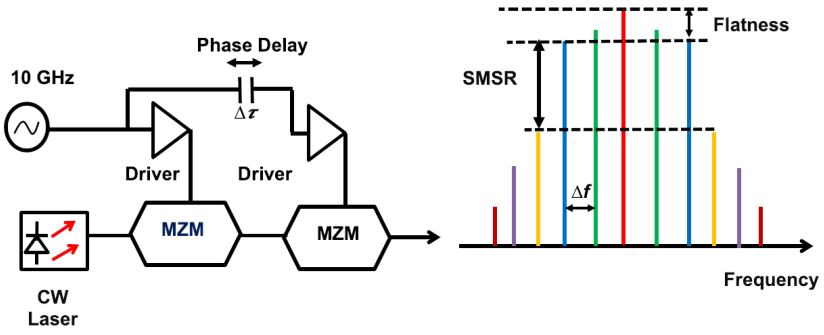
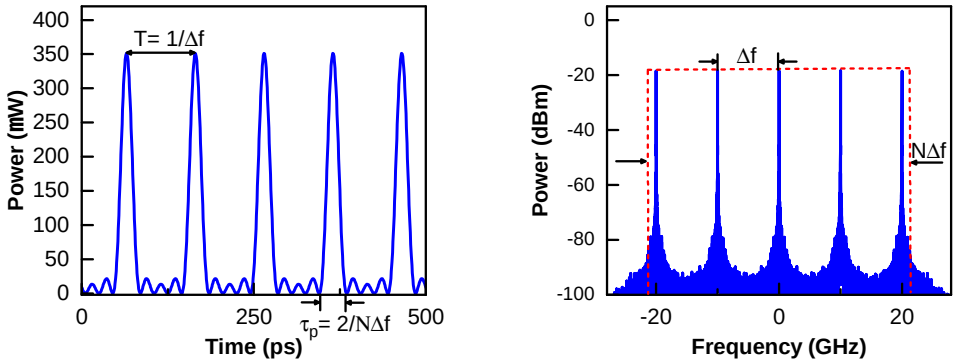


Figure 4.1: Schematic of Optical Frequency Comb Generation.

is launched to the first amplitude modulator. If a sine wave of frequency (f=10 GHz, in this case) is applied, it generates spectral side-bands separated by Δf. The same effect should occur when this signal is launched to a second amplitude modulator. However, the balanced modulator bias and precise

phase control are necessary to enable a flat comb and flatter the comb, and better is the coherence. In our simulations, both MZMs have the same extinction ratio of 30 dB. Both MZMs are biased with the same DC bias voltage of 1.9 V. The MZMs are driven with the amplitude of 0.5 V_π and the frequency of the sinusoidal signal of 10 GHz. The V_π is the switching voltage. To obtain the flat comb, the DC voltage is swept from 1 to 5 V. The best spectrum flatness (0.12 dB) of an optical frequency comb is found when the DC voltage is 1.9 V. The frequency spacing (Δf) between adjacent spectral lines



(a) Time (b) Frequency

Figure 4.2: Time–frequency correspondence for sinc-shaped pulses.

determines the pulse repetition period $T = \frac{1}{\Delta f}$, and the rectangular bandwidth $N \times \Delta f$ (N being the number of lines) defines the zero-crossing pulse duration $\tau_p = \frac{2}{N \times \Delta f}$ as shown in Fig. 4.2. Hence, the pulse width and repetition rate can be changed by tuning the frequency comb parameters. This feature offers a highly flexible and simple method to adjust the bit rate and bandwidth allocation in an optical network as per requirements.

4.1.1 Theoretical Analysis

The principle of the method is based on the time–frequency duality described by Fourier analysis. A sinc pulse can be represented by a rectangular spectrum in the Fourier domain, while the frequency content of a train of sinc pulses corresponds to a flat comb with equally spaced components within the bandwidth defined by the single-pulse spectrum. The comb generator produced a sequence of sinc pulses directly having uniformly spaced components with narrow linewidth, equal amplitude and linear-locked phase, together with strong outer-band suppression. The pulse sequence obtained from this rectangular frequency comb is strictly identical to the summation of

individual time-unlimited sinc pulses. The time-domain representation of the optical field of a frequency comb with N lines, having the same amplitude $\frac{E_0}{N}$ and frequency spacing Δf around the central frequency f_0, can be expressed in equation 4.1 (Soto et al. 2013).

$$\begin{aligned} E(t) &= \frac{E_0}{N} \sum_{n=-\frac{N-1}{2}}^{\frac{N-1}{2}} e^{2i\pi(f_0+n\Delta f)t+i\phi} \\ &= \frac{E_0}{N} e^{2i\pi f_0 t+i\phi} \sum_{n=-\frac{N-1}{2}}^{\frac{N-1}{2}} e^{2i\pi n\Delta f t} \\ &= \frac{E_0}{N} e^{2i\pi f_0 t+i\phi} \frac{e^{i\pi\Delta f(N+1)t} - e^{-i\pi\Delta f(N-1)t}}{e^{2i\pi\Delta f t} - 1} \\ &= E_0 \frac{sin(\pi N\Delta f t)}{N sin(\pi\Delta f t)} e^{2i\pi(f_0 t+i\phi)} \end{aligned} \tag{4.1}$$

It is assumed that all frequency components have the same phase ϕ. The normalized envelope of the optical field is calculated to be $\frac{sin(\pi\Delta f t)}{N sin(\pi\Delta f t)}$ denominated as periodic sinc function. To verify that this envelope actually corresponds to a train of sinc-shaped Nyquist pulses, it is convenient to start from its frequency domain representation. The Fourier transform is shown in equation 4.2.

$$\begin{aligned} F\{\frac{sin(\pi N\Delta f t)}{N sin(\pi\Delta f t)}\} &= F \sum_{n=-\frac{N-1}{2}}^{\frac{N-1}{2}} e^{2i\pi\Delta f t} \\ &= \sum_{n=-\frac{N-1}{2}}^{\frac{N-1}{2}} \delta(f - n\Delta f) \end{aligned} \tag{4.2}$$

Introducing the rectangular function $\prod(\frac{n}{N})$ that is 1 for all integers n where $n \leq \frac{N-1}{2}$ and 0 elsewhere, the above equation can be replaced by equation 4.3.

$$\begin{aligned} \sum_{n=-\frac{N-1}{2}}^{\frac{N-1}{2}} \delta(f - n\Delta f) &= \sum_{n=-\infty}^{\infty} \delta(f - n\Delta f) \\ &= \prod(\frac{f}{N\Delta f}) \sum_{n=-\infty}^{\infty} \delta(f - n\Delta f) \end{aligned} \tag{4.3}$$

where the rectangular spectrum $\prod(\frac{f}{N\Delta f})$ covering a bandwidth NΔf, is represented in the time domain by the sinc-pulse NΔf sinc(NΔf). The temporal dependence of the above expression can then be obtained by taking

its inverse Fourier transform and using the Poisson summation formula expressed in equation 4.4 (Soto et al. 2013).

$$\begin{aligned} F^{-1}\{\prod(\frac{f}{N\Delta f})\sum_{n=-\infty}^{\infty}\delta(f-n\Delta f)\} &= Nsinc(N\Delta ft)\otimes\sum_{n=-\infty}^{\infty}\delta(t-\frac{n}{\Delta f}) \\ Nsinc(N\Delta ft)\otimes\sum_{n=-\infty}^{\infty}\delta(t-\frac{n}{\Delta f}) &= \sum_{n=-\infty}^{\infty}Nsinc(N\Delta f(t-\frac{n}{\Delta f})) \end{aligned} \tag{4.4}$$

The above equation can be rewritten as equation 4.5

$$\frac{sin(\pi N\Delta ft)}{Nsin(\pi\Delta ft)} = \sum_{n=-\infty}^{\infty}sinc(N\Delta f(t-\frac{n}{\Delta f})) \tag{4.5}$$

The optical intensity of the comb can be defined as equation 4.6.

$$I(t) = |E(t)|^2 \quad = E_0^2\frac{sin^2(\pi N\Delta ft)}{N^2sin^2(\pi\Delta ft)} \tag{4.6}$$

Consequently, it is proven that the field envelope of the time domain representation of a frequency comb of N identical and equally spaced lines corresponds to an infinite summation of sinc-shaped Nyquist pulses with period $\frac{1}{\Delta f}$ and zero-crossing pulse-width $\frac{2}{N\Delta f}$.

4.1.2 Result Analysis

A five-tone comb with frequency spacing of 10 GHz is simulated as shown in Fig. 4.3. However, more number of comb lines can be generated with this method, but the main objective of this thesis to study the impact of proposed spectral shaping at the transmitter side. For this each comb line to be demultiplexed and independently modulated before spectral shaping. Therefore, to avoid the complexity and to analyse the impact of spectral shaping without additional crosstalk from more channels, the five number of comb lines are chosen. The frequency spacing (10 GHz) is chosen in this work because with this small channel spacing, a large number of channels can be accommodated into a given bandwidth. This will help to use available bandwidth efficiently and thus increasing the spectral efficiency of the transmission system. The power variation (flatness) is within 0.12 dB, and the SMSR is 23.5 dB. The sinc pulse has τ_p of 29.4 ps and T = 100 ps. A more detailed analysis of the impact of the RF amplitudes and DC bias on the flatness of five-tone comb lines is shown in Fig. 4.4. The DC bias for both

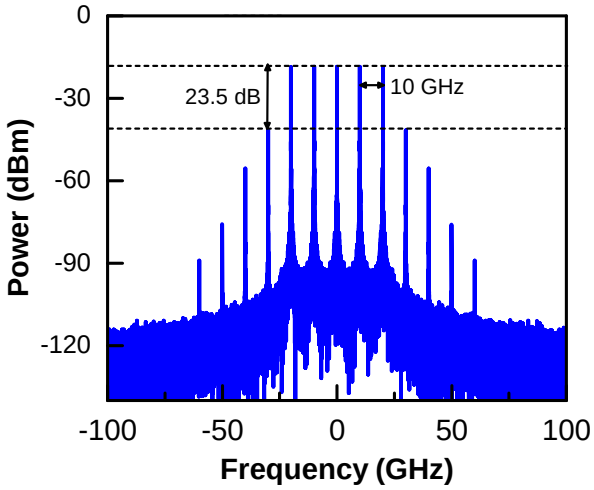


Figure 4.3: Simulated optical frequency comb spectrum with channel spacing of 10 GHz.

modulators are optimised, whilst setting RF amplitude at $0.5V_{\pi}$, where V_{π} is the switching voltage. It can be seen that the DC voltages from 1.5 V to 3.5 is

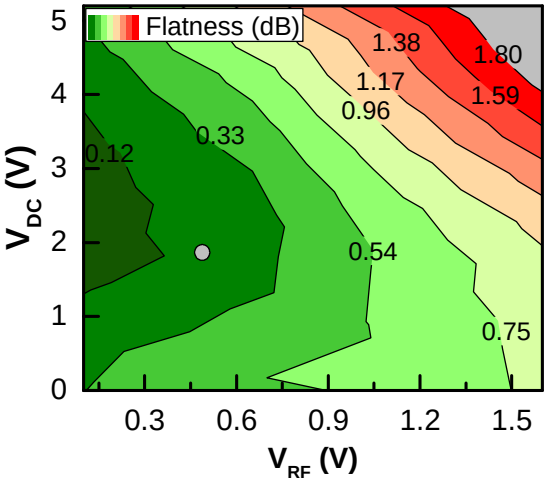


Figure 4.4: Optimised comb flatness versus drive (V_{RF}) and bias (V_{DC}) voltage.

required to achieve a flatness value of less than 1 dB. An ideal flatness of 0.12 dB is obtained around 1.9 V. The point marked with a circle in Fig. 4.4 represents the simulation operating position with a flatness within 0.12 dB. Similarly, the impact of the RF amplitudes and DC bias on the SMSR of comb line is illustrated in Fig. 4.5. SMSR is also a key parameter; the value of SMSR should be high so that unwanted side-bands can be suppressed. It can be seen that the DC voltages from 1.5 to 3.5 V are required to achieve an SMSR, more than 13 dB. The SMSR below 13 dB is not acceptable for optical transmission

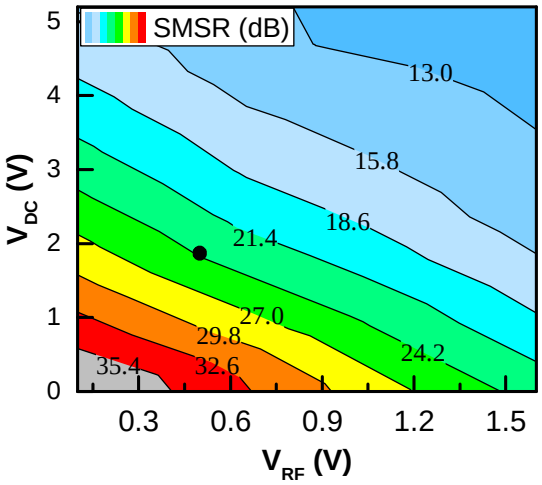


Figure 4.5: SMSR versus drive (V_{RF}) and bias (V_{DC}) voltage.

systems, as the unwanted side-bands may affect the adjacent channels in the optical link. However, SMSR greater than 20 dB can be considered a goal with a ratio of the optical power between the unwanted side-bands and the data-carrying channels. The higher SMSR can be achieved at other voltages as well but at the cost of reduced flatness. Therefore, the bias point should be chosen such that there should be an optimum trade-off between SMSR and flatness. The point marked with a circle in Fig. 4.5 represents the simulation operating position with SMSR of 23.5 dB. The comb channels are phase-locked to each other, which makes this comb generation technique suitable for use with a broad range of applications including Nyquist-WDM. These also allow a single laser to be used to generate carriers for several subchannels, reducing component count and cost.

4.2 Independent subcarrier modulation

In order to enable several optical subcarriers to be transmitted over the same medium, it is necessary to multiplex the signals. Before multiplexing, it is important to demultiplex the optical frequency comb so that each subcarrier can be independently modulated with the choice of modulation format at desired data rates. In this section, the demultiplexing of the comb is discussed, followed by its working principle.

4.2.1 De-multiplexing using Delay line Mach-Zehnder Interferometer

After the generation of the phase-locked optical carriers, the first step is to demultiplex the signal for independent modulation of each subcarrier. The optical carriers cannot be demultiplexed with conventional optical frequency filters because of the overlapping channel spectra. All the optical carriers must be demultiplexed in an appropriate approach. De-multiplexer can be structured using optical FFT in which components of MZDI act as spectral filter and splitter. By cascading N number of MZDIs, the N point optical FFT can be implemented (Hillerkuss et al. 2010) (Takiguchi et al. 2009).

Working Principle

FFT is considered equivalent to a cascade of delay interferometers and has exactly the frequency response of the DIs. The FFT of order N is able to separate N individual frequency components of the input signal, spaced $\Delta\,\omega = \frac{2\pi}{T_s}$. Thus, by cascading a sufficient number of DIs with correct delay and phase, any arbitrary frequency component can be isolated. All these equations for the analysis are taken from source (Hillerkuss et al. 2010). The DFT for continious input and output signal $x(t)$and $X_m(t)$ is presented in equation 4.7.

$$X_m(t) = \frac{1}{N}\sum_{n=0}^{N-1} exp(-j2\pi n\frac{m}{N}.\delta(t - n\frac{T}{N}) * x(t) \tag{4.7}$$

where δ(.) is the Dirac function used to sample the input signal $x(t)$ at N equidistant points within the interval T by means of the convolution operation ($*$). The transfer function $H_m(\omega)$ for the DFT can be obtained in equation 4.8 by using Fourier transform.

$$\begin{aligned} H_m(\omega) &= \frac{1}{N}\sum_{n=0}^{\frac{N}{2}-1}\{exp(-j2\pi[2n]\frac{m}{N})exp(-j\omega[2n]\frac{T}{N}) + exp(-j2\pi[2n+1]\frac{m}{N}) \\ &\qquad exp(-j2\omega[2n+1]\frac{T}{N})\} \\ &= \underbrace{\frac{2}{N}\sum_{n=0}^{\frac{N}{2}-1} exp(-j\frac{2n}{N}[2\pi m + \omega T])}_{FFT of order N/2} . \underbrace{\frac{1}{2}[1 + exp(-j[\omega\frac{T}{N} + \frac{2\pi m}{N}])]}_{H_{pm,1(\omega)}} \end{aligned} \tag{4.8}$$

$H_{pm,1}$ is the n-independent transfer function for the upper input of a delay interferometer with delay ϕ_{pm} is additional phase shift, obtained from the cascade of directional couplers and a delay line in the lower arm. as shown in equation 4.9

$$\begin{aligned} T_p &= \frac{T}{N} = \frac{T}{2^p} \\ \phi_{pm} &= 2\pi\frac{m}{N} - \pi \end{aligned} \tag{4.9}$$

Hence it is mathematically proven that the DFT of order $N = 2^p$ can always be replaced by an arrangement of p DI stages. The DFT acts as a periodic filter in the frequency domain with a free spectral range of $N\Delta\omega$, and each DI of the cascade is also a periodic filter with FSR $\frac{N\Delta\omega}{2^p}$ where p is the index of the FFT stage and N is the order of the FFT. In our case, the optical FFT processor consists only of $N-1$ cascaded DIs. We have five comb lines, so N=5. The mathematical expression is presented by equation 4.10 and the corresponding frequency transfer function is given by equation 4.11.

$$h(t) = \frac{1}{5}\left[\sum_{n=0}^{\frac{3}{2}} \delta\left(t - \frac{2n+1}{5}T\right) - \sum_{k=0}^{\frac{3}{2}} \delta\left(t - \frac{2n}{5}T\right)\right] \tag{4.10}$$

$$H(\omega) = \frac{1}{5}\left[1 + \exp\left(-\mathrm{j}\left[\omega\frac{T}{2}\right]\right)\right]\left[1 + \exp\left(-\mathrm{j}\left[\omega\frac{T}{4}\right]\right)\right]\left[1 + \exp\left(-\mathrm{j}\left[\omega\frac{T}{8} + \pi\right]\right)\right] \tag{4.11}$$

A schematic diagram of the proposed all-optical de-multiplexer is shown in Fig. 4.6. The structure combines three-stage cascaded MZI and adjacent stages of the MZIs. The differential path length of each stage MZI has a specific path length and delay. The first stage has the longest length; the second stage has a length half of that of the first stage. The third stage has a length half of the second stage. On one arm of each stage MZI, there is a phase shifter, which is used to tune the phase difference between the two arms. With the specific phase difference on each stage MZIs as shown in Fig. 4.6, the five-tone comb can be demultiplexed into individual subcarriers (Yu et al. 2016). In the first stage, a half bit delay is used in one arm of first MZI. This half bit delay introduces the phase shift of $180°$ in one of MZI arm, which result in FSR of 20 GHz. This FSR of 20 GHz separate the comb into odd (three) and even (two) lines. In the second stage, a 1/4 bit delay and an additional phase shift of $90°$

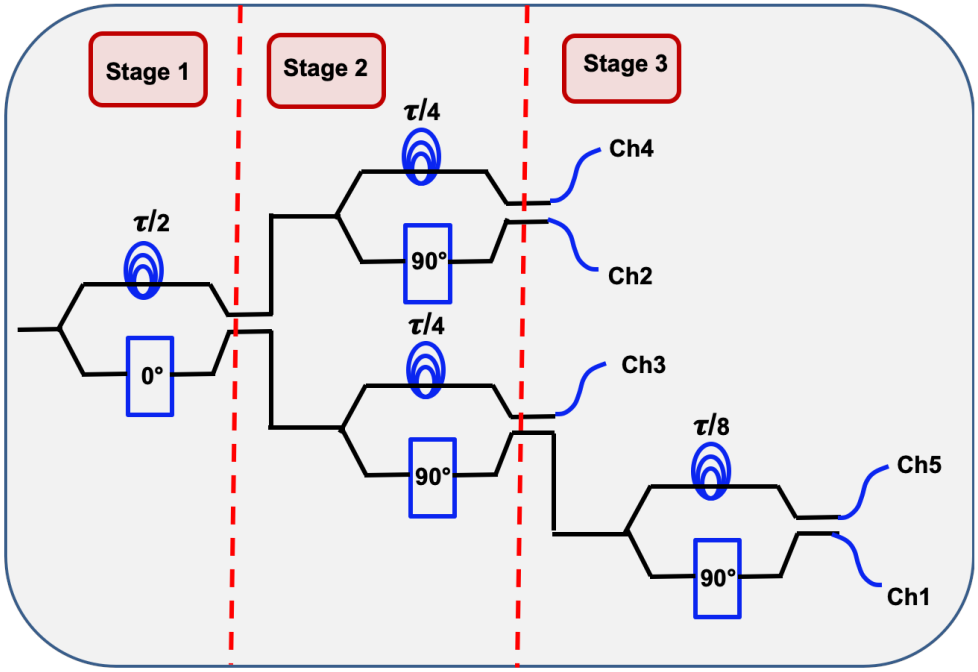


Figure 4.6: Implementation of optical FFT using cascaded stages of MZDI

is required to separate the pair of comb lines into an individual one. With same delay and phase shift, one odd comb line out of three can be separated. For the third stage, to separate a pair of odd lines, an additional 1/8 bit delay and $90°$ is on the arm of the fourth MZI as seen in Fig. 4.6. This way, each individual subcarrier can be demultiplexed, with an extinction ratio of 60 dB, ensuring minimal crosstalk and also preserving the phase relationship between subcarriers.

4.2.2 Phase Monitoring of subcarriers

The source for the Nyquist-WDM transmitter is optical frequency comb with phase-locked subcarriers. For the ideal transmitter implementation, each of the optical channels is separated by cascaded delay line interferometers and independently encoded in a phase preserving modulator array before being wavelength-multiplexed at the output of the transmitter. The optical phase difference between adjacent optical channels needs to be controlled in order to create a deterministic interference signal. If five individual optical subcarriers with non-optimal phase differences are multiplexed together to form superchannel, then the waveforms of these subcarriers will not be aligned with each other. Without phase alignment, the eye at the crossing point cannot be aligned, which can lead to errors and distortions, as shown in Fig. 4.7. The

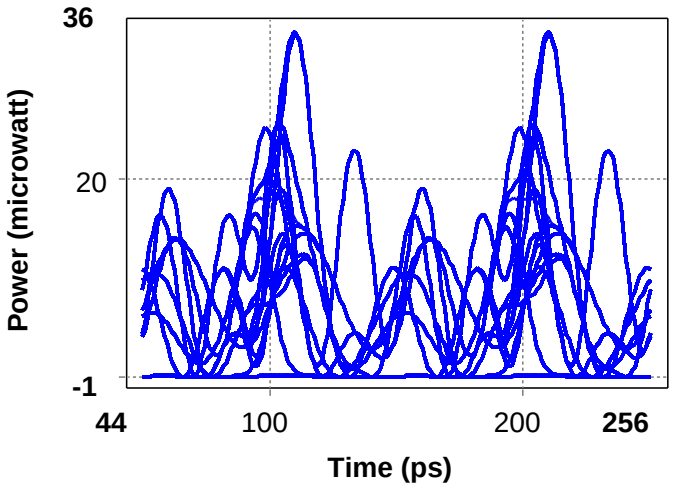


Figure 4.7: Eye diagram after multiplexing of five optical channels with non-optimal phases.

reason behind this misalignment is that Ch1 and Ch5 have an additional MZDI which causes an extra phase shift in both channels as shown in stage 3 in Fig. 4.6. To counteract with this extra phase shift, a pair of delay lines are used

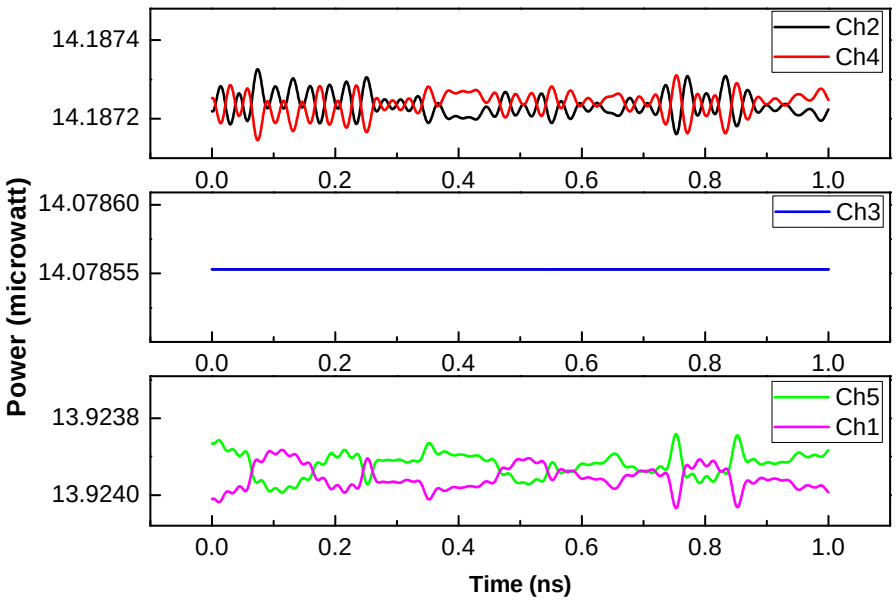


Figure 4.8: Optical waveform before combining five channels to form a super-channel.

for both channels. With this extra delay lines, the impact of the extra phase shift is cancelled, and the amplitude of Ch1 and Ch5 remains the same as the

rest of the channels. With this step, the phase relationship of all-optical subcarriers is also preserved, and their waveforms are aligned with each other, as seen in Fig. 4.8. After multiplexing, the eye is aligned without many

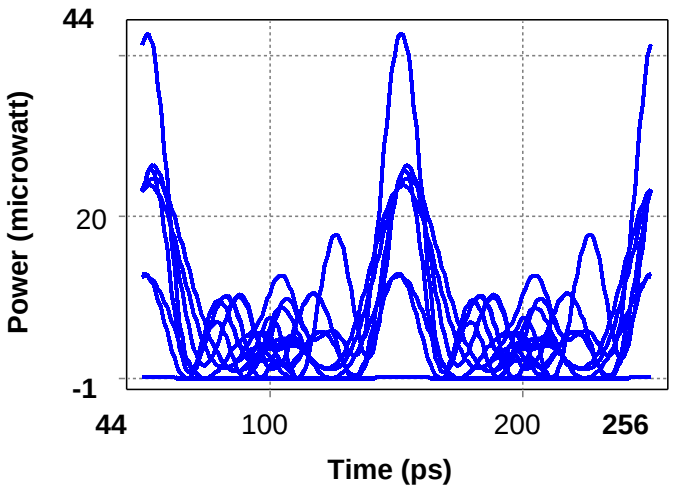


Figure 4.9: Eye diagram after multiplexing of five channels with optimal phases.

distortions as depicted in Fig. 4.9. Therefore, the optical phase relationship between the channels in the transmitter must be preserved throughout the entire transmitter, from comb generation, demultiplexing and data encoding, as it has a significant impact on the overall performance of the system. After phase monitoring of subcarriers, the next step is modulation. In the next section, modulations formats and their generation are explained in detail.

4.3 Employing high order modulation formats

Modulation is a process of converting information onto a light-wave in which base-band signal uses high-frequency carrier signal is upconverted to become more suitable for transmission over long optical fibre distances. An optical signal produced from a laser source is commonly used as a carrier signal. The optical signal is then modulated and propagated through a medium such as silica fibre, which confines the light and guides it to the receiver where the signal is detected and decoded. The information can be conveyed by varying any one or a combination of the amplitude, frequency, phase and polarisation of the carrier. The modulation format is a key parameter which determines the transmission quality. The choice of optical modulation format depends on various factors such as data rate, fibre types and channel spacing where the

compromise between the complexity, optical power and bandwidth is important. Recently, the use of advanced modulation formats is motivated for high transmission capacity and better system reliability. The ideal modulation format has a narrow spectral width, low susceptibility to fibre non-linearities, large dispersion tolerance, simple and cost-effective configuration for a generation. The modulation is achieved by different technologies, which include directly modulated lasers (DML), electro-absorption modulators (EAM) and Mach-Zehnder modulators (MZM) (Stavdas 2010). In order to realise high-speed modulation, an optical modulator should have high electro-optical bandwidth, low optical insertion loss and a high extinction ratio. A DML is a very cost-efficient modulation technique as it can be easily realised by direct modulation of the laser drive current. This modulation presents a large chirp that defined as a rapid variation in the instantaneous frequency of the laser caused by the refractive index changes in the active layer due to the carrier density population (Shalom et al. 1998). The chirp introduces pulse broadening, which is considered a serious problem as it can introduce crosstalk between the adjacent wavelengths in DWDM systems. For this reason, the performance of this modulation class is still limited for data rate (< 10 Gb/s) and short distance transmission (Matsui et al. 2006). To overcome these limitations of the chirp in the intensity of the direct modulation, external modulators like EAMs and MZMs are generally required as they result in a nearly chirp-free signal (Borne 2008). An external modulator switches the incoming CW laser output "ON or OFF", depending on the electrical drive signal applied to the modulator.

4.3.1 Electro-absorption Modulator

An EAM modulates the optical field by changing the absorption properties of the device material using the externally applied voltage. The modulation with an EAM can result in an optical signal with lower chirp than a DML, and high electro-optical bandwidth can be realised (Yichuan Yu et al. 2005). However, EAMs have a wavelength-dependent performance, low extinction ratio (<10 dB), high insertion loss (10 dB) and a limited optical input power (Borne 2008). The extinction ratio is defined as the ratio of the transmission in the ON state to the transmission in the OFF state, and it is typically measured by varying a DC phase bias to one of the modulator arms to find the absolute maximum and minimum transmission of the modulator. The high insertion losses of EAMs can be eliminated by integrating with semiconductor optical

amplifiers (SOAs), which can even yield some net fibre-to-fibre gain.

4.3.2 Mach–Zehnder Modulator

The most commonly used external optical modulator is MZM due to its ability to produce both intensity-modulated (OOK) and phase-modulated formats (e.g. BPSK). It was first proposed by Ernst Mach and Ludwig Zehnder in 1891(Zehnder 1891). MZMs are fabricated using electro-optically active

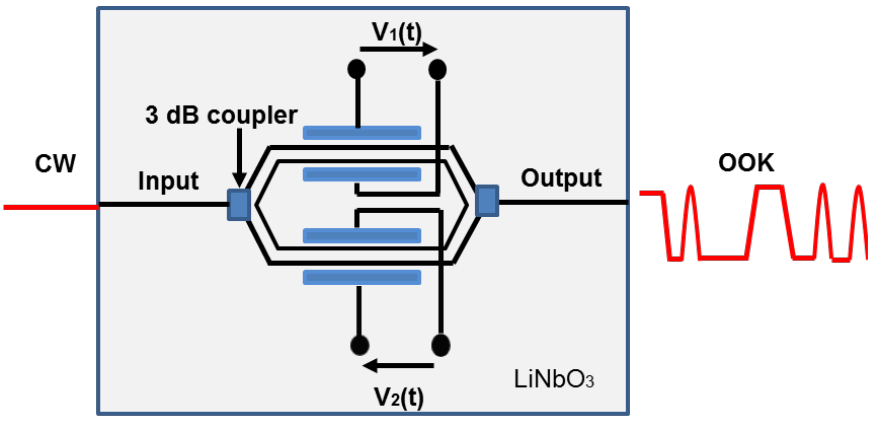


Figure 4.10: Mach-Zehnder Modulator architecture.

materials such as Lithium-Niobate $(LiNbO_3)$ by diffusing titanium through the material to increase the local refractive index without altering its electro-optics (EO) properties (Doi et al. 2006). An MZM consists of two 3-dB couplers with two interconnecting waveguides of equal length to create an interferometer, as shown in Fig. 4.10. When both waveguides are coupled together, the condition is known as single-drive operation. However, two waveguides of an MZM can be modulated separately, which is known as dual-drive operation. When an electric field is applied across the phase shifter, the refractive index of the crystal changes, which in turn changes the velocity of the light propagating through the waveguide. By choosing the electrical drive voltage level appropriately, the interference in the second 3-dB coupler can be either constructive (the phase of the light in each branch is the same) or destructive (the phase in each branch differs by π). The drive voltage required to achieve π phase difference between two arms is defined as the switching voltage (V_π). The optical field at the output of the MZM and by neglecting the insertion loss, the effect of temperature with an equal power division between the two arms

of the interferometer, is expressed by the following equation 4.12.

$$\frac{E_{\text{out}}(t)}{E_{\text{in}}(t)} = \frac{1}{2} \cdot \left(e^{j\varphi_1(t)} + e^{j\varphi_2(t)}\right) \tag{4.12}$$

with E_{in} in and E_{out} are the electric fields at the input and output of the MZM, respectively. $\varphi_1(t)$ and $\varphi_2(t)$ are the phase shifts in the upper and the lower arms of the interferometer which are given by equation 4.13

$$\begin{aligned} \varphi_1(t) &= \pi \frac{V_1(t)}{V_\pi} \\ \varphi_2(t) &= \pi \frac{V_2(t)}{V_\pi} \end{aligned} \tag{4.13}$$

V_1 and V_1 present the applied voltages to the two arms of the MZDI composed by the modulation voltage V_{RF} and the bias voltage V_{DC}. In case that $\varphi_1(t) = \varphi_2(t) = \varphi(t)$, an identical phase shift is obtained in the two arms of the MZM. Then, a phase modulation is obtained, the electric field at the input and the output of the MZM are given by the following equation 4.14

$$\frac{E_{\text{out}}(t)}{E_{\text{in}}(t)} = e^{j\frac{V(t)}{V_\pi}\pi} \tag{4.14}$$

The MZM operates as a single phase modulator in push-push mode. The intensity transfer function is shown in Fig. 4.11. In this case, the power transfer function is unit function which is defined as equation 4.15

$$\frac{P_{\text{out}}(t)}{P_{\text{in}}(t)} = \left|\frac{E_{\text{out}}(t)}{E_{\text{in}}(t)}\right|^2 = 1 \tag{4.15}$$

In the equation 4.16, an opposite phase shift is induced in the two interferometer arms of MZM. This is called the push-pull configuration of MZM.

$$\begin{aligned} \varphi_1(t) &= -\varphi_2(t) = \varphi(t) \\ V_1(t) &= -V_2(t) = \frac{V(t)}{2} \end{aligned} \tag{4.16}$$

The relation between the electric field at the input and the optical field at the output of the MZM is defined as function 4.17

$$\frac{E_{\text{out}}(t)}{E_{\text{in}}(t)} = \cos\left(\frac{\Delta\varphi(t)}{2}\right) = \cos\left(\pi\frac{V(t)}{2V_\pi}\right) \tag{4.17}$$

The phase difference between the upper and lower arms of the interferometer is given by equation 4.18

$$\varphi(t) = \varphi_1(t) - \varphi_1(t) = 2\varphi(t) \tag{4.18}$$

The MZM power transfer function is given by the following equation 4.19

$$\begin{aligned} \frac{P_{\text{out}}(t)}{P_{\text{in}}(t)} = \left|\frac{E_{\text{out}}(t)}{E_{\text{in}}(t)}\right|^2 &= \frac{1}{2} + \frac{1}{2}\cos\left(\Delta\varphi(t)\right) \\ &= \frac{1}{2} + \frac{1}{2}\cos\left(\pi\frac{V(t)}{V_\pi}\right) \end{aligned} \tag{4.19}$$

The power transfer function of the MZM is shown in Fig. 4.11. The behaviour

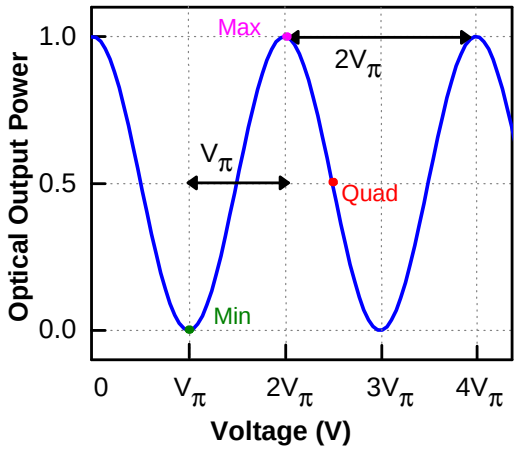


Figure 4.11: Power Transfer Characteristics of Mach-Zehnder Modulator.

of the MZM depends on the operating point. For an intensity modulation, the MZM can operate at the quadrature operating point (Quad) with peak-to-peak voltage V_{RF} equal to V_π. In case that the MZM is operated at minimum or maximum operating point (Min or Max) with a peak-to-peak voltage equal to $2V_\pi$ as shown in Fig. 4.11. An MZM is a promising device for long-haul transmission as it has a high extinction ratio (>20 dB), low insertion loss (4 dB). With the benefit of independently modulating intensity and phase of the optical field, MZMs form the basis of many advanced optical modulation formats by controlling the bias voltage of the RF signal.

4.3.3 Intensity Modulation Format- NRZ-OOK

A typical amplitude shift keying modulation format used in optical communication systems is NRZ-OOK in which binary information is

represented by the presence or absence of an optical signal. When using an

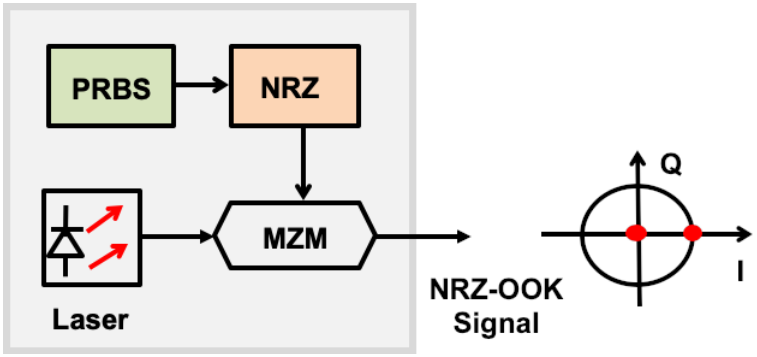
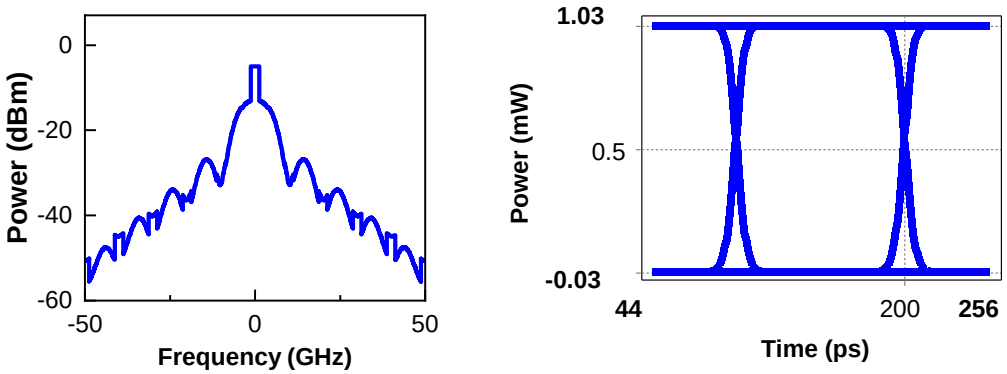


Figure 4.12: Transmitter Schematic for optical NRZ-OOK.

MZM, the modulator is biased at 50 % transmission which is called quadrature point ($Quad$) and indicated by a red dot in Fig. 4.11, and applying an electrical drive signal with a peak-to-peak amplitude of V_π will produce an OOK signal. As the applied RF electric field, V_{RF}, varies from peak-to-peak (V_π to $2V_\pi$), the optical output sweeps from to a 0 to 1. The schematic diagram of NRZ-OOK transmitter is shown in Fig. 4.12. The NRZ transmitter consists of a continuous laser (CW) which is modulated by MZM at 10 Gb/s PRBS sequence of 2^7 -1. A convenient representation of amplitude obtained via a constellation diagram – the representation of signal symbols on a complex plane. The horizontal axis of the constellation plane represents the In-phase (I) component of the signal and the vertical axis the Quadrature (Q) component. The constellation of OOK signals lies in a single axis, with one symbol in origin (bit 0) and the other on the I axis (bit 1) to emphasise that no phase modulation is present. The optical



(a) (b)

Figure 4.13: (a) Optical spectra and (b) Direct-detected eye diagram of NRZ-OOK system.

spectrum and direct-detected eye diagram of an NRZ-OOK modulated signal

which is operated at PRBS bit rate of 10 Gb/s are depicted in Fig. 4.13. The optical spectrum is taken with OSA resolution of 0.02 nm. The optical spectrum shows the power spectral density as a function of optical frequency. It has a strong component at the carrier frequency, which contains half the optical power. The side-bands are also present in the spectrum and are spaced at multiples of the symbol rate. The bandwidth of the optical spectrum is approximate twice the symbol rate. NRZ-OOK modulation is the most widely deployed modulation format due to its simplicity and low cost compared with other modulation formats. NRZ-OOK is highly sensitive to non-linear impairments due to the presence of the strong optical carrier.

4.3.4 Quadrature Phase Shift keying

In optical communications, QPSK is one of the advanced optical multi-level modulations formats which is widely used in optical communication to meet the increasing demand on spectral efficiency. In QPSK, the information bits are encoded into the phase of the optical carrier, and the amplitude of the signal remains constant. The optical transmitter is based on a CW laser and two MZMs, having a $\frac{\pi}{2}$ difference between them as shown in Fig. 4.14. The extinction ratio of MZM is 30 dB in this work. The MZM modulators are biased

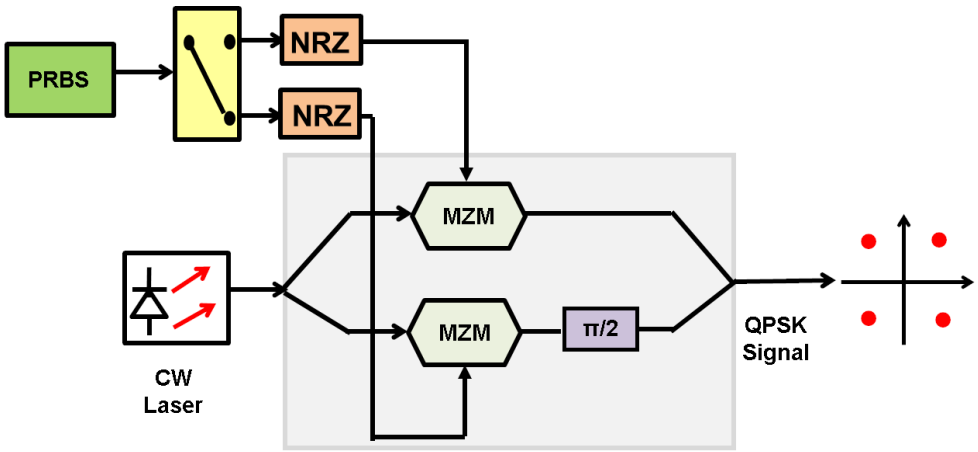


Figure 4.14: Transmitter Schematic for optical QPSK.

at the null point shifting the transfer-function such that the cosine transfer-function becomes a sine. Both of these two embedded MZMs are fully-driven by RF signal of the amplitude of $2V_\pi$ operating at a data rate of 10 Gb/s, i.e. the symbol rate is 5 Gbaud/s in this case. Fig. 4.15 shows the optical spectrum of QPSK modulation at 193.1 THz. The upper MZM forms in-phase (I) signal and the lower MZM (passing through a $\frac{\pi}{2}$ phase shift) forms the

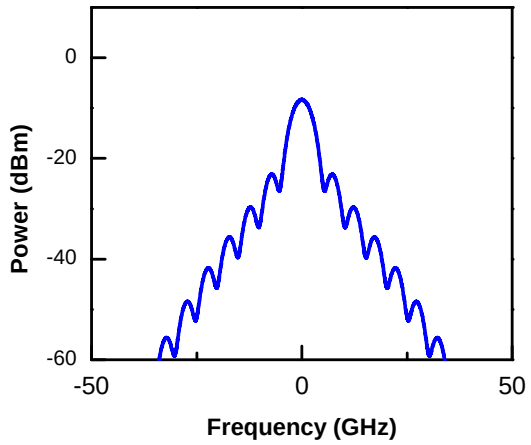
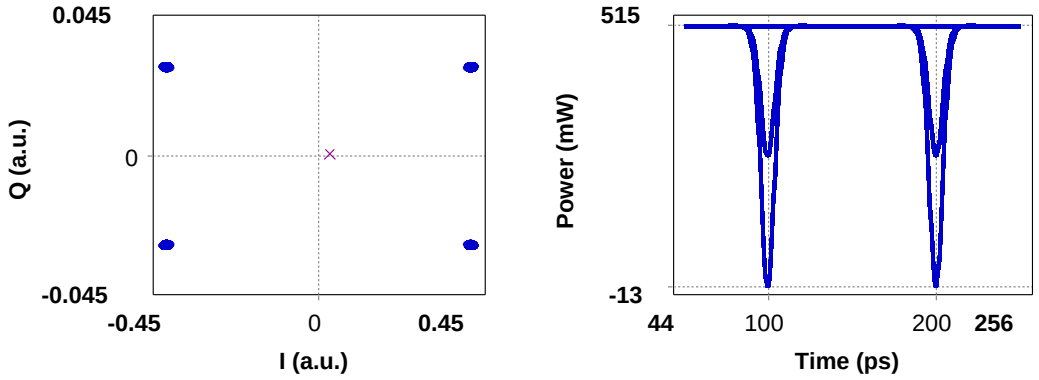


Figure 4.15: Optical Spectra of QPSK signal at 10 Gb/s.

quadrature (Q) signal for QPSK. This leads to 4 possible combinations of the $\pm$ signs representing the four symbols of the QPSK. Fig. 4.16 illustrates the constellation diagram and the simulated QPSK direct-detected eye diagram.



(a) (b)

Figure 4.16: (a) Constellation diagram and (b) Direct-detected eye-diagram of QPSK system at 10 Gb/s.

The eye diagram shows the dips at transition symbols which is characteristic for QPSK signal generated with two MZMs. In comparison to NRZ-OOK, QPSK enables the data rate to be doubled while keeping the same bandwidth. QPSK is commonly used for data rates of 100 Gb/s. Coherent techniques are needed for detecting the phase of the signal.

4.3.5 Quadrature Amplitude Modulation

The transmission capacity of optical communication systems can be increased by a factor of 4 over traditional NRZ-OOK systems by employing signals with the 16-QAM format. 16-QAM offers a high spectral efficiency, which makes it a

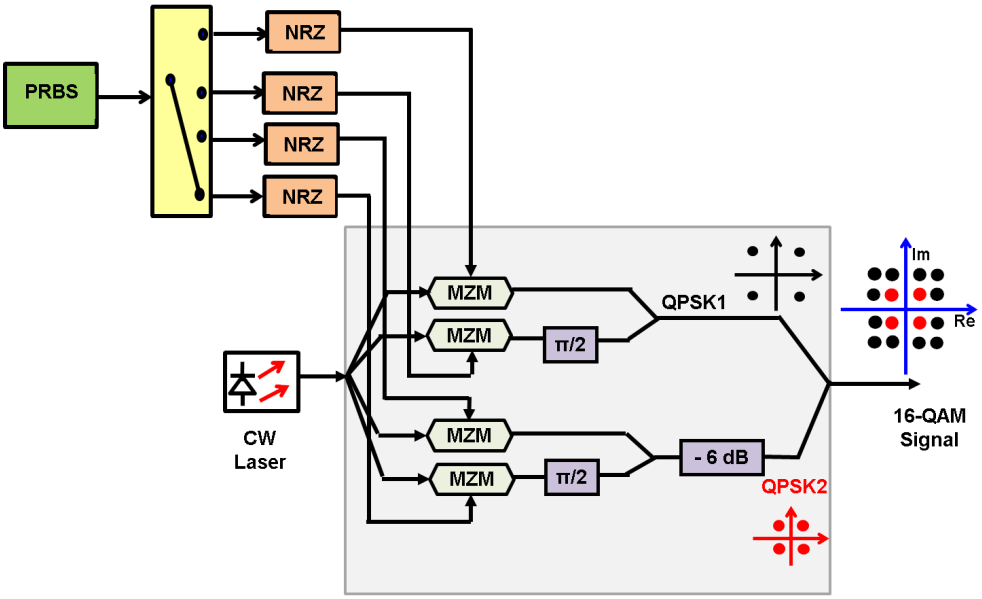


Figure 4.17: Transmitter Schematic for optical 16-QAM.

promising candidate for future high spectrally efficient transmission systems. For 16-QAM modulation, two QPSK modulators are embedded together, as shown in Fig. 4.17. The large amplitude QPSK1 is created in the upper arm by two 2^7-1 PRBS outputs with an amplitude of $2V_\pi$ to drive the MZM modulator at its null transmittance point. The overall data rate, in this case, is 10Gb/s, hence the symbol rate is 2.5 Gbaud/s in this case. The small-amplitude QPSK2 is obtained with a different amplitude of V_π to drive the MZM modulator at its null transmittance point followed by 6 dB attenuation in the lower arm. This 6 dB value of attenuation fixes the position of symbols within the quadrant, and the interference of the two signals with different amplitude levels yield a 16-QAM signal. The optical spectrum of the 16-QAM signal is shown in Fig. 4.18 measured at 10 Gb/s. The constellation diagram and eye diagram of 16-QAM, where each symbol represents four bits, are depicted in Fig. 4.19. Each point indicates a unique amplitude and phase of the signal. The constellation diagram is slightly rotated due to a phase shift of 6 dB attenuator. However, an effort to add small attenuation to the non-attenuated side is made but is remained unsuccessful. As it disturbs the entire quadrant and all the constellation points moved away from their ideal places. However, this slight

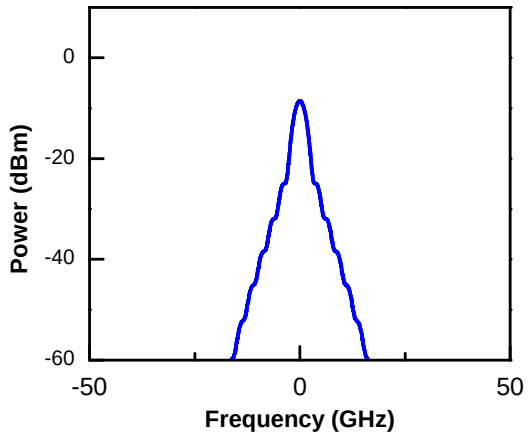
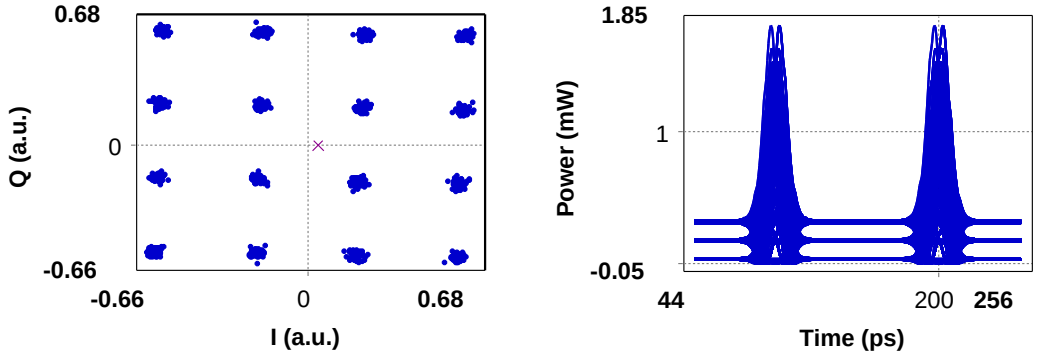


Figure 4.18: Optical spectrum of 16-QAM signal at 10 Gb/s with OSA resolution of 0.02 nm.



(a) (b)

Figure 4.19: (a) Constellation diagram and (b) Direct-detected optical eye diagram of 16-QAM.

rotation has not any significant impact on a signal; therefore, it can be ignored. The inherent advantage of this method is that no complicated set-up for obtaining a multi-level electrical signal is needed.

4.3.6 Spectral characteristics comparison of modulation formats

The optical power spectrum of the three modulation formats has been compared at the transmitter. The bandwidth occupied by the NRZ-OOK signal is larger than the others, as seen in Fig. 4.20. The spectrally broadened channels can overlap with their neighbouring channels which can lead to degradation of the modulated information. Unlike NRZ-OOK, QPSK reduces

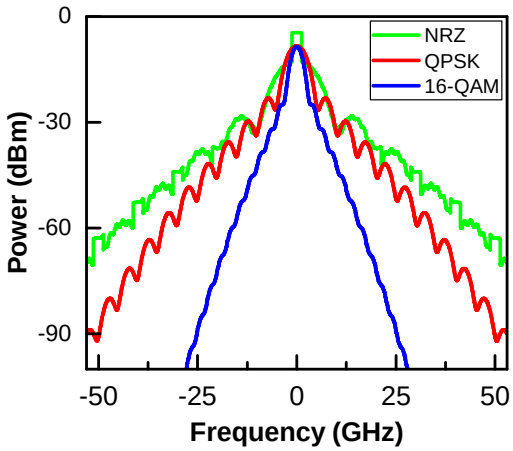


Figure 4.20: Optical spectral comparison of different modulation formats.

the required bandwidth to half, by sending two bits per symbol. 16-QAM modulation offers two times higher spectral efficiency than QPSK and further reduces the required symbol rate to obtain the equivalent overall bit rate, albeit, at the expense of an increased required OSNR. In addition to transmitting several information bits in each symbol period, additional spectral shaping of the transmitted pulses is required to retain the most of the modulated signal energy in a minimum frequency band. This can significantly reduce the required spacing between carriers enabling high spectral efficiency.

4.4 Detection of Nyquist-WDM

In optical transmission systems, two detection methods can be employed to demodulate and recover the data in the receiver: (1) direct and (2) coherent detection. The direct detection is the most simple technique to detect the signals with the help of the preamplified photodetector. The demultiplexing of the optical carriers is done similarly.

4.4.1 Direct Detection

The simplest form of optical detection is a direct detection receiver which detects the intensity of light and converts it to an electrical signal. With direct detection, only intensity-modulated formats like NRZ-OOK can be detected. A photodiode is used for this purpose which is a photosensitive device, thereby converting optical intensity into electrical current. The generated photocurrent is proportional to the responsivity of the receiver and intensity of an optical

signal, as shown in equation 4.20.

$$\begin{aligned} I &= R \cdot P \\ P &= \frac{|A|^2}{2} \\ E(t) &= A(t)e^{j(\omega t+\phi)} \end{aligned} \tag{4.20}$$

where P is the time-varying signal power which is related to the amplitude $(A(t))$ of incident light field $(E(t))$ and R is the responsivity of the photodiode which is given in equation 4.21.

$$R = \eta \frac{e}{h\nu} \tag{4.21}$$

$h\nu$ is the photon energy, η is the quantum efficiency, and e is the electron charge. The electrical current generated by the photodiode can be detected by a simple detection circuit to convert it to data bits. The phase information carried in the optical signal is lost when applied to a conventional square-law detector. The direct-detection based receiver is illustrated in Fig. 4.21 and is

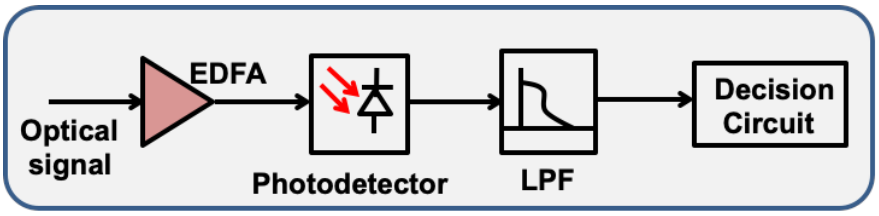


Figure 4.21: Direct detection of an optical signal.

used for all investigations presented in this thesis for NRZ-OOK direct-detection scheme. It consists of an optical pre-amplifier followed by a semiconductor photodetector (PIN-diode in our case) and an electrical filter. The optical signal is received by a photodetector which converts optical signal to an electrical signal. The converted signal is then passed through low pass filter (LPF) that rejects out of band noise. The filtered signal is fed to the data-recovery section consists of a decision circuit and a clock-recovery circuit. The clock-recovery circuit provides information about the bit slot to the decision circuit and helps to synchronise the decision process. The decision circuit compares the output from the linear channel to a threshold level, at sampling times determined by the clock-recovery circuit, and decides if the signal corresponds to bit "1" or a bit "0".

4.4.2 Coherent Detection

When a phase-modulated optical signal is applied to a conventional square law detector, the phase information is lost. A receiver that can detect both the amplitude and phase of the received signal is required to detect the phase-modulated signals. Coherent detection allows access to both amplitude and phase components of the transmitted optical field and enables the use of high spectral efficient modulation formats. The fundamental concept behind coherent detection is that the beating product of electric fields of the modulated signal light and the local oscillator (LO) that can be processed electrically. To detect both IQ components of the signal, optoelectronic components such as 90 % hybrid mixer and two pairs photodetectors are required. A hybrid is a 2x2 optical coupler with its property of a 90° phase shift between its direct-pass and cross-coupling outputs. By combining such optical couplers into the configuration shown in Fig. 4.22, together with an additional 90° phase shift in one arm a detection of real and imaginary parts of in-phase (I) and quadrature signals (Q) can be achieved. The expressions for

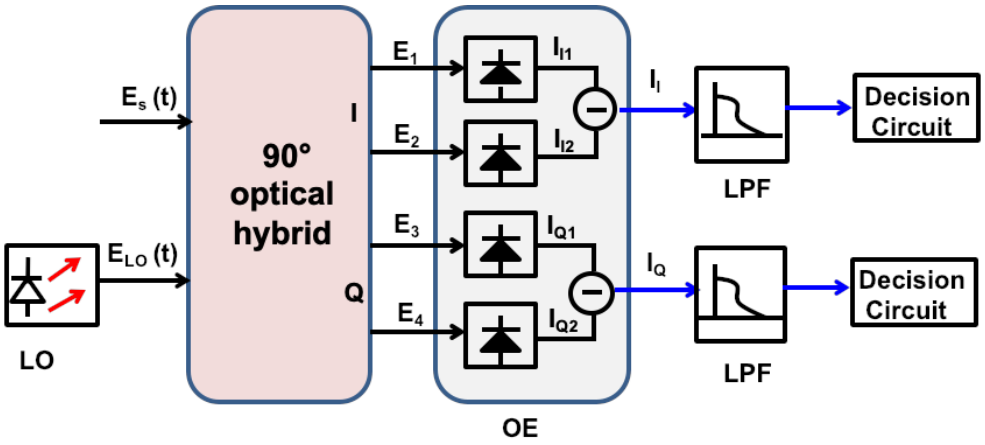


Figure 4.22: Configuration of Phase-diversity Coherent Receiver.

the input fields are given in equation 4.22 below (Ip et al. 2008).

$$\begin{aligned} E_1 &= \tfrac{1}{2}\left(E_s + E_{LO}\right), \quad E_2 = \tfrac{1}{2}\left(E_s - E_{LO}\right) \\ E_3 &= \tfrac{1}{2}\left(E_s + jE_{LO}\right), \quad E_4 = \tfrac{1}{2}\left(E_s - jE_{LO}\right) \end{aligned} \tag{4.22}$$

The output photocurrent from balanced photodetectors is presented in equation 4.23.

$$\begin{aligned} I_I(t) &= I_1(t) - I_2(t) = R\sqrt{P_s P_{LO}}\cos\left\{\varphi_s(t) - \theta_{LO}(t)\right\} \\ I_Q(t) &= I_3(t) - I_4(t) = R\sqrt{P_s P_{LO}}\sin\left\{\varphi_s(t) - \theta_{LO}(t)\right\} \end{aligned} \tag{4.23}$$

where $R$is the responsivity of the photodiode, P_s andP_{LO} are the power of the optical fields for incoming and LO signal respectively. The receiver thus leads to the recovery of both the sine and cosine components. It is possible to estimate the phase noise varying with time and restore the phase information through subsequent DSP. This coherent receiver is used in Chapter 5 for the detection of QPSK and 16-QAM Nyquist-WDM superchannels.

Summary

In this chapter, all-optical generation and detection of the Nyquist-WDM system are discussed. The comb generation is first explained, and simulation results of a five-tone optical frequency comb are presented. A detailed description of the demultiplexing of the optical frequency comb with all-optical FFT de-multiplexer is described, and simulation results are presented to describe the impact of the phase monitoring on the superchannel-transmitters. From the simulations results, it is found that phase monitoring is a crucial part of the Nyquist-WDM transmitter, and for the optimum system performance, the proper phase has to be preserved before modulation. The extensive description of individual modulation of subcarriers using an MZM device is discussed. It can be seen using MZM, different modulation formats like NRZ-OOK, QPSK and 16-QAM are generated. The optical spectra of NRZ-OOK, QPSK and 16-QAM, are compared for most spectral efficient modulation format. The detection techniques such a direct and coherent detection are described with their merits and demerits.

Chapter 5

Enabling Nyquist-WDM Transmission with Adaptive Spectral Shaping

In this chapter, the implementation of Nyquist-WDM superchannel based on different modulation format like (NRZ-OOK, QPSK and 16-QAM) at different data rates of 10 Gb/s and 28 Gb/s with our proposed, a low-complexity spectral shaping technique is considered. We investigate the impact of narrow-band spectral shaping at the transmitter side and also evaluate the performance originating from effective channel bandwidth reduction.

5.1 NRZ-OOK based Nyquist-WDM Superchannel

Optical communication systems have been long employing primarily conventional on-off keying (OOK) signals, which convey the information in the amplitude in non-return-to-zero (NRZ) format. The main reason for using NRZ-OOK modulation is its simplicity of implementation. A five-channel NRZ-OOK based superchannel system is simulated in VPI version 9.2. as shown in Fig. 5.1. The first stage of Nyquist-WDM system is the generation of equally spaced subcarriers at a frequency equal to the symbol rate by using a comb generator. A CW laser with a linewidth of 100 kHz and emission frequency of 193.1 THz is used as source for comb generator. A linewidth of 100 kHz can support higher order modulation formats up to 64 QAM at 10 Gbaud (Pfau et al. 2009). Five coherent optical subcarriers with equal

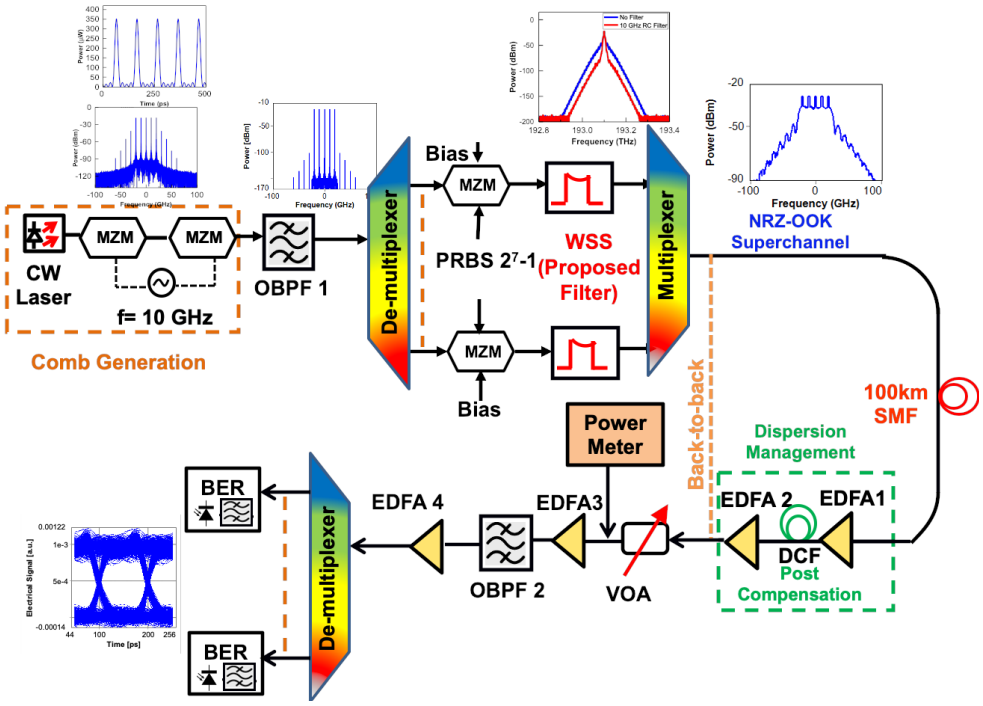


Figure 5.1: Schematic of NRZ-OOK based Nyquist-WDM system.

intensities and phases are generated using two cascaded $LiNbO_3$-based MZM driven by sinusoidal signals with a frequency of 10 GHz. The flatness of OFC is 0.12 dB, and the SMSR is 23.5 dB. The five-tone OFC is de-multiplexed into individual optical subcarriers with the help of four cascaded MZDIs. The first MZI has separated the comb into odd (three) and even (two) lines by using a half bit delay in one of the MZI arms. Then, two even comb lines are further separated by applying 1/4 bit delay and an additional phase shift of $90°$. The other two MZIs are used to separate odd lines using 1/4 bit delay and 1/8 bit delay in each of their respective arms with SMSR of more than 60 dB. The whole process of de-multiplexing is explained in Fig. 4.6 in Chapter 4. Each comb line is modulated independently by different seeds PRBS data sequences of $2^7 - 1$ length at 10 Gb/s by biasing the MZM in linear regime with an amplitude of V_π. The data sequence of $2^7 - 1$ is chosen to save the simulation time. After this, each modulated subcarrier is spectrally shaped by our proposed optical filter, followed by passive multiplexing to form the superchannel. The superchannel signal is then amplified by EDFA 1 and EDFA 2 to compensate for the realistic losses incorporated throughout the transmitter. At the receiver side, the superchannel is de-multiplexed in a similar way as before with the aid of MZI, before being detected by individual PIN photodetectors per subcarrier with a responsivity of 0.8 A/W. The

Table 5.1: Parameters for NRZ-OOK based superchannel.

Parameters	**Value**	**Unit**
Emission Frequency	193.1	THz
Noise Figure	4	dB
Bit Rate	10	Gb/s
Channel Spacing	10	GHz
EDFA 1-gain	10	dB
Output Power of EDFA 1	0	dBm
EDFA 2- gain	10	dB
Output Power of EDFA 2	0	dBm
EDFA 3-gain	20	dB
Output Power of EDFA 3	10	dBm
EDFA 4- gain	20	dB
Output Power of EDFA 4	4.8	dBm
Thermal Noise	10^{-12}	A/$\sqrt{Hz}$
Responsivity	0.8	A/W

bandwidth of photodetector is determined by the bandwidth of the electrical lowpass filter (LPF) in VPI software. The bandwidth of LPF is 50 GHz for 10 Gb/s and 75 GHz for 28 Gb/s scenario and has a Bessel transfer function of order 5. The parameters which are considered to evaluate the performance of the simulated system are mentioned in Table. 5.1. The performance of the optical spectral shaping is evaluated in terms of the BER and received power sensitivity. The RC filter is chosen because it has a rectangular spectrum in the frequency domain and has a sinc-shape pulse in the time domain which is the main requirement for Nyquist -WDM system. In this work, two different RC optical filters are considered and are benchmarked against the scenario where no spectral shaping is applied.

5.1.1 Performance Evaluation at 10 Gb/s

In this section, the impact of narrow-band spectral shaping at the transmitter side over system performances is evaluated. The desired spectral shaping can be achieved by optical filtering of the optical signal after modulation by Mach-Zehnder modulator. Normally, a spectral filter would contain the full bandwidth of a modulated signal, which can be roughly estimated to be at least twice the frequency of the modulation (Dorf 2006). So for a 10 Gb/s NRZ-OOK system, one would expect a -3 dB optical fibre bandwidth around 20 GHz to avoid errors or penalties.

Hence, the analysis of a signal under different optical filter constraints, in order to study the penalty associated with narrow filters is presented. The RC filter has been simulated with different values for -3 dB bandwidth (B_{FWHM}) ranging from 10 GHz to 60 GHz. The filter bandwidth (B_{FWHM}) is normalized by the resolution of the WSS (r), which is 10 GHz in our case. The value of the (B_{FWHM}) is an integer in our case, however, non -integer values will also have similar behaviour. Considering, the performance of the system with spectral shaping using the RC filter, the impact of different B_{FWHM}/r of filters on each of the subcarrier with small channel spacing of 10 GHz is discussed here. In the first case, the performance is assessed without any spectral shaping in back-to-back (B2B) transmission scenario. The back-to-back transmission means that the length of optical fibre is 0 km. The performance is analyzed in terms of bit error rate (BER). The BER is calculated by keeping the noise power constant and the varying the optical power using variable optical attenuator (VOA). The more details of BER estimation is explained in section A of Appendix A. Fig. 5.2 shows the performance of the centre (Ch3), inner (Ch2/Ch4), and outer subcarriers (Ch1/Ch5). In theory, to achieve BER of

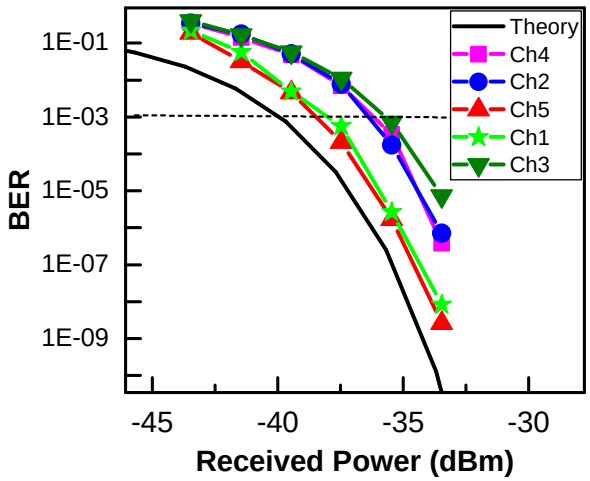
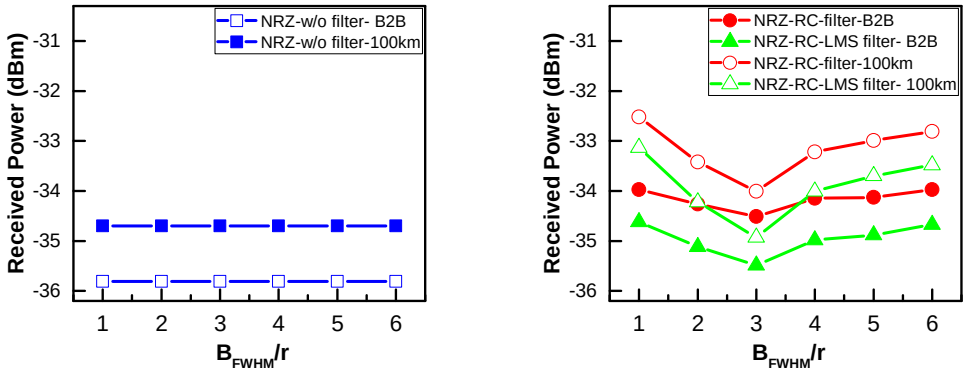


Figure 5.2: Five Channel NRZ-OOK system performance in the absence of spectral shaping.

10^{-3}, the optical power required by five-channel NRZ-OOK system is -39.95 dBm. The details of how the theoretical value is calculated are detailed in section 2.8.3 in Chapter 2. The optical power received by Ch5 and Ch1 is -38.54 dBm and -37.98 dBm respectively. These two outer channels have only one inner neighbour; therefore, they outperform the other channels in terms of received power sensitivity. There is a 1.41 dB power penalty between

theoretical value and simulated channel Ch5 (best performance) without any filtering. This discrepancy between theory and simulated results is due to crosstalk from neighbouring channels and independent de-multiplexing and modulation of each channel. Ch4/Ch2 has two inner neighbours; hence, they need more power (-37. 98 dBm and -36.39 dBm respectively) than outer channels to achieve the same BER. Ch3 has the worst performance (-35.81 dBm) as it is more affected by the interference of the adjacent subcarriers carrying different data. Therefore Ch3 has incurred an additional 2.73 dB power penalty as compared to best performance channel (Ch5). For further



(a) (b)

Figure 5.3: Received power at BER of 10^{-3} for Ch3: (a) without shaping and (b) after shaping with an RC filter and RC-LMS filter of different bandwidth.

performance analysis, the worst channel Ch3 is considered. Ch3 is shaped with an RC filter of 10 GHz, which is equal to channel spacing. The performance of Ch3 is compared without any filter and with a typical RC filter required for Nyquist-WDM. When Ch3 is shaped with the RC filter, which has B_{FWHM}/r=1, which is equal to symbol rate, the received optical power is -33.87 dBm as shown in Fig. 5.3(b). Due to this narrow-band filtering, the bandwidth of the channel has reduced, resulting in signal spectrum being clipped in the frequency domain, leading to ISI in the time domain and inducing a power penalty of 1.94 dB in comparison to the back-to-back case. For B_{FWHM}/r=2, the received power required for the same target BER is -34.26 dBm. There is an improvement of 0.39 dB in receiver sensitivity than the previous case. Nevertheless, ISI is still dominant. The best received power of -34.51 dBm is obtained when the signal is shaped with an optical filter having B_{FWHM}/r equal to three times of symbol rate. At this point, the contributions of ISI is minimized and therefore, the penalty is reduced to 1.30 dB as compared to 1.94 dB. It can be seen from the Fig. 5.4 that the received

eye diagram for Ch3 without any filtering is open with less distortions. The

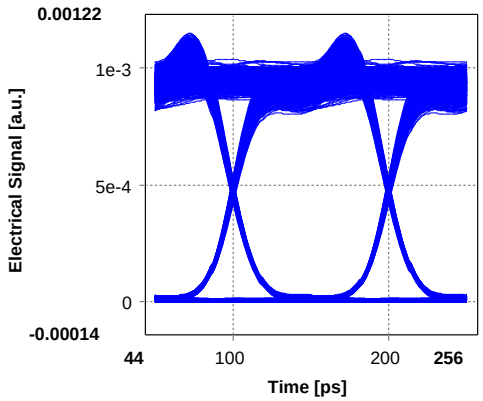
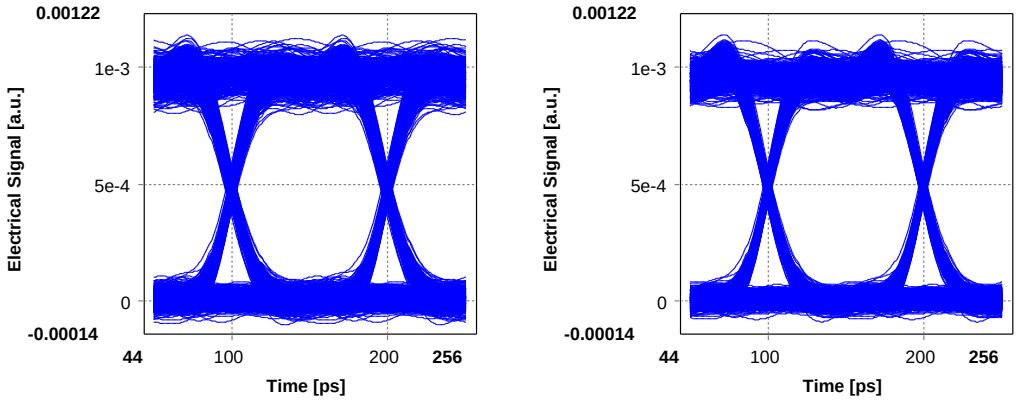


Figure 5.4: Received eye diagram of the Ch3 without filtering after back to back transmission at 10 Gb/s.

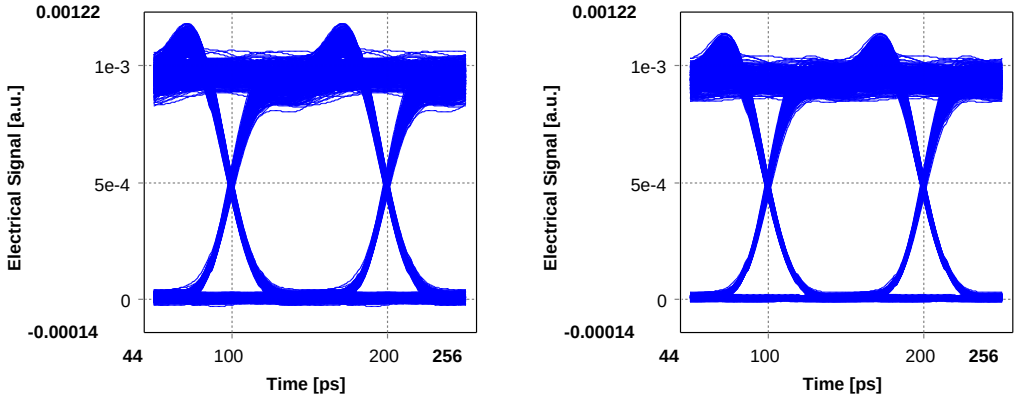
unit of eye diagram on the y-axis is "amplitude units" (a.u.) which are acceptable in optical communication and has been already used by different researchers. The eye diagram represents a qualitative analysis, unlike BER, which gives quantitative measure. More details on the comparison of BER and eye diagrams have been presented in subsection 2.8.4 in Chapter 2.

After filtering the Ch3 with RC filter of $B_{FWHM}/r = 1$, there is a significant amount of noise which mark a reduction in the size of the eye-opening as seen in Fig. 5.5(a). As the filter B_{FWHM}/r is increased to 3, the improvement in eye-opening is evident. The received power is again reduced to -34.15 dBm when the B_{FWHM}/r is increased from 3 to 4. This means the filter bandwidth is wider, hence introducing ICI. Further increasing the B_{FWHM}/r to 5 and 6, the contribution of interchannel crosstalk has increased further. This results in a further reduction in optical received power. From this analysis, one can observe that when the signal is narrowly filtered, the induced power penalties increase due to ISI. On the other hand, the choice of larger filter bandwidth reduces the induced ISI, but the increase in spectral occupancy of each subcarrier results in stronger interchannel crosstalk. This results in imposing the use of larger interchannel spacing (thus reducing the spectral efficiency). Therefore, it is crucial to choose the optimum filter bandwidth at which there is a fair trade between ISI and ICI. For our system, the optimum filter bandwidth (B_{FWHM}/r) is 3, where the impact of power penalties is minimum.



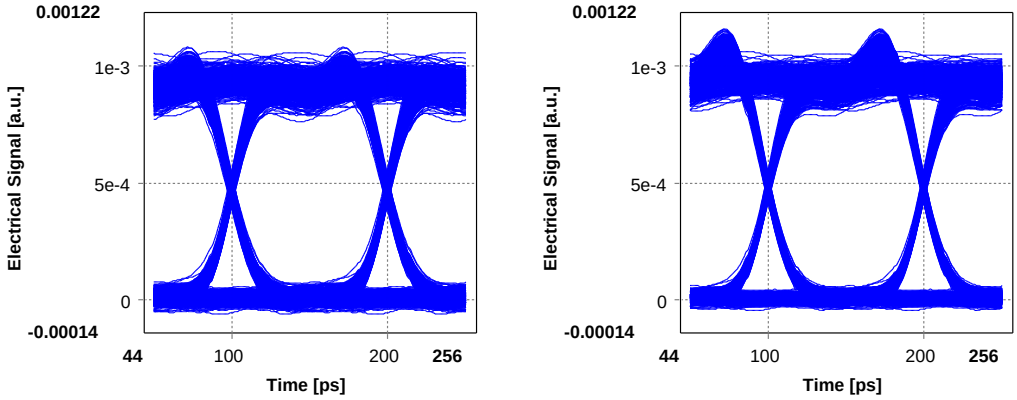
(a) RC filter = 1

(b) RC-LMS filter = 1



(c) RC filter = 3

(d) RC-LMS filter = 3



(e) RC filter = 6

(f) RC-LMS filter = 6

Figure 5.5: Received eye diagram of the Ch3 after shaping with an RC filter and RC-LMS filter of different B_{FWHM}/r after back-to-back transmission at 10 Gb/s.

5.1.2 Optical Adaptive Spectral Shaping

In Nyquist-WDM, the goal is to place the optical subcarriers as close as possible to the symbol rate either by minimizing the interchannel crosstalk through the formation of the rectangular spectrum shape of each channel either by electrical filtering or optical filtering. Electrical filtering can be achieved by shaping the modulator driving signals through analogue filters or DSP employing high-speed DACs at the transmitter side. Although this method can provide a good roll-off factor, the speed of the DAC restricts the symbol rate. Alternately, optical pulse shaping methods like programmable optical filter such as WSS can help to reduce the complexity of the current state-of-the-art. However, the current generations WSS has a limited resolution of $\sim$10 GHz, so it is impossible to obtain spectra with zero roll-off. Hence, a novel and simple solution to reduce the roll-off factor by optimizing the input response of WSS for best filter performance in a "set-and-forget" scenario is proposed. This method is feedback-based optimization known as LMS algorithm. LMS algorithm serves the purpose to reduce the MSE between the desired filter shape and the measured WSS filter shape output. The working principle of LMS is discussed in detail in Chapter 3. The process is repeated until the MSE is minimized and a new output has a more accurate representation of the desired filter profile. Fig. 5.6(a) shows the optical spectrum of Ch3 without shaping, after shaping with a typical RC filter and our proposed RC-LMS filter. It can be seen that, with the implementation of RC-LMS, the roll-off factor is improved. As per section 5.1.1, the initial power penalty for a simple RC filter

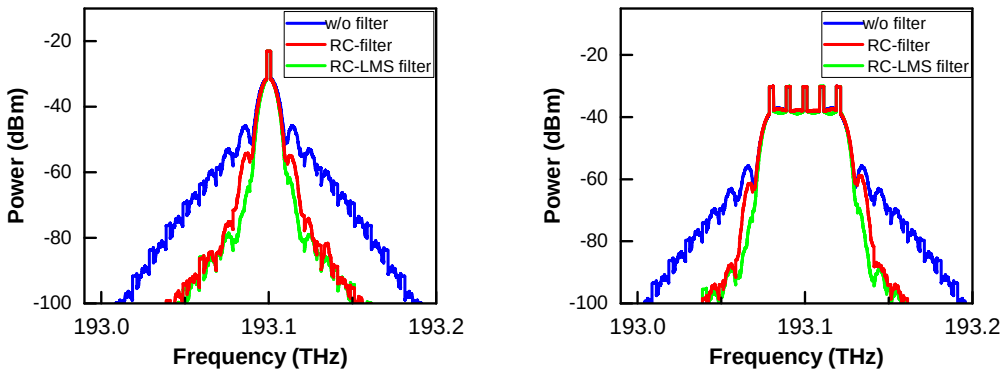
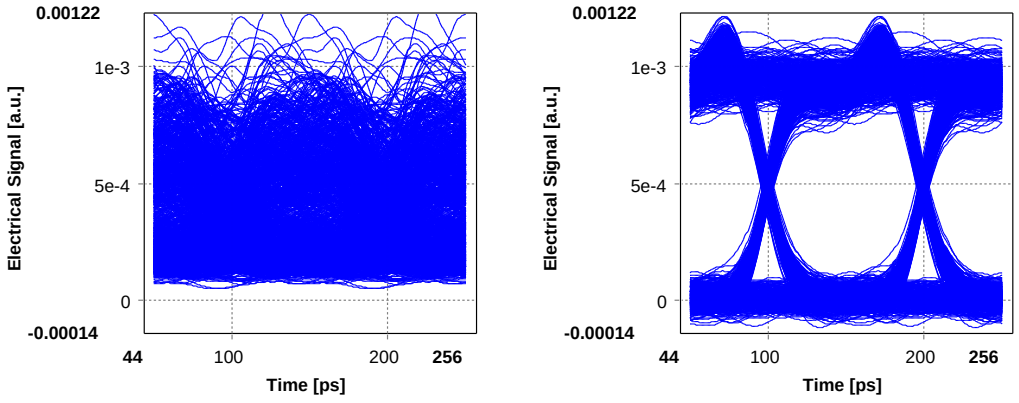


Figure 5.6: Optical Spectrum of: (a) Ch3 and (b) NRZ-OOK superchannel before and after spectral shaping with RC filter of B_{FWHM}/r=1 at 10 Gb/s.

with B_{FWHM}/r= 1 is 1.94 dB when compared to back-to-back performance.

When using our proposed LMS optimized RC filter, the power penalty is reduced to 1.19 dB, with ∼0.75 dB improvement in received power. When the B_{FWHM}/r increases from 1 to 3, the improvement in received power sensitivity also increases from 0.75 to 0.98 dB. As $B_{FWHM}/r = 4$, the improvement in received sensitivity is no longer significant due to an increase in crosstalk. It is reduced from 0.98 to 0.83 dB. Similarly, for the B_{FWHM}/r= 5 and 6, the improvement is roughly 0.75 dB and 0.70 dB. Here, it can be noted that B_{FWHM}/r= 3, the improvement is biggest and thus reducing the induced filtering penalty to just 0.32 dB, which is minimal given the benefits associated with adding the optical spectral shaping.

The performance of the superchannel is also analyzed after 100 km transmission over single-mode fibre (SMF), in order to figure out if the shaping is still practical and necessary. In long-distance transmission, chromatic dispersion directly affects the quality of the data transmission and causes a blurring of the bitstream. The value of dispersion in regular fibre is around 17 ps/nm at 1550 nm. Over the distance of 100 km, the value of the



(a) (b)

Figure 5.7: Eye diagram of the Ch3: (a) without and (b) with dispersion compensation after 100 km transmission.

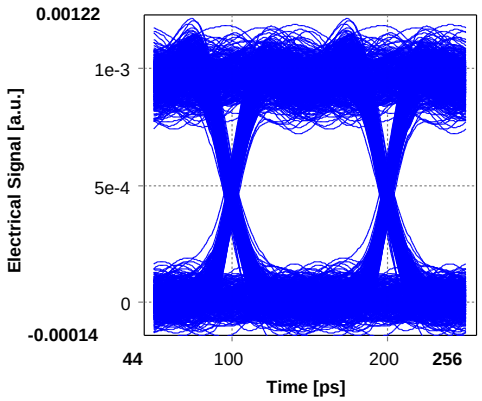
dispersion is calculated as Dispersion×Length = 17 ps/(nm×km)×100 km = 1700 ps/nm. The maximum allowable accumulated chromatic dispersion at 10 Gb/s provided by ITU standards is 800 to 1000 ps/(nm×km) (Kaushik 2002). Therefore, dispersion management is a vital part of designing a fibre optic transmission system. To properly manage this, the dispersion compensation management (DCM) is built using a special type of dispersion compensating fibre inside the module that has a negative value of dispersion coefficient, ranging from -32 ps/(nm×km) to -300 ps/(nm×km). Fig. 5.7 shows the eye

diagram of Ch3 with and without dispersion compensation. It is clear from eye diagram that the output signals overlap due to ISI caused by the broadening of pulses due to dispersion. Due to this overlapping of the pulses, the output becomes undetectable. On the other hand, with the use of DCM, an impressive improvement in the performance is evident. The eye is more open and free of distortions.

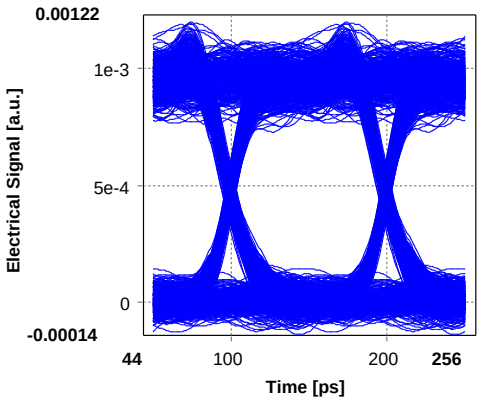
After 100 km transmission, it is observed that the received power for Ch3 without any spectral shaping is -34.7 dBm. Comparing this with the B2B scenario, there is a power penalty of around 1.11 dB due to a noise figure of additional EDFAs in DCM modules. After 100 km transmission when the signal is shaped with an RC filter of B_{FWHM}/r= 1, the observed power penalty is 2.22 dB. The induced penalty of 2.84 dB is reduced to 1.57 dB with our proposed RC-LMS filter. So there is 0.61 dB improvement. For the B_{FWHM}/r = 2, the improvement is 0.80 dB. Following a similar trend like B2B scenario, the system performance is best at B_{FWHM}/r = 3, with the addition of 0.92 dB in received power. A clear and distortion-free eye is seen in Fig. 5.8(d). With the further increase in B_{FWHM}/r from 4 to 6, the received power is enhanced by 0.79 dB, 0.71 dB and 0.67 dB respectively by our RC-LMS filter as compared to typical RC filter. From the results, it can be estimated that the filter induced penalty is negligible for B_{FWHM}/r= 3, hence a judicious choice for filtering.

5.1.3 Performance Evaluation at 28 Gb/s

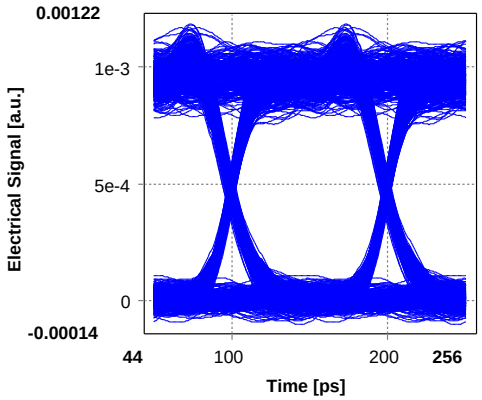
The demand for higher bandwidth is growing fast; therefore, the service providers are moving from 10 Gb/s to higher data rates. In this section, the impact of transmitter-side optical filtering on the performance of Nyquist-WDM at 28 Gb/s is evaluated for testing the practicality of shaping at higher data rates. The performance is evaluated in terms of required received optical power to achieve the target of BER of 10^{-3} under the scenario of B2B and 100 km transmission. The channel spacing of 10 GHz is too narrow for data rate of 28 Gb/s. Therefore, the channel spacing of 28 GHz is considered. The received optical power for Ch3 without any spectral shaping is -32.71 dBm in back-to-back scenario. When Ch3 is shaped with the RC filter which has B_{FWHM}/r=1, the received optical power is -31.22 dBm as shown in Fig. 5.9(b). In this case, a large portion of the signal spectrum is clipped as the signal bandwidth is quite larger than the filter bandwidth. At this narrow bandwidth region, the crosstalk due to ISI is strongly present, inducing a



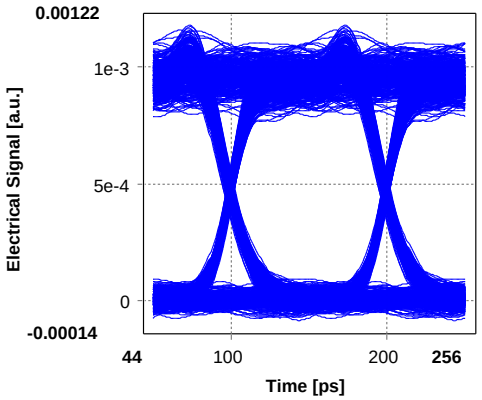
(a) RC filter = 1



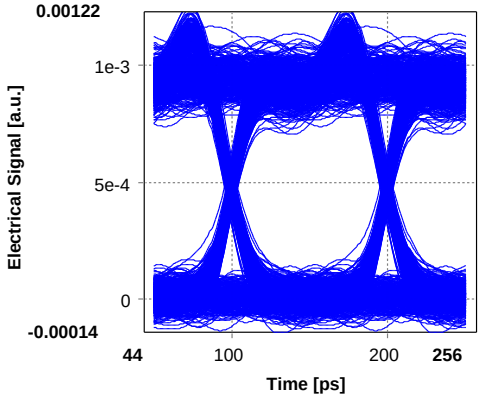
(b) RC-LMS filter = 1



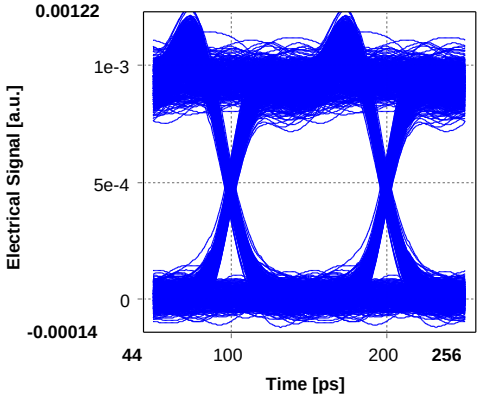
(c) RC filter = 3



(d) RC-LMS filter = 3

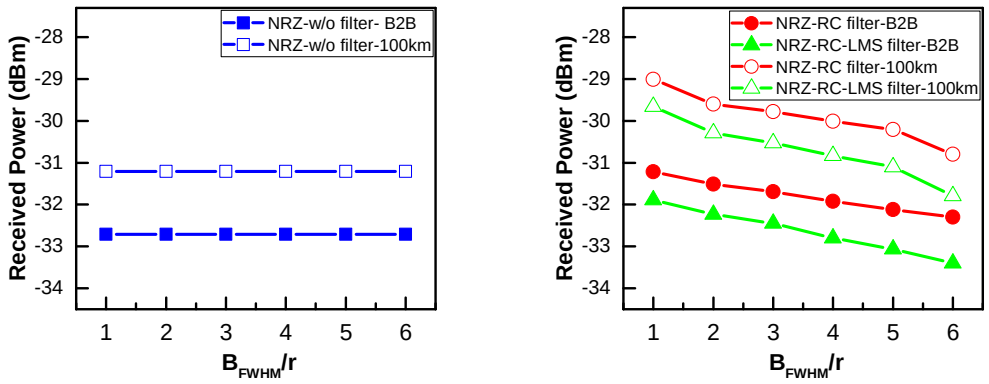


(e) RC filter = 6



(f) RC-LMS filter = 6

Figure 5.8: Received eye diagram of the Ch3 after shaping with an RC filter and RC-LMS filter of different B_{FWHM}/r after 100 km.

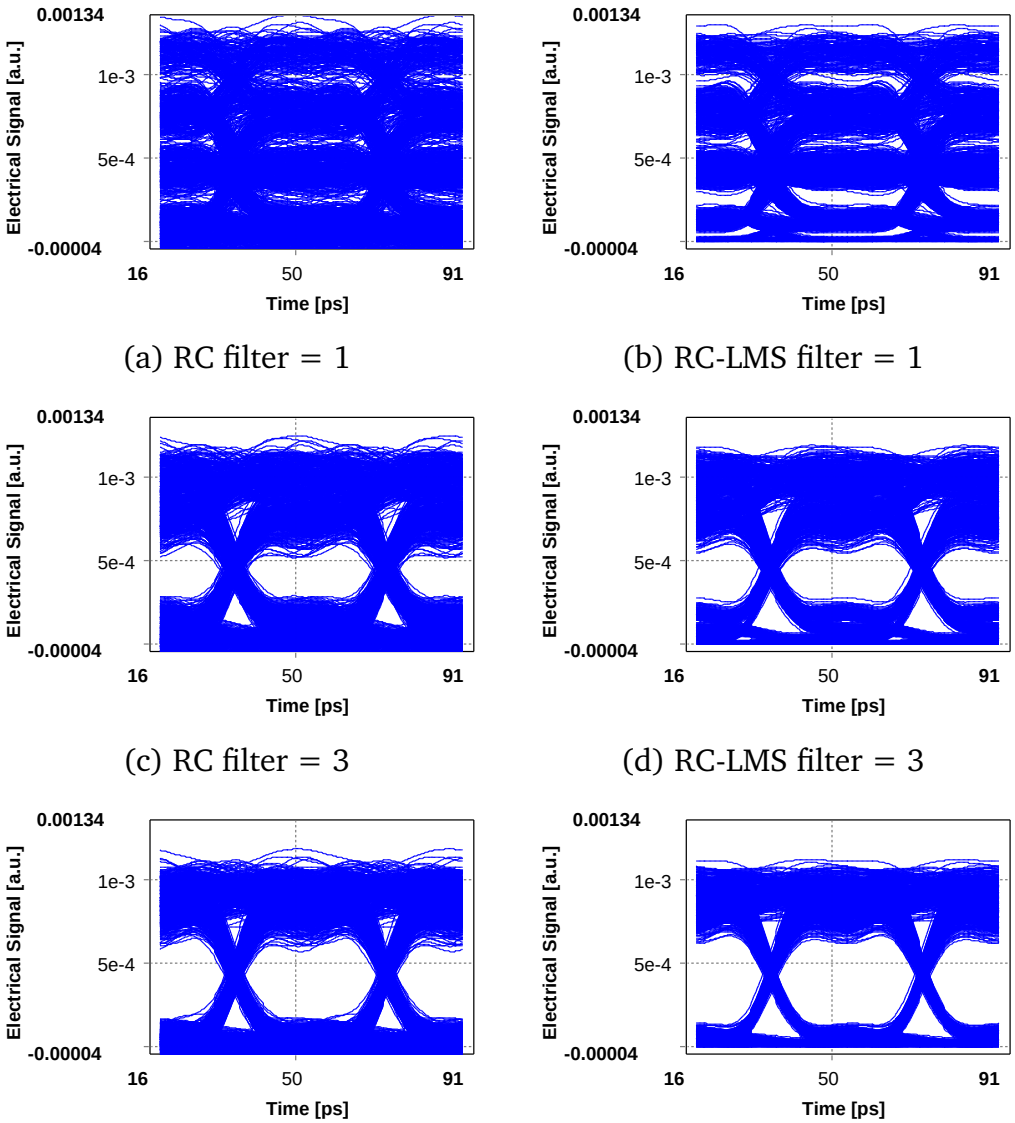


(a) (b)

Figure 5.9: Received power at BER of 10^{-3} for Ch3: (a) without shaping and (b) after shaping with a RC filter and RC-LMS filter of different bandwidth.

power penalty of 1.49 dB in comparison to back-to-back case. The eye of Ch3 is distorted and closed as most of the information of the channel is cut due to extensive shaping as seen in Fig. 5.10 (a). For B_{FWHM}/r=2, the received power required for the same target BER is -31.51 dBm. There is an improvement of 0.29 dB in receiver sensitivity than the previous case. As the filter B_{FWHM}/r is increased to 3, the improvement in eye opening is evident. Further increasing the B_{FWHM}/r to 3 and 6, the contribution of ISI is reduced and the best received power of -32.81 dBm is achieved at 6, which is also seen from Fig. 5.10 (e).

A similar trend is also followed when the performance is evaluated after 100 km transmission. When B_{FWHM}/r=1, the impact of ISI has become more severe at a high data rate, thereby degrading the system performance significantly. Even after increasing the B_{FWHM}/r to 3, the filter bandwidth is around 1.07$\times$ Δf (channel spacing), which is still not enough for the optimum performance. However, from the eye diagram, the improvement is apparent from the previous case. As the B_{FWHM}/r is moved to 6, the filter bandwidth is now almost 2$\times\Delta f$, results in the opening of the eye and hence improvement in system performance is quite visible from the eye diagram in Fig. 5.11(e). The system performance is further assessed with the implementation of our proposed RC-LMS filter. The proposed method adds improvement of 0.67 dB and 0.65 dB for B2B and 100 km transmission for B_{FWHM}/r= 1. Following the improvement trend, the gain of 0.72 dB and 0.76 dB add up for the B_{FWHM}/r= 2 and 3 for B2B scenario. The highest improvement of 1.1 dB and 0.99 dB is noted when the filter bandwidth is



(a) RC filter = 1

(b) RC-LMS filter = 1

(c) RC filter = 3

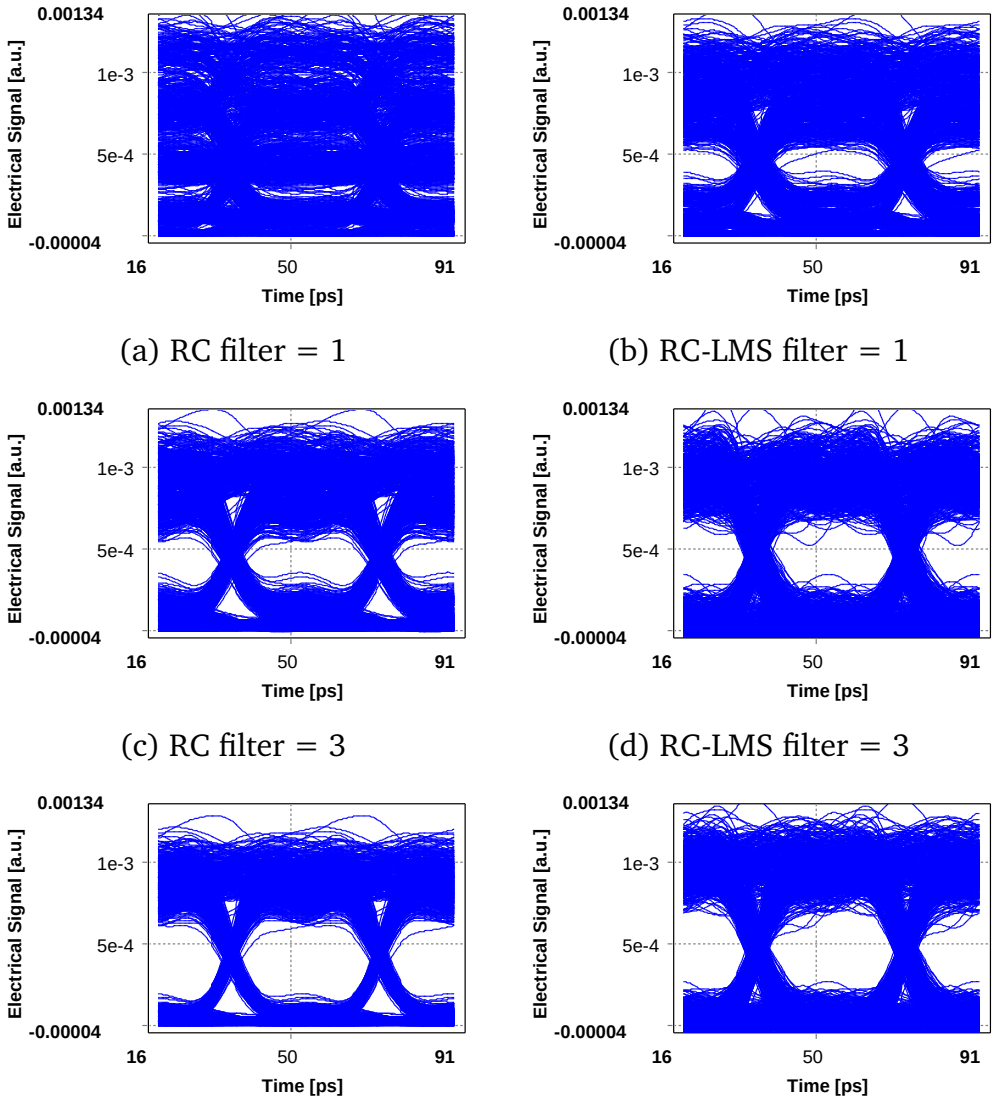
(d) RC-LMS filter = 3

(e) RC filter = 6

(f) RC-LMS filter = 6

Figure 5.10: Received eye diagram of the Ch3 after shaping with a RC filter and RC-LMS filter of different B_{FWHM}/r after back-to-back transmission at 28 Gb/s.

twice of the channel spacing, i.e. B_{FWHM}/r= 6 for both back-to-back and 100 km transmission. Moreover, from Fig. 5.9(b), it can be seen that at B_{FWHM}= 6, with our proposed RC-LMS filter, there is no filter induced penalty; instead, the received power is even better than no spectral shaping scenario.



(a) RC filter = 1

(b) RC-LMS filter = 1

(c) RC filter = 3

(d) RC-LMS filter = 3

(e) RC filter = 6

(f) RC-LMS filter = 6

Figure 5.11: Received eye diagram of the Ch3 after shaping with an RC filter and RC-LMS filter of different B_{FWHM}/r after 100 km at 28 Gb/s.

5.2 QPSK based Nyquist-WDM Superchannel

A move away from OOK to more complex modulation schemes, such as quadrature phase-shift keying (QPSK), is necessary for high-speed transmission to increase the spectral efficiency and capacity further. Dual-polarisation QPSK, for example, is the standardized modulation format for 100G transceivers, based on a 32 Gbaud (Gringeri et al. 2012). QPSK modulated signals use four possible positions in the constellation diagram. The four constellation points differ in phase by $\frac{\pi}{2}$, and the amplitude remains constant. Each phase state now encodes two bits. The symbol rate is therefore

halved, so the bandwidth requirement is reduced to half.

5.2.1 Schematic setup for QPSK Superchannel

A schematic of the 5-channel 10 Gb/s QPSK superchannel transmission system is illustrated in Fig. 5.12. The output of a CW laser with a linewidth of 100 kHz is passed through an OCG that consist of two cascaded MZM both over-driven with an amplified sinusoidal wave frequency of 10 GHz. OCG

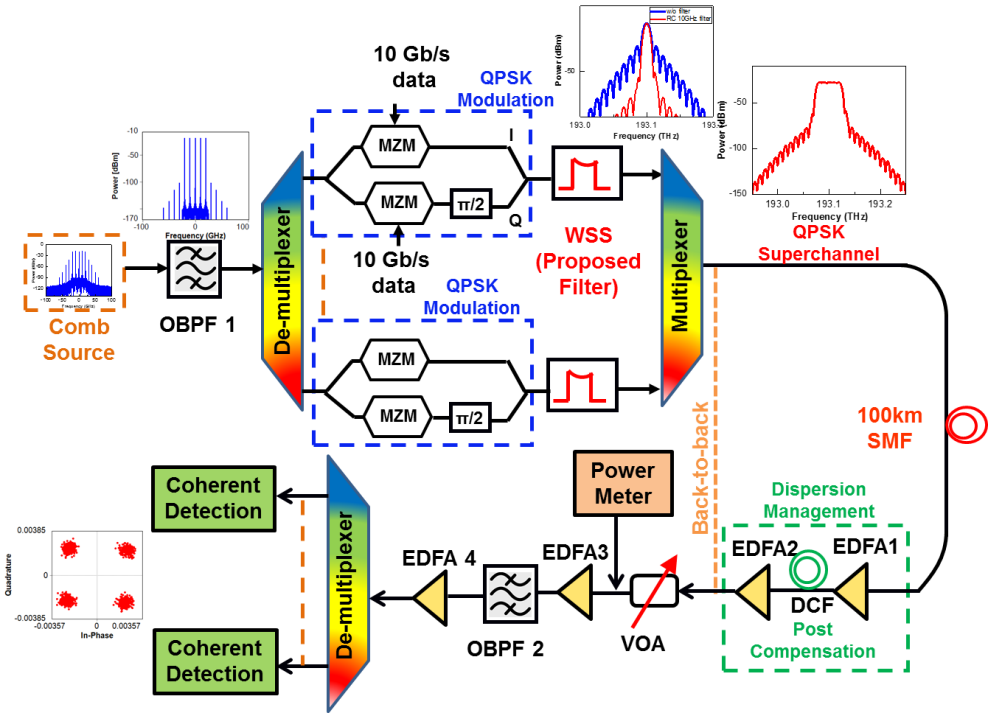


Figure 5.12: Schematic of QPSK based Nyquist-WDM system

generates a five-tone, evenly spaced, frequency-locked comb, with the channel spacing of 10 GHz. The comb is de-multiplexed into individual optical subcarriers with the help of four cascaded MZDIs. Each comb line is modulated independently by using QPSK modulation. QPSK modulator is composed of parallel MZMs arranged within a Mach-Zehnder super-structure. Each of the MZMs is biased at a minimum DC transmission point and driven with an electrical signal with an amplitude of $2V_\pi$. Quadrature phase control is required to maintain an optical phase difference of $\frac{\pi}{2}$ between upper and lower branches to generate I (in-phase) and Q (quadrature) components of the QPSK signal. The optical combiner receives I and Q components and ensures quadrature addition of the optical fields on recombination.

Each QPSK modulated subcarrier is then shaped with our proposed filter for

pre-spectral shaping, followed by passive multiplexing to form the superchannel. The superchannel signal is transmitted over SMF having a span of 100 km with a dispersion management system and then preamplified by two EDFAs to compensate for the realistic losses incorporated throughout the transmission system. At the receiver side, the superchannel is de-multiplexed in a similar way as before with the aid of MZI, before being detected. An individual coherent receiver detects each subcarrier with a local oscillator tuned to the central frequency (193.1 THz) of each detected channel. The photodetectors in the balanced detectors are PIN diodes with a responsivity of 0.8 A/W and thermal noise equal to $10^{-12}\ A/\sqrt{Hz}$. The bandwidth of photodetector is considered as 50 GHz for 10 Gb/s and 75 GHz for 28 Gb/s scenario and has a Bessel transfer function of order 5. The logical channels are used to obtain the bit sequence sent by the transmitter for BER estimation.

5.2.2 Performance Evaluation at 10 Gb/s

The pre-shaping performance is evaluated in the tightly spaced superchannel where the centre channel (Ch3) is chosen for investigation. In theory, to

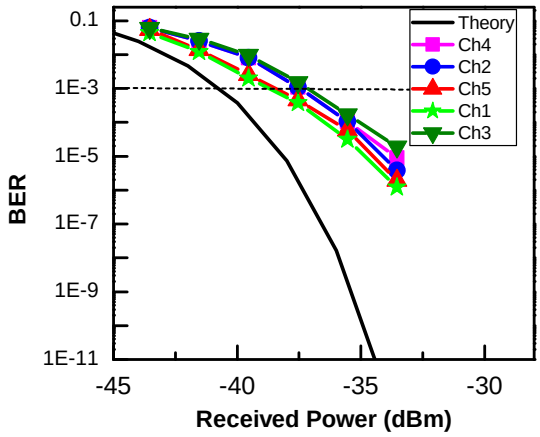
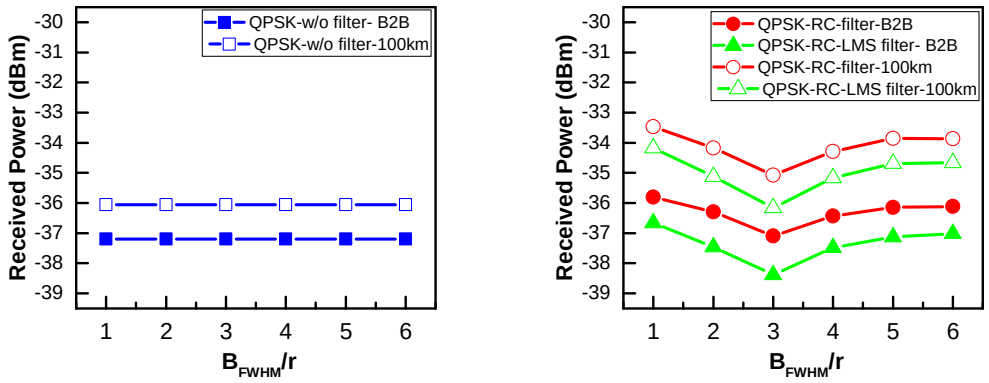


Figure 5.13: Five Channel QPSK system performance in the absence of spectral shaping.

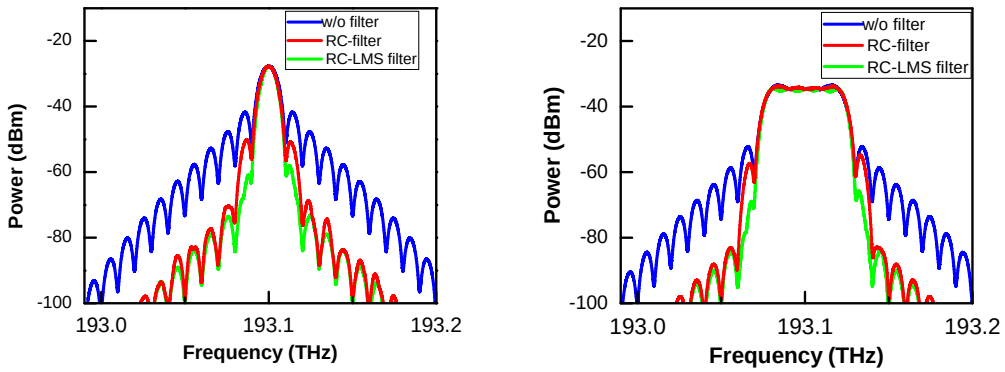
achieve the BER of 10^{-3}, the required optical received is -41 dBm for five channel system as seen in Fig. 5.13. The first step of the analysis is to study the impact of the different B_{FWHM}/r filter on the system performance under the scenario of back-to-back transmission. The received power sensitivity for Ch3 is -37.2 dBm without any spectral shaping. When the Ch3 is shaped with a typical RC filter of B_{FWHM}/r= 1, a significant portion of signal is filtered out

incurring a power penalty of 1.39 dB as seen in Fig. 5.14(b). It can seen from Fig 5.15, that the spectral shaping has limited the bandwidth occupied by the



(a) (b)

Figure 5.14: Received power at BER of 10^{-3} for Ch3: (a) without shaping and (b) after shaping with a RC filter and RC-LMS filter of different bandwidth for QPSK-Nyquist-WDM superchannel at 10 Gb/s.



(a) Ch3 (b) QPSK superchannel

Figure 5.15: Optical spectrum before and after spectral shaping with RC filter having B_{FWHM}/r=1 at 10 Gb/s.

transmitted signal as compared with no shaping case. After shaping with our proposed RC-LMS filter, the optical spectra of Ch3 and QPSK superchannel become closer to the desired rectangular spectrum. There is an improvement of 0.85 dB in received power with our proposed filter. Fig 5.16 shows the constellation diagram for Ch3 before shaping, and a clear constellation is observed. This narrow optical filtering, smears the transmitted signal in time, causing the symbol to spread to adjacent symbols, thus introducing ISI as seen in Fig. 5.17(a). With the introduction of ISI, there is little spread and displacement in the constellation points when the signal is shaped with

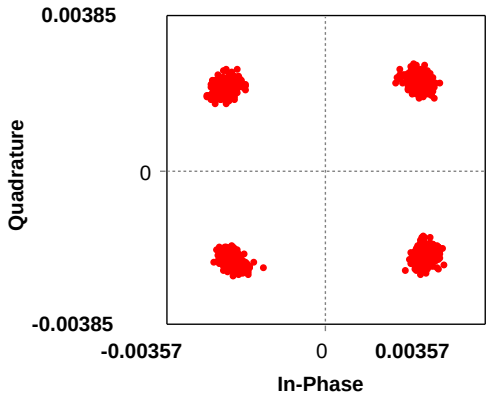
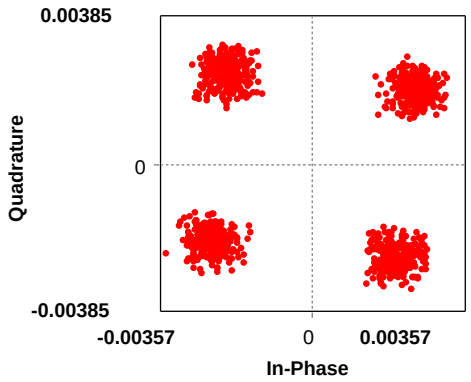


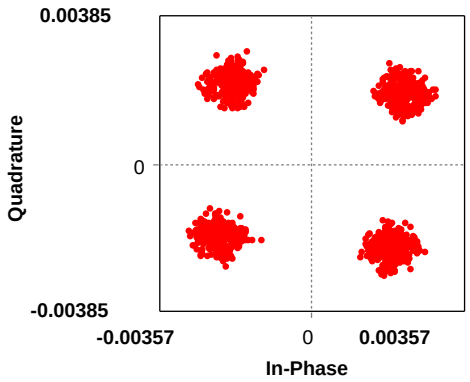
Figure 5.16: QPSK Constellation diagram of Ch3 without spectral shaping after back-to-back transmission.

B_{FWHM}/r= 1. When optical filter bandwidth is swept from 1 to 3, the impact of ISI is reduced, the filtering penalty, which is 1.39 dB in the previous case is now just reduced to 0.11 dB. Moreover, not only this lost power is recovered with our proposed method, but there is the additional power gain of 1.18 dB with RC-LMS filtering. The improvement is evident from the constellation diagram, where, the constellations points are more aligned and clear. Moving further, when the filter bandwidth is increased to 6, the signal bandwidth becomes wider than the channel band and start interfering with the neighbouring channels. Therefore, the received optical power is reduced to -36.11 dBm. While shaping with the RC-LMS filter, there is 0.9 dB improvement in received power. It can be noted that B_{FWHM}/r should be less than 6 to avoid crosstalk penalties.

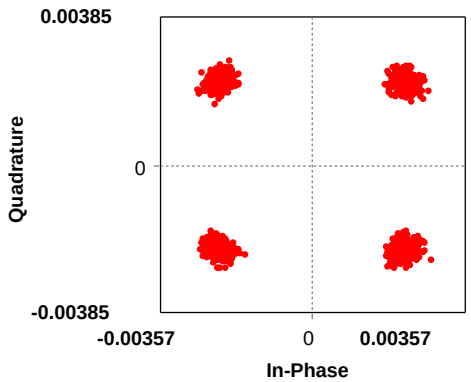
The performance of the system is assessed after the transmission of 100 km. Without dispersion compensation, the constellation diagram is heavily distorted, and it is impossible to recover the information from Ch3 at all. With the implementation of the dispersion compensation module, the QPSK system has excellent tolerance towards chromatic dispersion, as seen in Fig 5.18(b). After 100 km transmission, it is observed that the received power for Ch3 without any spectral shaping is -32.70 dBm. When the Ch3 is filtered with an RC filter of B_{FWHM}/r= 1, the observed power penalty is 2.18 dB as compared to without any shaping case. However, the induced penalty is further improved by 0.61 dB with our proposed RC-LMS filter. The best performance is achieved when Ch3 is shaped with RC-LMS filter at B_{FWHM}/r = 3, with received power of -34.93 dBm. In this case, there is no filter induced penalty



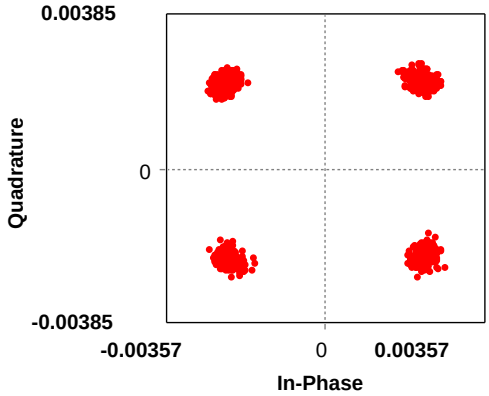
(a) RC filter = 1



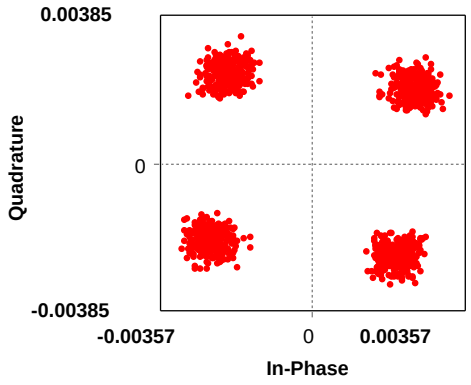
(b) RC-LMS filter = 1



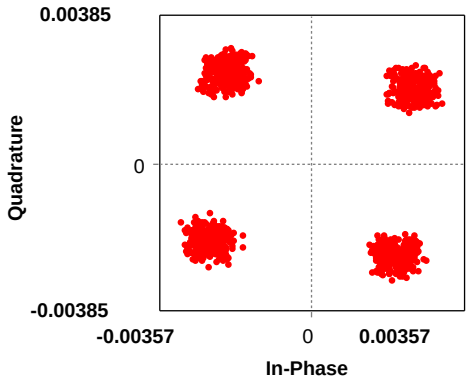
(c) RC filter = 3



(d) RC-LMS filter = 3

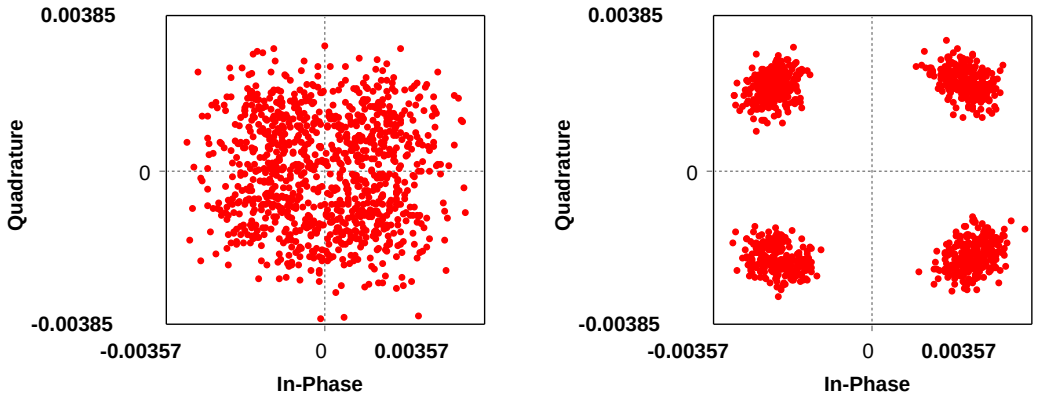


(e) RC filter = 6



(f) RC-LMS filter = 6

Figure 5.17: QPSK Constellation diagram of the Ch3 after shaping with an RC filter of different B_{FWHM}/r after back to back transmission at 10 Gb/s.



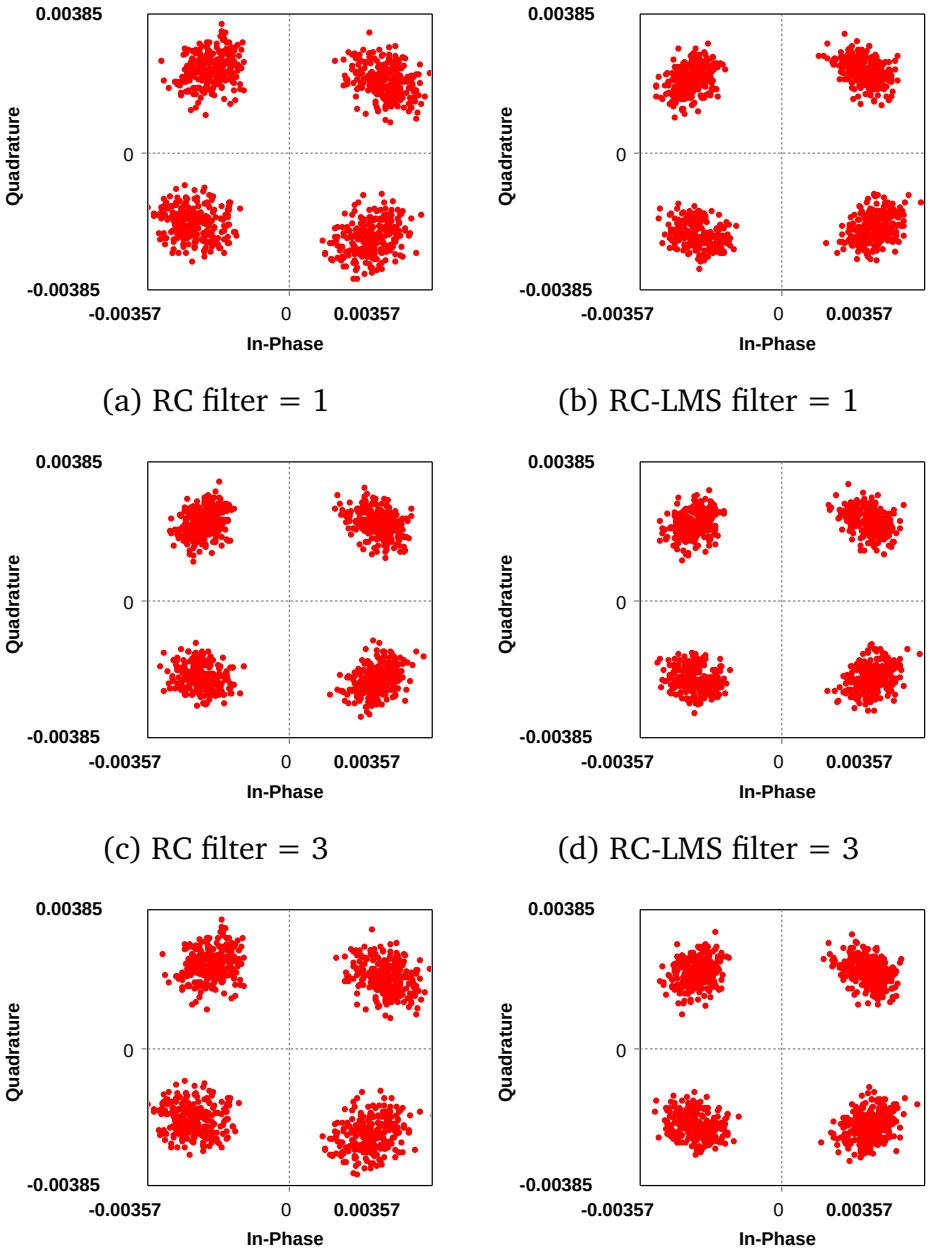
(a) (b)

Figure 5.18: Constellation diagram of the Ch3: (a) without and (b) with dispersion compensation after 100 km transmission at 10 Gb/s.

at all, but there is an improvement of 0.92 dB than a typical RC filter case. The I/Q constellation diagrams are in agreement, as shown in Fig 5.19. With the increase in B_{FWHM}/r from 4 to 6, the received power is enhanced by 0.79 dB, 0.71 dB and 0.67 dB respectively as depicted from Fig. 5.14. Finally, when optical filters are used at the multiplexer side, the crosstalk penalty reduces especially with RC-LMS method and pre-shaping is still useful in saving allocated optical spectrum.

5.2.3 Performance Evaluation at 28 Gb/s

As mentioned before, the spectral efficiency of the system can be increased by using modulation formats like QPSK at higher data rates. In this section, the impact of transmitter side optical pre-shaping on the QPSK based Nyquist-WDM superchannel is evaluated at 28 Gb/s. The channel spacing of the optical frequency comb is 28 GHz. The received optical power for Ch3 is -34.48 dBm without any spectral shaping, as shown in Fig. 5.20(a). As a consequence of narrow-band filtering (B_{FWHM}/r= 1), the strong ISI occurs between adjacent symbols as narrow filter suppresses the spectral components of the optical spectrum. The constellation diagram of I/Q plane at 28 GHz channel spacing presented in Fig. 5.21(a) confirm the presence of excessive distortions degrading the signal. The crosstalk due to ISI is strongly present, inducing a power penalty of 3.01 dB in a back-to-back case as compared to no spectral shaping. As the bandwidth is increased to 3, the received power required is -32.02 dBm. It can be noticed that system's performance is better



(a) RC filter = 1

(b) RC-LMS filter = 1

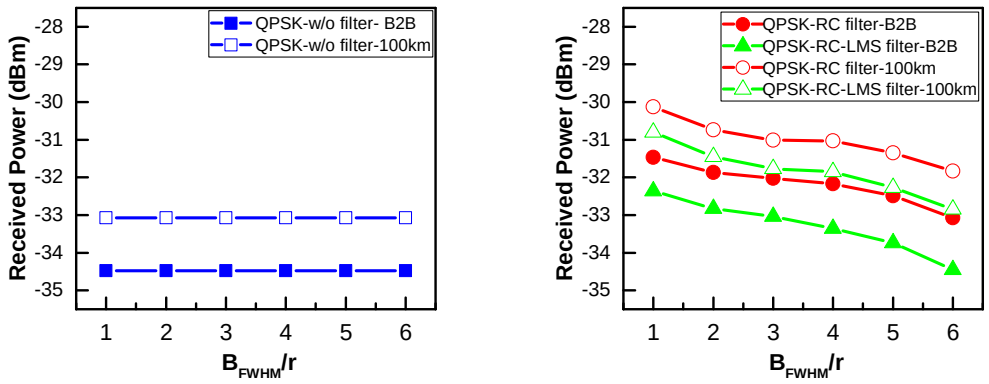
(c) RC filter = 3

(d) RC-LMS filter = 3

(d) RC filter = 6

(e) RC-LMS filter = 6

Figure 5.19: Constellation diagram of the Ch3 after shaping with an RC filter of different B_{FWHM}/r after 100 km transmission at 10 Gb/s.



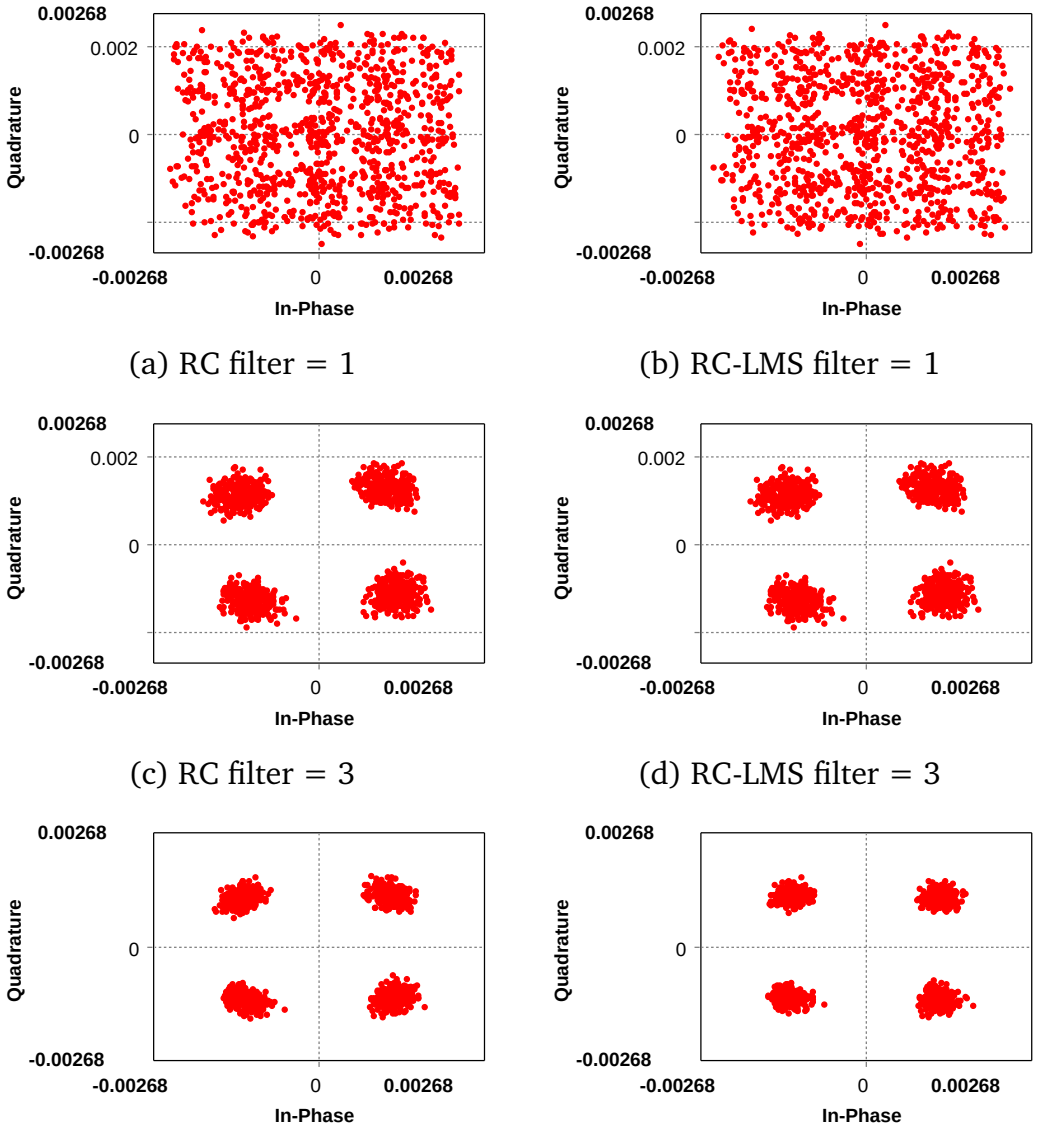
(a) (b)

Figure 5.20: Received power at BER of 10^{-3} for Ch3: (a) without shaping and (b) after shaping with a RC filter and RC-LMS filter of different for QPSK-Nyquist-WDM superchannel at 28 Gb/s.

when B_{FWHM}/r is larger than 1. The constellation points are linearly distributed and separated for B_{FWHM}/r=3. When the bandwidth of the filter is further increased to 6 which is approximately twice of the symbol rate. At this point, the contributions of ISI is minimised, and filter induced losses are reduced, and the received power is -33.07 dBm. The improvement in constellation points are quite evident. The system performance is further assessed with the implementation of RC-LMS filter for back-to-back transmission. It can be seen from the Fig. 5.21 that the proposed method add improvement of 0.89 dB, 1.02 dB and 1.38 for B_{FWHM}/r= 1, 3 and 6 respectively as compared to typical RC filter. The constellation point for all the cases are more confined and aligned with RC-LMS filter.

After 100 km transmission, the impact of narrow filtering is very severe, and it is tough to decode the proper symbols as the constellation points are heavily distorted as seen in Fig. 5.22(a). Although there is an improvement with RC-LMS method, the improvement is not sufficient to decode the symbols properly. Therefore, filtering with B_{FWHM}/r=1 is not good choice for 28 Gb/s. When filter bandwidth is swept from 1 to 3, which is $\sim$1.07 times the symbol rate. The constellation points are more localized than the previous case. However, with the RC-LMS filtering, there is a further 0.76 dB gain in received power. When the filter bandwidth is doubled the symbol rate, the clear and aligned constellation points are observed, and best results are achieved with RC-LMS method with negligible power penalty.

Finally, optical pre-filtering is a critical need to ensure high spectral efficiency



(a) RC filter = 1

(b) RC-LMS filter = 1

(c) RC filter = 3

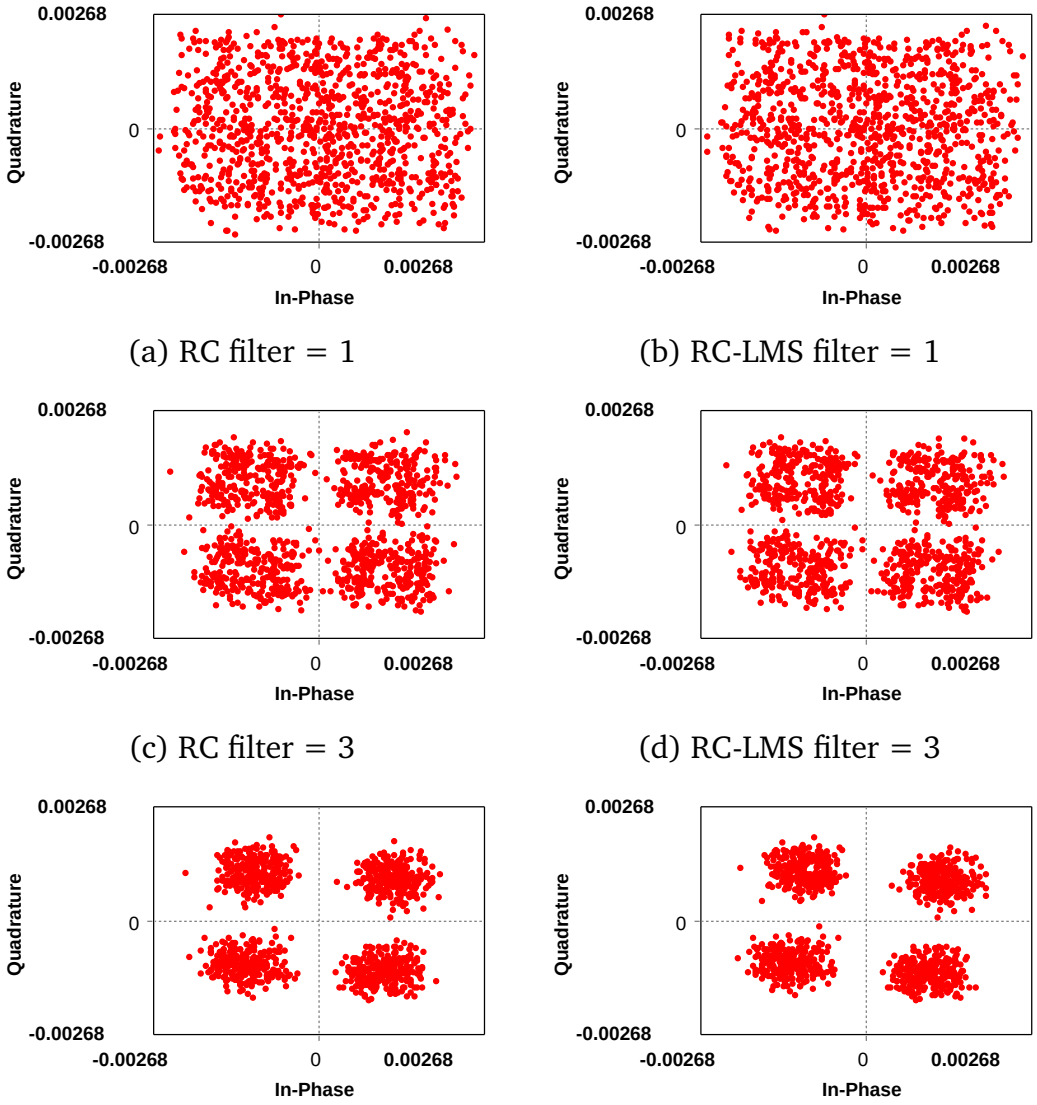
(d) RC-LMS filter = 3

(e) RC filter = 6

(f) RC-LMS filter = 6

Figure 5.21: QPSK Constellation diagram of the Ch3 after shaping with a RC filter of different B_{FWHM}/r after back to back transmission at 28 Gb/s.

with the possibility of low crosstalk during transmission with optimum filter bandwidth. In order to meet the growing demand for transmission rates while maintaining the 100 Gb/s standardized transmission structures, the use of dual-polarization 16-quadrature amplitude modulation (DP-16QAM) modulation format is presented as a potential solution and its use in coherent optical systems (Gnauck et al. 2011). In the next section, the impact of transmitter side filtering is investigated on 16-QAM at 10 Gb/s and 28 Gb/s.



(a) RC filter = 1

(b) RC-LMS filter = 1

(c) RC filter = 3

(d) RC-LMS filter = 3

(e) RC filter = 6

(f) RC-LMS filter = 6

Figure 5.22: QPSK Constellation diagram of the Ch3 after shaping with a RC filter of different B_{FWHM}/r after 100 km transmission at 28 Gb/s.

5.3 16-QAM based Nyquist-WDM Superchannel

QAM is a modulation format that combines two carriers whose amplitudes are modulated independently with the same optical frequency and whose phases are 90 degrees apart. These carriers are called in-phase carriers (I) and quadrature-phase carriers (Q). The QAM can assign 2^N states by using I and Q, which is called 2^N-QAM where N is (2,4,8). 2^N QAM signal processes N bits in a single-channel so that it can realize N times the spectral efficiency of OOK. For QAM, the most common forms are 16-QAM, 64-QAM, 128-QAM and 256-QAM. It is possible to transmit more bits per symbol by moving to a

higher-order, but more points in the constellation will make it more susceptible to noise. This results in a higher bit error rate, hence higher-order QAM can deliver more data, less reliably than lower-order QAM. Therefore, 16-QAM modulation is a promising candidate for doubling the overall bit rate as compared QPSK format for the same symbol rate and is an effective solution to obtain spectral efficient optical systems.

5.3.1 Schematic setup for 16-QAM Superchannel

A CW laser with 100 kHz linewidth is used to seed an optical comb generator resulting in five subcarriers spaced at 10 GHz. The comb is de-multiplexed into individual optical subcarriers with the help of four cascaded MZDIs before modulation. For 16-QAM modulation, two QPSK modulators are embedded together. The large amplitude QPSK1 is created in the upper arm by two $2^7 - 1$ PRBS outputs with an amplitude of $2V\pi$ to drive the MZM modulator at its null transmittance point. The small-amplitude QPSK 2 is obtained with a different amplitude of $V\pi$ to drive the MZM modulator at its null transmittance

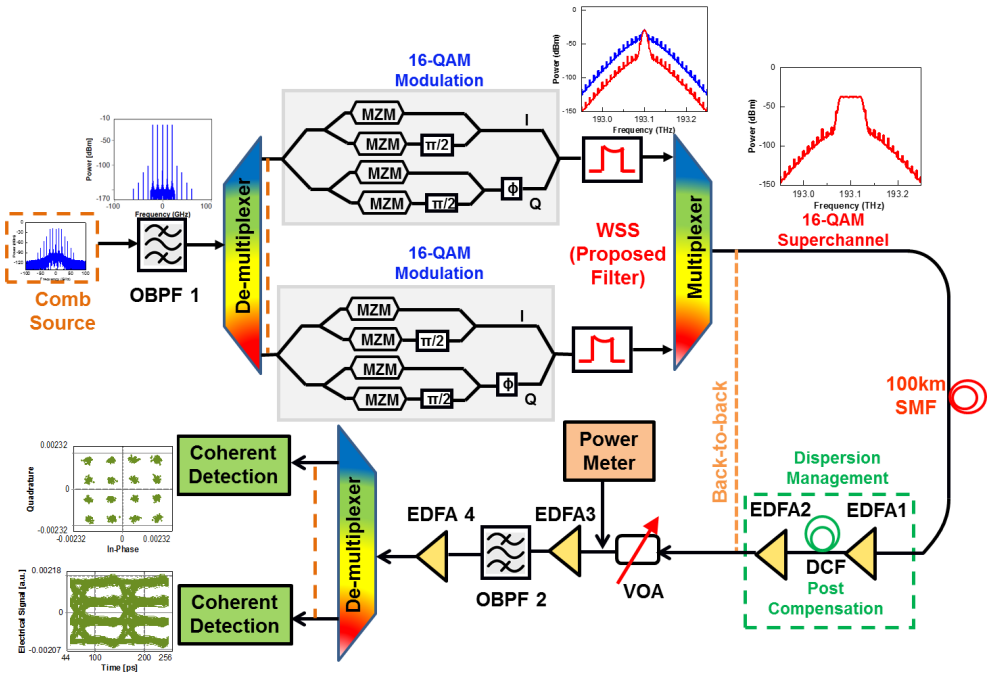


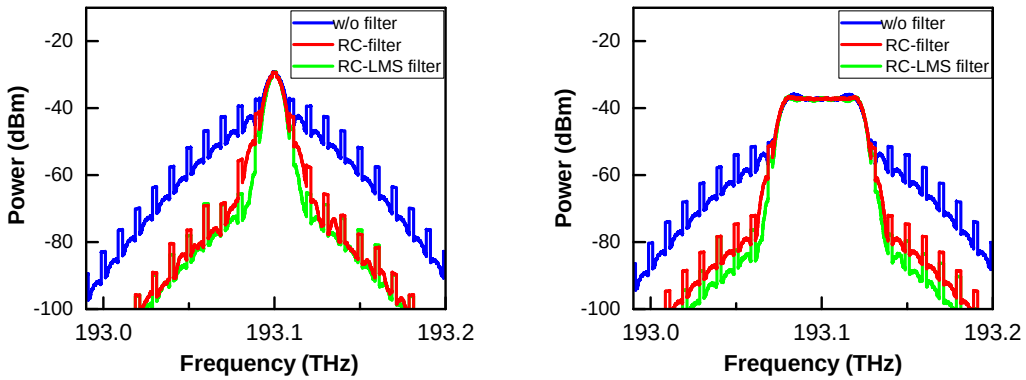
Figure 5.23: Five channel spectrally shaped 16-QAM Nyquist-WDM transmission system.

point followed by 6 dB attenuation in the lower arm. This attenuation of 6 dB fixes the position of symbols within the quadrant, and the interference of the two signals with different amplitude levels yield a 16-QAM signal. The

resultant 16-QAM signal is launched into 100 km SMF span with an overall chromatic dispersion of 17 ps/nm×km. The noise figure of the EDFAs used is 4 dB. The optical band-pass filter (OBF) used in the simulation has a bandwidth of 1 nm. At the receiver side, the superchannel is de-multiplexed in a similar way as before with the aid of MZI, before being detected. Each subcarrier is detected by an individual coherent receiver, as shown in Fig. 5.23.

5.3.2 Performance Evaluation at 10 Gb/s

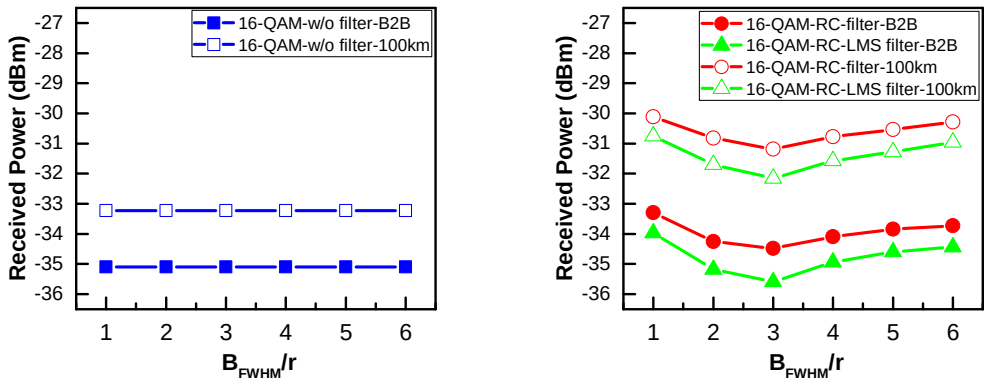
The pre-shaping performance of the 16-QAM is evaluated in the tightly spaced superchannel, and Ch3 is chosen for investigation. The optical spectrum of Ch3 and 16-QAM superchannel is shown in Fig. 5.24. In theory, to achieve the



(a) Ch3 (b) 16-QAM superchannel

Figure 5.24: Optical spectrum of 16-QAM before and after spectral shaping with RC filter having B_{FWHM}/r=1 at 10 Gb/s.

BER of 10^{-3}, the required optical received power is -37.41 dBm. The received power sensitivity for Ch3 is -35.1 dBm and -33.07 dBm without any spectral shaping for back-to-back and 100 km transmission respectively as shown in Fig. 5.25. Ch3 suffers from a performance degradation of 1.8 dB and 3.11 dB with narrow channel spacing, due to the existence of ISI when the channel spacing is reduced to the symbol rate for back-to-back and 100 km transmission respectively. With the narrow-band spectral shaping, the symbols are spread to adjacent symbols, thus introducing ISI as seen in the constellation diagram in Fig. 5.26(a). Due to the presence of ISI, there is displacement in the constellation points when the signal is shaped with B_{FWHM}/r= 1. When optical filter bandwidth is increased from 1 to 3, the impact of ISI is reduced, the filtering penalty, which is 1.8 dB in the previous case is now just reduced to 0.62 dB. The improvement is evident from the

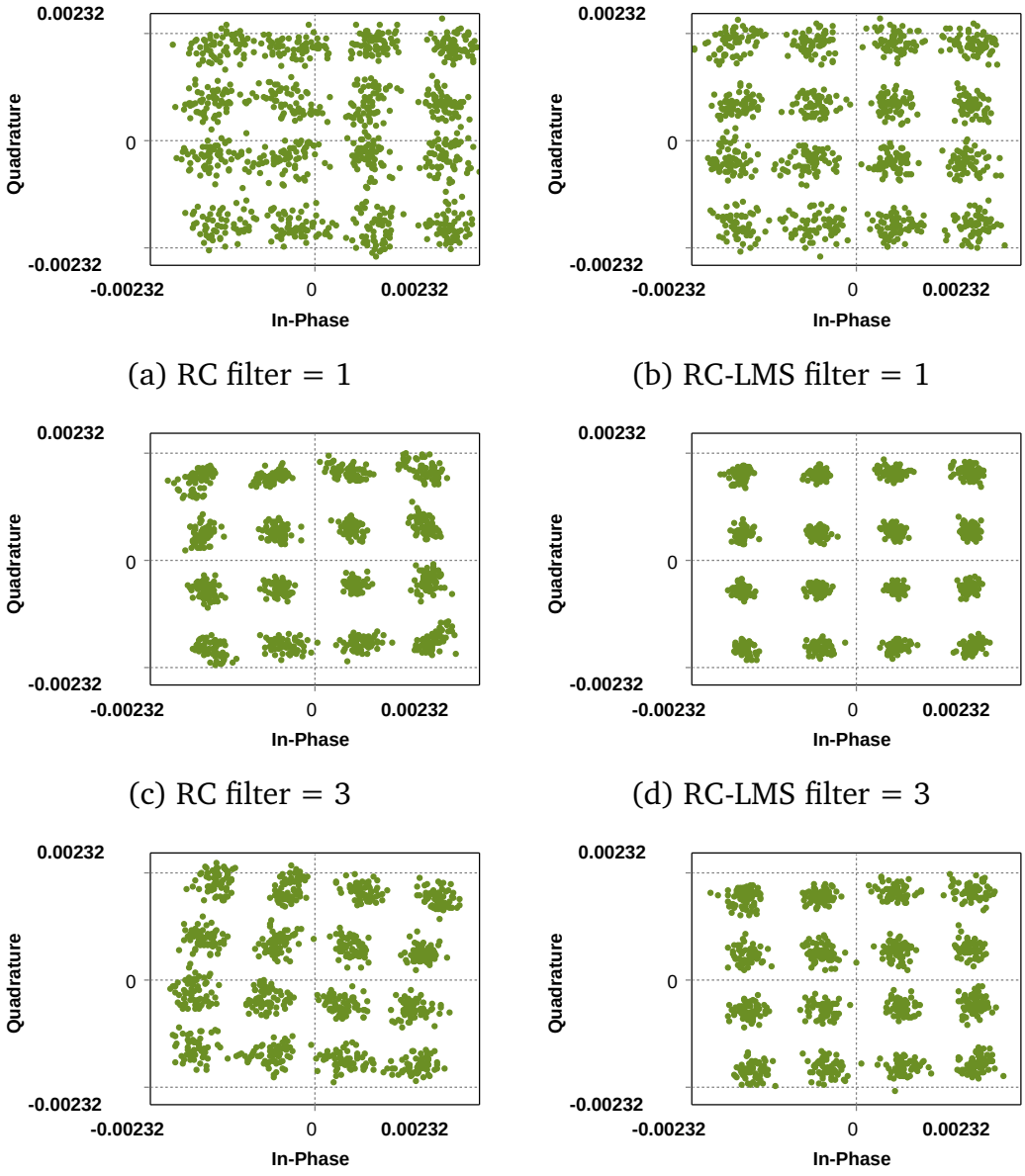


(a) (b)

Figure 5.25: Received power at BER of 10^{-3} for Ch3: (a) without shaping and (b) after shaping with a RC filter and RC-LMS filter of different B_{FWHM}/r for 16-QAM based Nyquist-WDM superchannel at 10 Gb/s.

constellation diagram, where, the constellations points are more aligned and clear with our proposed RC-LMS filtering with the received power is -35.59 dBm. In this case, all filter induced penalties are recovered. Furthermore, when the filter bandwidth is further increased to 6, the signal bandwidth becomes broader than the channel band and start interfering with the neighbouring channels. This results in degradation of received power, which is reduced to -34.44 dBm. The imperfections present in the channel cause the ideal points of the constellation diagram to spread and to tilt in Fig. 5.26(e) indicates that there is a slight phase difference between the I and Q signal. While shaping with the RC-LMS filter, compensates for the distortions and overcome the phase errors along with 0.71 dB improvement in received power for the back-to-back scenario. Like QPSK, it is also true for 16-QAM that filter bandwidth should be less than the 6 to avoid crosstalk penalties.

Following similar tend for 100 km transmission, the impact of narrow filtering is powerful, it is hard to decode the symbols as they are spread and interfering with the adjacent symbols. Although, there is a slight improvement with RC-LMS method. With, the increase in improvement is not sufficient to decode the symbols correctly. When filter bandwidth is swept from 1 to 3, the constellation points are more localized than the previous case. However, with the RC-LMS filtering, there is a further 0.76 dB gain in received power. When the filter bandwidth is twice of the symbol rate, the clear and aligned constellation points are observed, and the best results are achieved with RC-LMS method with negligible power penalty.



(a) RC filter = 1

(b) RC-LMS filter = 1

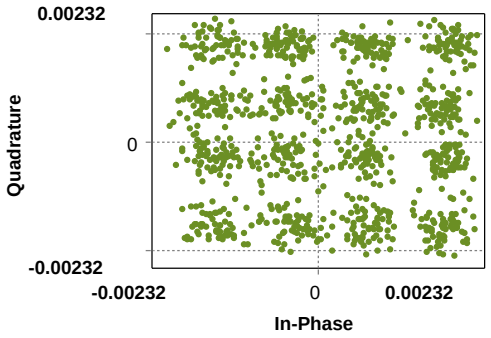
(c) RC filter = 3

(d) RC-LMS filter = 3

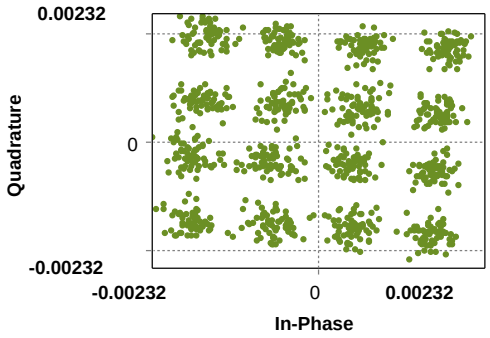
(e) RC filter = 6

(f) RC-LMS filter = 6

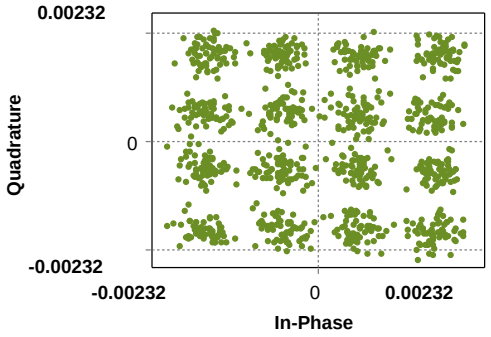
Figure 5.26: 16-QAM Constellation diagram of the Ch3 after shaping with a RC filter of different B_{FWHM}/r back-to-back transmission at 10 Gb/s.



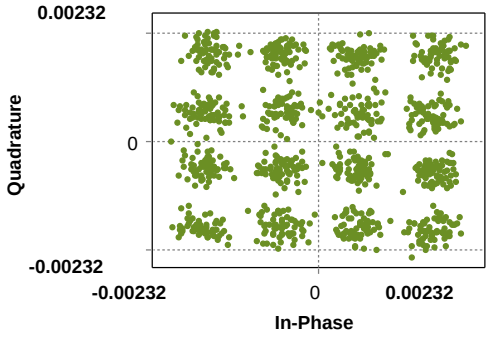
(a) RC filter = 1



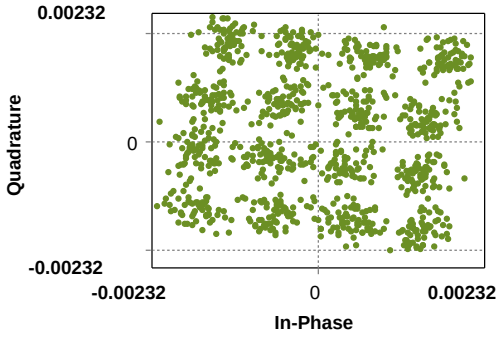
(b) RC-LMS filter = 1



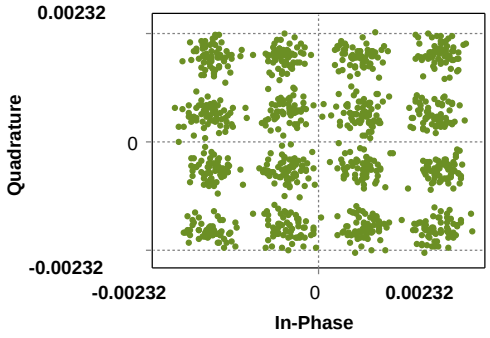
(a) RC filter = 3



(b) RC-LMS filter = 3



(a) RC filter = 6

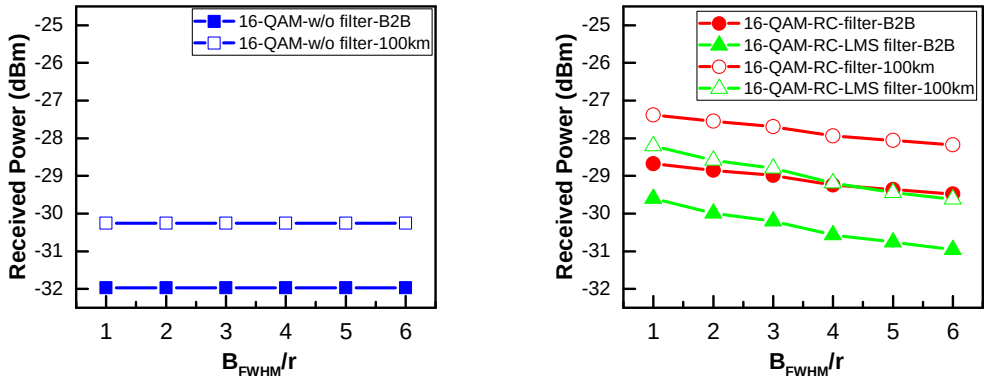


(b) RC-LMS filter = 6

Figure 5.27: 16-QAM Constellation diagram of the Ch3 after shaping with a RC filter of different B_{FWHM}/r after 100 km transmission at 10 Gb/s.

5.3.3 Performance Evaluation at 28 Gb/s

As mentioned before, the spectral efficiency of the system can be increased by using higher modulation formats at higher data rates. In this section, the impact of transmitter side optical pre-shaping on the 16-QAM based Nyquist-WDM superchannel is evaluated at 28 Gb/s with channel spacing of 28 GHz. Due to narrow-band filtering ($B_{FWHM}/r = 1$), strong ISI is present between adjacent symbols because a significant portion of the optical spectrum is filtered out, which reduces the overall optical power of the signal. The received optical power for Ch3 is -31.97 dBm without any spectral shaping, as shown in Fig. 5.28(a). The crosstalk due to ISI is strongly present, inducing a

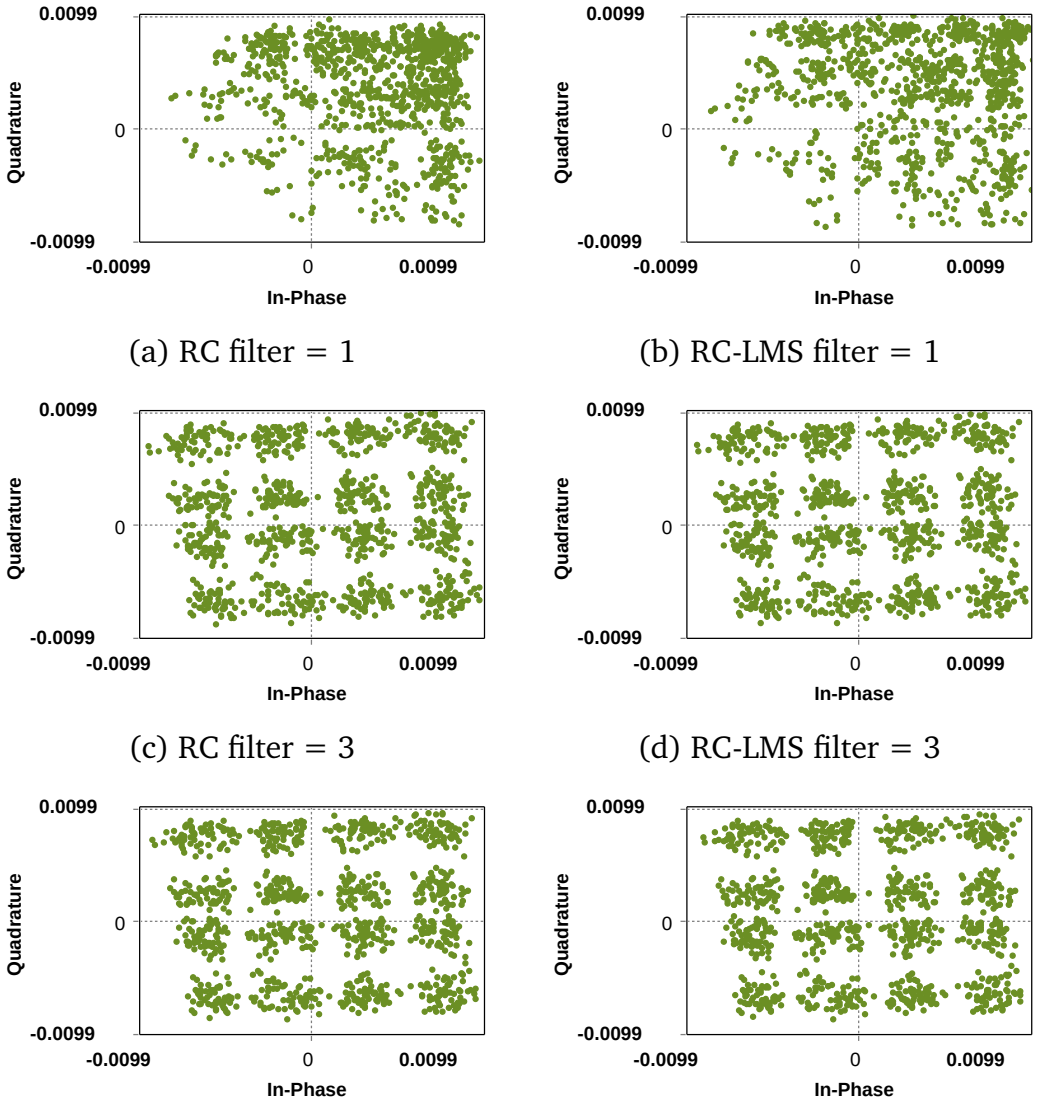


(a) (b)

Figure 5.28: Received power at BER of 10^{-3} for Ch3: (a) without shaping and (b) after shaping with a RC filter and RC-LMS filter of different bandwidth for 16-QAM based Nyquist-WDM superchannel at 28 Gb/s.

power penalty of 3.29 dB in the back-to-back case as compared to no filtering case. As the filter bandwidth is increased to 3, the received power required is -30.02 dBm. When the bandwidth of the filter is further increased to 6, which is almost twice of the symbol rate, the contributions of ISI is minimum and filter induced losses are reduced at this point. The system performance is further assessed with the implementation of RC-LMS filter for back-to-back transmission. The proposed method add improvement of 0.92 dB, 1.21 dB and 1.48 dB for $B_{FWHM}/r = 1$, 3 and 6 respectively as compared to typical RC filter. The constellation points for all the cases are more confined and aligned with RC-LMS filter as shown in Fig. 5.29.

After 100 km transmission, the impact of narrow filtering is very intense, and it is very hard to decode the proper symbols as the constellation point are heavily distorted. Although there is an improvement with RC-LMS method,



(a) RC filter = 1

(b) RC-LMS filter = 1

(c) RC filter = 3

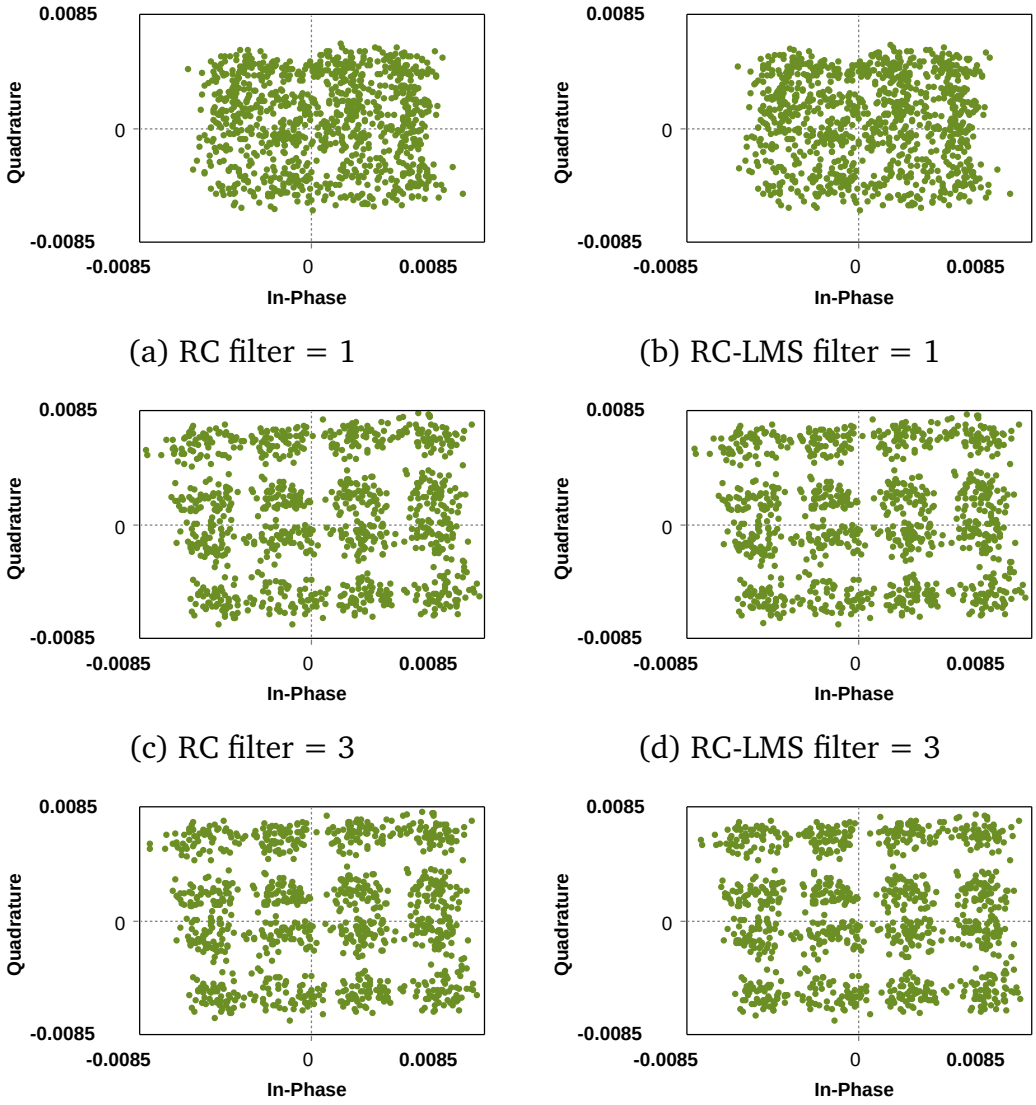
(d) RC-LMS filter = 3

(e) RC filter = 6

(f) RC-LMS filter = 6

Figure 5.29: 16-QAM Constellation diagram of the Ch3 after shaping with a RC filter of different B_{FWHM}/r after back-to-back transmission at 28 Gb/s.

the improvement is not sufficient to decode the symbols properly. When filter bandwidth is swept from 1 to 3, the constellation points are more local than the previous case. However, with the RC-LMS filtering, there is a further 1.3 dB gain in received power. The best performance is achieved when the filter bandwidth is at least twice the symbol rate. The clear and aligned constellation points are observed, and the best results are achieved with RC-LMS method with negligible power penalty. Generally, it is anticipated at this point that broader filtering is to be preferred over narrow filtering since the degrading effect of increasing noise power is less severe than spectrally



(a) RC filter = 1

(b) RC-LMS filter = 1

(c) RC filter = 3

(d) RC-LMS filter = 3

(e) RC filter = 6

(f) RC-LMS filter = 6

Figure 5.30: 16-QAM Constellation diagram of the Ch3 after shaping with an RC filter of different B_{FWHM}/r after 100 km transmission at 28 Gb/s.

truncating the signal as seen in constellation diagram in Fig. 5.30.

Summary

The main idea of Nyquist-WDM transmission technique is to have a Nyquist-shaped pulse in the temporal domain, and square-like shaped spectrum that limits the bandwidth of the signal within the Nyquist frequency. This technique improves the spectral efficiency by placing Nyquist filtered WDM channels closer to each other. Spectral shaping of optical signals

provides a method to use channel bandwidth efficiently. However, it commonly takes much effort and complexity to realize rectangular spectra in both digital and optical ways of spectral shaping. Although tight filtering can be employed to constrain the bandwidth of each WDM channel, the filtering process itself results in significant ISI within each channel. However, if an appropriate filter like raised cosine with a corresponding rectangular spectrum is chosen, then the Nyquist criterion for ISI can be closely achieved. Optical spectral shaping at the transmitter can help to reduce the overall optical bandwidth requirement, albeit at the cost of reduced receiver sensitivity. Our proposed adaptive RC-LMS filter is suitable for making superchannel transmission robust to the degradation of received power sensitivities. For a given interchannel spacing, a range of suitable values for filter bandwidth is determined.

Table 5.2: Improvement in optical received power with RC-LMS filter using different modulation formats in back-to-back scenario.

Modulation Format	NRZ-OOK		QPSK		16-QAM	
Data Rate	10 Gb/s	28 Gb/s	10 Gb/s	28 Gb/s	10 Gb/s	28 Gb/s
B_{FWHM}/r	Improvement in optical received power (dB)					
1	0.65	0.67	0.85	0.89	0.67	0.92
2	0.86	0.72	1.16	0.96	0.92	1.14
3	0.98	0.76	1.29	1.02	1.11	1.21
4	0.83	0.88	1.05	1.19	0.85	1.33
5	0.75	0.94	0.98	1.25	0.76	1.4
6	0.7	1.1	0.9	1.38	0.71	1.48

The table 5.2 highlights the improvement in optical received power with the implementation of our proposed RC-LMS filtering using different modulations formats in back-to-back scenario. The simulation results indicate that with our proposed filter, the filter induced penalties can be reduced and lost optical power can be recovered back.

Similarly, the table 5.3 concludes the results after spectral shaping with RC-LMS filter in case of 100 km transmission using different modulation formats at 10 Gb/s and 28 Gb/s respectively. From the simulation results, it is estimated that using narrow optical filtering; one has to accept a compromise between ICI and ISI for the case of the all modulations formats used above. It is concluded that the B_{FWHM}/r= 3 is the best filtering bandwidth where the impact of crosstalk is minimum and transmission is achieved without any significant penalty for NRZ-OOK, QPSK and 16-QAM at 10 Gb/s. For 28 Gb/s,

Table 5.3: Improvement in optical received power with RC-LMS filter using different modulation formats after 100 km transmission.

Modulation Format	NRZ-OOK		QPSK		16-QAM	
Data Rate	10 Gb/s	28 Gb/s	10 Gb/s	28 Gb/s	10 Gb/s	28 Gb/s
B_{FWHM}/r	Improvement in optical received power (dB)					
1	0.61	0.65	0.7	0.67	0.63	0.82
2	0.8	0.69	0.95	0.71	0.88	1.04
3	0.92	0.75	1.08	0.76	0.96	1.11
4	0.79	0.82	0.88	0.825	0.79	1.25
5	0.71	0.89	0.83	0.92	0.74	1.38
6	0.67	0.99	0.79	1.02	0.67	1.44

the best performance is obtained when B_{FWHM}/r= 6 for all the cases with channel spacing of 28 GHz. However, QPSK outperformed the NRZ-OOK and 16-QAM with highest received power sensitivity in both data rates as expected from their theoretical values. Furthermore, the carrier spacing has to be slightly larger than the symbol rate to ensure acceptable linear crosstalk due to the imperfect rectangular spectral shape in practical implementations. However, it is true that the current available WSS has not enough resolution to perform the optical shaping perfectly but implementing our proposed adaptive optical filter at the transmitter can help to relax the complexity of the state-of-art to some extent and also help to mitigate signal degradation in Nyquist-WDM systems.

Chapter 6

Conclusion

In this chapter, the major works presented in this thesis are summarised, and potential research directions for future works are proposed.

6.1 Summary

A rapid growth in data-rate intensive applications has been witnessed in recent years. This trend is likely to continue in the future as well, which will continuously increase the data-traffic demands over the underlying transmission infrastructure. The global data-traffic is transported by optical fibre networks; the data-carrying capacity of those networks will lead to a capacity crunch. To enable faster-growing system capacity, coherent optical communications are revived, which has triggered the employment of advanced modulation formats. Employing higher-order modulation formats (64-QAM) can increase the data rate per channel. However, there are both electrical and optical restrictions on spectrally efficient modulation formats. A currently proposed solution for maximising the capacity of optical communications is superchannels. In superchannels, WDM channels are placed closer together, potentially at the symbol rate, and more channels can be transmitted through the same bandwidth. Efficient utilisation of the available spectral bandwidth can be enabled with the introduction of AO-OFDM and Nyquist-WDM modulation techniques in optical communication systems.

Nyquist-WDM is found to be the best candidate in terms of its performance and low-complexity of implementation. Nyquist-WDM systems require more tightly spaced subcarriers, achievable through narrow spectral shaping in the

digital domain using FIR filters and in the optical domain by using optical filters. It is found that that DSP-based approach is limited by the complexity and finite sampling speed which limits the achievable symbol rate. This thesis addresses that spectral shaping by programmable optical filters like WSS at the transmitter side can be an alternative solution to minimise the complexity and potential cost of the current state-of-the-art. As optical filtering can avoid the limitation of electronics bandwidth, it may become the preferred approach if the desired filter shape can be easily achieved. Optical filters with a very steep profile are required to approximate the desired rectangular spectrum, which is critical to design and build using state-of-the-art technology. Due to the limited number of pixels available on the current generation of LCoS based devices, its resolution is limited to $\sim$10 GHz.

In this thesis, the limitations of the WSS's accuracy and resolution in terms of a roll-off factor are explored. It is found that, when the filter bandwidth is equal to the WSS's resolution, the roll-off factor is capped to 0.67 for a narrowband RC filter with -3dB of 10 GHz. However, implementing signal processing with full control of amplitude and phase to the input response of WSS can help to approximate the filter transfer function closer to the desired shape. Two novel filter input optimisation approaches are proposed for enhancing the output response of the WSS. The first method is reducing spectral roll-off factor by introducing amplitude dip in input filter response of WSS. With this proposed method, for the filter with $B_{FWHM/r}$=1, 4 and 5, the roll-off factor is reduced by a factor of 10.1 %, 8 % and 5 % respectively when amplitude dip is changed from 0 to 5 %. A single-channel optical system is simulated to observe the total power penalty caused by different types of WSS generated filters. From the simulation results, our proposed RC filter has performed better by 1 dB in terms of power penalty than Gaussian and Butterworth filters.

In the second method, an effective tool for adapting the spectral roll-off factor of programmable optical filters for optical shaping of superchannels using least mean square algorithm, achieving a significant (19.8 %) reduction in roll-off factor is presented. To validate the performance of the filter with the proposed algorithm, the impact of narrowband spectral shaping at the transmitter is investigated in five-channel Nyquist-WDM superchannel using different modulation formats at different data rates.

The basic building blocks for generating Nyquist-WDM are optical frequency comb, de-multiplexers, higher-order modulations formats, spectral shaping

filters and coherent detection. For Nyquist-WDM, optical frequency comb features like frequency and amplitude stability (spectral flatness) and free spectral range (repetition rate) play a significant role. For our proposed system, an optical frequency comb with flatness within 0.12 dB and the SMSR is 23.5 dB achieved by cascading two MZMs. All-optical FFT circuits can be applied to demultiplex the optical frequency comb without the need for optical to electrical (O-E) or (E-O) electrical to optical conversion. The cascaded delay interferometers to achieve FFT/IFFT functions, which largely reduces the number of phase shifters and delay is implemented. From the simulations results, it is found that phase monitoring is a crucial part of the Nyquist-WDM transmitter, and for the optimum system performance, a proper phase has to be preserved before modulation.

The extensive description of individual modulation of subcarriers using an MZM device is discussed. Using MZM, different modulation formats like NRZ-OOK, QPSK and 16-QAM are generated. The optical spectra of NRZ-OOK, QPSK and 16-QAM are compared for most spectral efficient modulation format, and 16-QAM is found to be most spectral efficient.

Tight filtering can be employed to constrain the bandwidth of each channel in Nyquist-WDM, the filtering process itself results in significant ISI within each channel. Optical spectral shaping at the transmitter can help to reduce the overall optical bandwidth requirement, albeit at the cost of reduced receiver sensitivity. Our proposed adaptive RC-LMS filter is suitable for making superchannel transmission robust to the degradation of received power sensitivities. For a given channel spacing, a range of proper values for filter bandwidth is determined.

From the simulation results, it is clear that using narrow optical filtering, and one has to accept a compromise between crosstalk from neighbouring channels and ISI for the case of all modulations formats used above. It is found that the $B_{FWHM}/r = 3$ is the best filtering bandwidth where the impact of crosstalk is minimum and transmission is achieved without any significant penalty for NRZ-OOK, QPSK and 16-QAM at 10 Gb/s. However, if the performance is considered in case of 28 Gb/s with the channel spacing of 28 GHz, the best performance is obtained at $B_{FWHM}/r = 6$. However, QPSK outperformed the NRZ-OOK and 16-QAM by providing the highest sensitivity received in both data rates. Furthermore, the carrier spacing has to be slightly larger than the symbol rate to ensure acceptable crosstalk due to the imperfect

rectangular spectral shape in practical implementations. Indeed, the current available WSS has not enough resolution to perform the optical shaping correctly but implementing our proposed adaptive optical filter at the transmitter along with the DSP will help reduce the filter taps required in the electronic/digital domain.

Since the work on this thesis has started in 2015, the researchers from various groups are looking at different innovative ideas to improve the state-of-the-art systems. With the advancement in photonic integration technology, the improvements in the resolution and variety of optical filters to separate Nyquist WDM channels has been enabled (Goh et al. 2015). Many chip-based passive optical filters and the tapped-delay-line-based interferometric filters architectures are characterised by a finite-impulse response (FIR) with multiple optical delays to implement a filter circuit (Xie et al. 2017). A large number of delays and phase tuning elements increase circuit complexity, crosstalk and power consumption. This intrinsic trade-off between performance and complexity poses barriers to the practical photonic integration of such filters for use in Nyquist-WDM systems. While effort is still needed to reach industrial maturity, a resolution-enhanced WSS, a RAMZI chip as a wavelength interleaver is used to pre-process the incoming superchannel before launch into a commercial WSS (Corcoran et al. 2016). The use of ring resonators in RAMZI can introduce dispersion to the signal. Low cost colourless, directionless, and contention-less (CDC) technologies based WSS (Yang et al. 2017) is also reported. The applications of these new variations are expected to improve the optical performance and the switching functionalities of the LCOS-WSS with low cost and complexity.

6.2 Main contributions

The main objective of this thesis is to investigate the novel spectral shaping techniques, which can reduce the complexity of the current state-of-the-art in Nyquist-WDM by utilising now commercially available optical filters such as WSS. The device WSS has been already used for spectral shaping. The novelty of this work is that the reduction of the spectral roll-off has not been investigated before using this device. Some of the main contributions of the work in this thesis, to the field of optical communication systems, are highlighted below:

- Two low-complexity novel filter input optimisation approaches-Spectral amplitude dip and Adaptive spectral shaping were investigated to overcome the limitations of WSS resolution.
- Roll-off-factor was reduced by 10.1 %, with the implementation of spectral dip approach (Kaur & Garcia Gunning 2018).
- Roll-off-factor was reduced by 19.8 %, with the implementation of amplitude spectral shaping.
- A five-channel Nyquist-WDM superchannel with proposed adaptive spectral shaping at transmitter side demonstrated, with 10 GHz spacing between channels using different modulation formats at 10 Gb/s and 28 Gb/s.

6.3 Future Work

The research in this thesis has presented the novel optimisation techniques for the optical spectral shaping at the transmitter side of Nyquist-WDM. Potential future work in need of further investigation is described below:

- To validate the performance of the proposed optimised optical filters in Nyquist-WDM, the simulations are carried out in VPI Transmission Maker. For future work, a similar test-bed can be implemented in the lab to carry out experimental validation. The simulated and experimental results can be compared for the better analysis. All components used in VPI simulated testbed are required for the practical implementation of the system as a hardware point of view. Most of the components are available in the Photonics Systems lab. However, for the digital signal processing, high precision DACs, ADCs and FPGA are required.
- In this work, two novel filter input optimisation approaches for enhancing the output response of the WSS are implemented at the transmitter side. The next step is to implement the combination of our proposed optical filtering along with the DSP at the transmitter side. The proposed method is illustrated in Fig. 6.1. Alone DSP will need a large number of filter taps, but this optimised optical filtering will help to relax the complexity to some extent and also help to mitigate signal degradation in Nyquist-WDM systems.
- As mentioned above, the combination of DSP and optimised optical

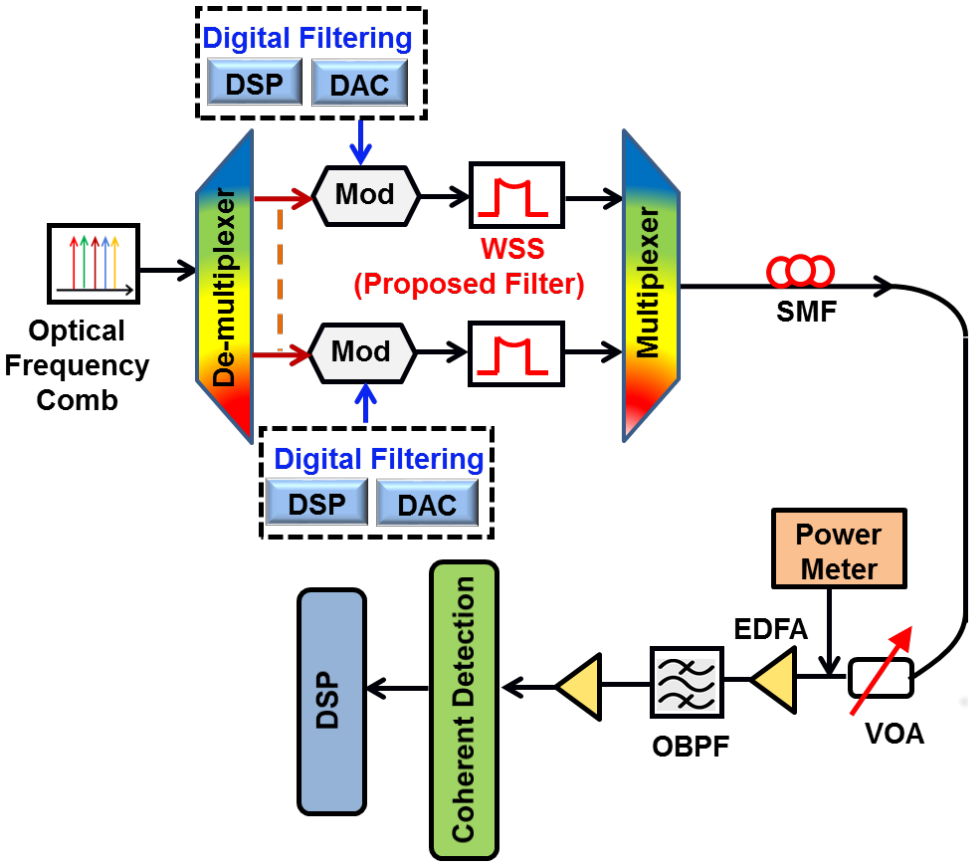


Figure 6.1: Proposed Experimental Set for Nyquist-WDM Superchannel

filtering with WSS can be a potential solution. However, the chances of the improvement will increase further, if the similar optimisation will be implemented on the DSP side along with our proposed optical spectral shaping. Then, the performance of the Nyquist-WDM can be compared experimentally with the optimisation at both digital and optical side and optimisation at just optical side.

- The photonic integrated circuits (PIC) are considered key enablers of future WDM systems. With densely integrated high bandwidth optical transceivers, the footprint and power consumption of WDM systems will be dramatically reduced compared to current solutions using bulky discrete optical components. In future, with technology advancement, if it is possible to integrate the WSS to the available PIC transceivers, then the flexibility and low complexity of our proposed optical spectral shaping can take the current PICs to another level.

Appendix A

VPI Images

Parameter Editor Window

The parameter editor of a module can be accessed by right-clicking on it and selecting the edit parameters option, or just by double-clicking on the module. Fig. A.2 is an example of a parameter editor window corresponding to a laser

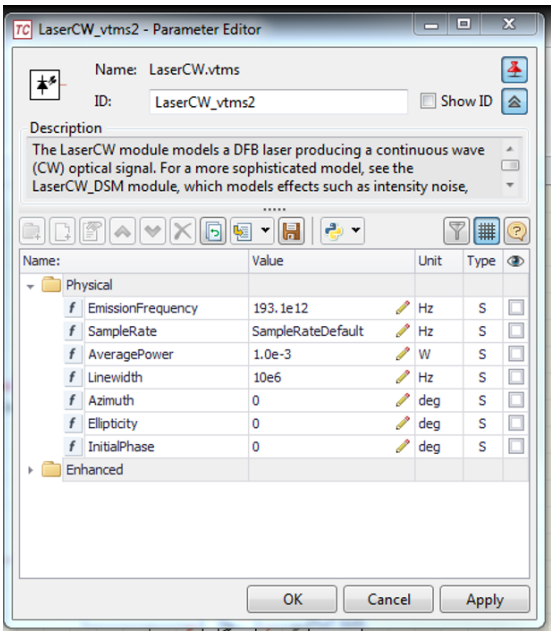


Figure A.1: Simualtion parameter editor window of a VPI laser module.

module.

VPIphotonicsAnalyzer™

VPIphotonicsAnalyzer™ establishes a universal framework for data display and analysis. The data visualisation can be achieved in form of multi-input

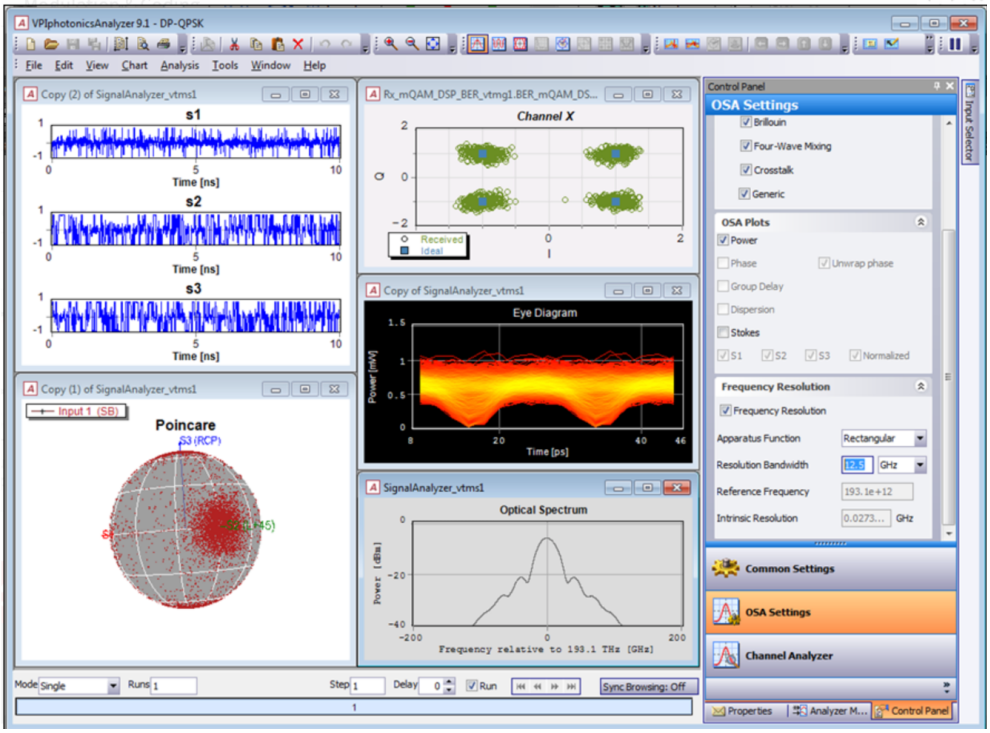


Figure A.2: Data visualization and analysis using VPIphotonicsAnalyzer™.

optical, electrical oscilloscope, eye plots featuring color-grading, BER plots, constellation diagrams, and optical spectrum analyzer with phase, delay and dispersion plots as shown in Fig. A.2 (VPIphotonics GmbH 2014). VPIphotonicsAnalyzer™ framework provides visualizers and analyzers that accurately represent laboratory test and measurement equipment for detailed results display, component characterization and system performance analysis functions.

BER Estimation

Bit Error Ratio estimation requires a knowledge of which channel is being detected from a group of transmitters in order to recover the clock information properly, and allow a comparison between the transmitted and received sequences. For this purpose, VPI software provides logical channels which trace a connection between transmitter and receiver. A logical channel allows

a channel to be traced from its transmitter to the receiver. This allows a receiver to compare modulation type and the received bit sequence with the transmitted sequence, for the purposes of BER clock recovery and then BER estimation. The time needed for BER calculation depends on the time window of simulation. In our case, the time window is $1024/10^9$ seconds where 1024 is the number of bits and 10^9 b/s is the bit rate.

Parameters for Chapter 5

This section includes parameters used by different components in Chapter 5 for the generation of Nyquist-WDM using NRZ-OOK, QPSK and 16-QAM. The value of parameters is same of all three modulation formats. Fig. A.5 shows global parameter related to 10 Gb/s Nyquist-WDM system.

.

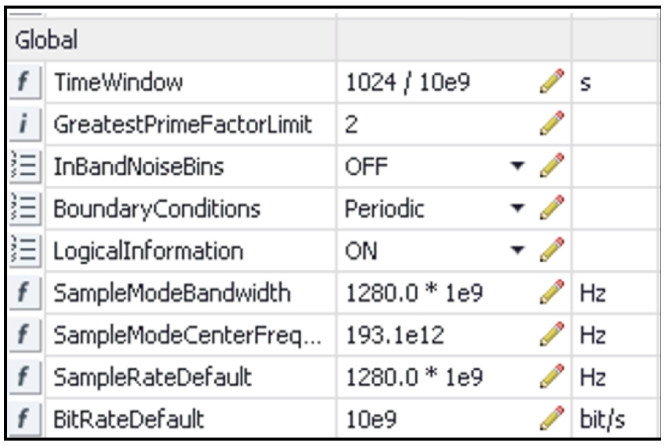


Figure A.3: Global parameters for 10 Gb/s Nyquist-WDM system.

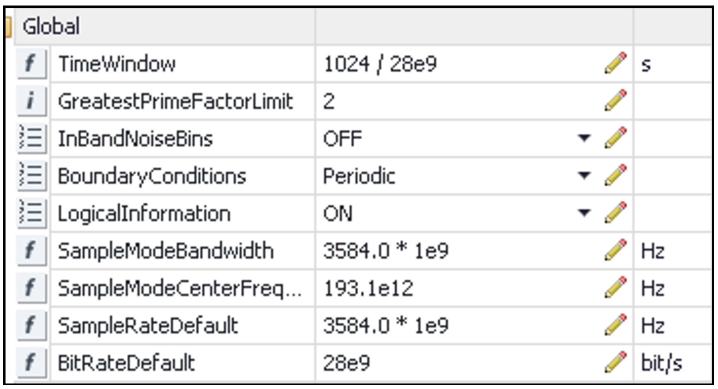


Figure A.4: Global parameters for 28 Gb/s Nyquist-WDM system.

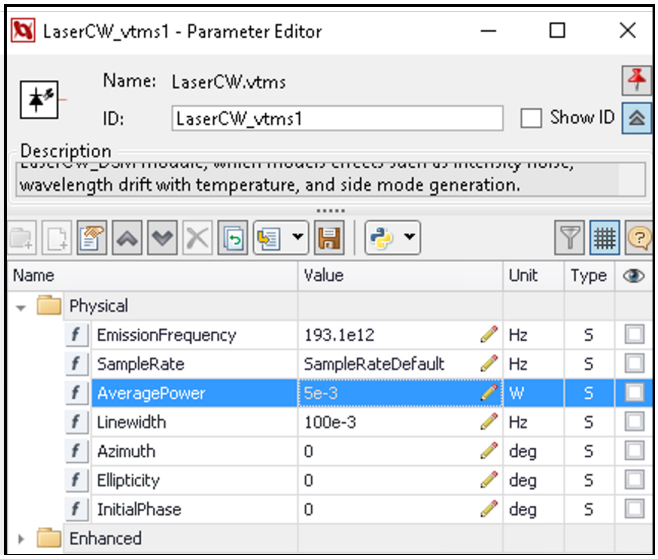


Figure A.5: Parameters for the CW laser.

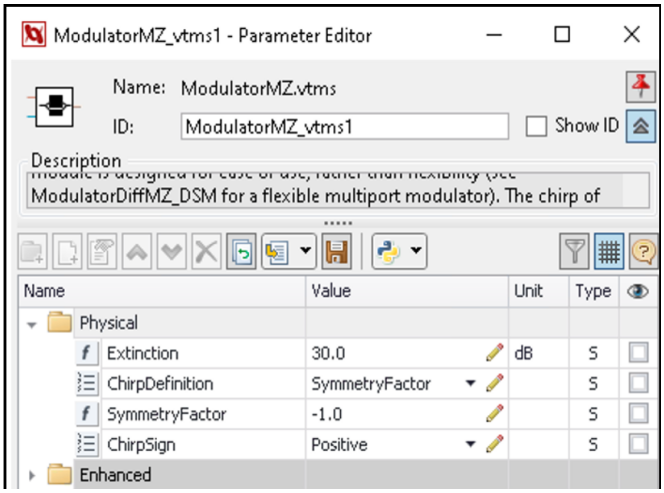


Figure A.6: Parameters for the Mach Zehnder Modulator.

Appendix B

Publications

- A. Kaur and F. C. Gunning (2020), “Improvement of spectral roll-off in superchannels with simple "set and forget" LMS algorithm for optical filter profile optimisation”, Optics Letters (To be submitted).
- A. Kaur and F. C. Gunning (2018), “Impact of analogue pre-filtering for spectral roll-off improvement in efficient spectral transmitter”, 20th International Conference on Transparent Optical Networks (ICTON), Bucharest, Romania, 1-5 July.
- A. Kaur and F. C. Gunning (2017), “Analogue Pre-filtering Using WSS for spectral efficient transmitters”, IEEE Photonics Conference (IPC), Orlando, USA, 1-5 October.
- A. Kaur and F. C. G. Gunning (2017), “Spectral Roll-off Reduction using WSS”, Photonics Ireland Conference, Galway, 13-15 September.

Oral Presentations

- Superchannels to the rescue, Tyndall Internal Conference 2018.
- Busy Internet? Superchannels to the rescue!, UCC Doctoral Showcase.
- Light Solutions, UCC Entrepreneur of the Year 2016 (Finalist).

Awards

- IPC Women in Photonics Travel Grant 2017.

- Postgraduate Certificate in Innovation, Commercialisation and Entrepreneurship (ICE) 2018.

PG Certificate in ICE

Being registered as a structured PhD-Stream 2 student, I have completed total 55 credits during my PhD, out of which 30 ECTS credits are taken from modules related to innovation, commercialisation and entrepreneurship (ICE). After the successful completion of these modules, I have been awarded Postgraduate Certificate in Innovation, Commercialisation and Entrepreneurship (ICE) in 2018, which is equivalent to NFQ Level 9.

- AC6301 Innovation Finance.
- MG6705 Marketing for High Technology Entrepreneurs.
- IS6307 Creativity and Opportunity Recognition.
- IS6306 Technology Business Planning.
- LW6104 Intellectual Property Law for High-Tech Entrepreneurs.
- MG6704 Internationalisation and Sales

References

Abd el Samie, F. E., Ahmed, H. E. H., Elashry, I. F., Shahieen, M. H., Faragallah, O. S., El-Rabaie, E.-S. M. & Alshebeili, S. A. (2014), *Image encryption : a communication perspective*, CRC Press.

Adam, I., Ibrahim, M. H., andAbu Bakar Mohammad, N. M. K. & Supa'at, A. S. M. (2008), Design of Arrayed Waveguide Grating (AWG) for DWDM/CWDM Applications Based on BCB Polymer, *in* 'Elektrika', pp. 18–21.

Agrawal, G. P. (2011), *Fiber-Optic Communication Systems: Fourth Edition*, 4 edn, John Wiley & Sons, 2012.

Agrawal, G. P. (2016), Optical communication: Its history and recent progress, *in* 'Optics in Our Time', Springer.

Alard, M. & Lassalle, R. (1987), 'Principles Of Modulation And Channel Coding For Digital Broadcasting For Mobile Receivers', *EBU Technical Review* .

Antonio Teixeira, G. M. T. B. (2012), Optical Orthogonal Frequency Division Multiplexing, *in* 'Optical Transmission: The FP7 BONE Project Experience', 1 edn, Springer Netherlands, pp. 27–30.

Baeuerle, B., Josten, A., Eppenberger, M., Hillerkuss, D. & Leuthold, J. (2018), 'Low-complexity real-time receiver for coherent nyquist-FDM signals', *Journal of Lightwave Technology* **36**(4), 5728 – 5737.

Bell, A. G. (1880), 'Upon the production and reproduction of sound by light', *Journal of the Society of Telegraph Engineers* **9**(34), 404–426.

Bhasin, A., Kaushik, M. & Sharma, U. (2016), 'Wavelength Division Multiplexing Optical Networks', *International Journal for Research in Applied Science & Engineering Technology (IJRASET)* **4**(X), 556–559.

Borne, D. (2008), Robust optical transmission systems : modulation and equalization, PhD thesis, Department of Electrical Engineering.

Bosco, G., Pilori, D., Poggiolini, P., Carena, A. & Guiomar, F. (2017), Scalable modulation technology and the tradeoff of reach, spectral efficiency, and complexity, *in* G. Li & X. Zhou, eds, 'Next-Generation Optical Communication: Components, Sub-Systems, and Systems VI', Vol. 10130, International Society for Optics and Photonics, SPIE, pp. 68–84.

Chang, R. W. (1966), 'Synthesis of BandlimitedOrthogonal Signals for Multichannel Data Transmission', *Bell System Technical Journal* **45**(10), 1775–1796.

Chang, R. W. (1970), 'Orthogonal Frequency Multiplex Data Tranamission'.

Chen, C., He, C., Zhu, D., Guo, R., Zhang, F. & Pan, S. (2013), 'Generation of a flat optical frequency comb based on a cascaded polarization modulator and phase modulator', *Opt. Lett.* **38**(16), 3137–3139.

Chen, H., Chen, M. & Xie, S. (2009), 'All-optical sampling orthogonal frequency-division multiplexing scheme for high-speed transmission system', *Journal of Lightwave Technology* **27**(21), 4848–4854.

Chen, S., Ma, Y. & Shieh, W. (2010), 110-Gb/s multi-band real-time coherent optical OFDM reception after 600-km transmission over SSMF fiber, *in* '2010 Conference on Optical Fiber Communication (OFC/NFOEC), collocated National Fiber Optic Engineers Conference', pp. 1–3.

Cimini, L. J. (1985), 'Analysis and Simulation of a Digital Mobile Channel Using Orthogonal Frequency Division Multiplexing', *IEEE Transactions on Communications* **33**(7), 665–675.

Cincotti, G. (2015), 'Enhanced functionalities for AWGs', *Journal of Lightwave Technology* **33**, 998–1006.

Corbett, B., Li, Z., Buehler, K., Naumann, F., Krieger, U., Wicht, S. & Bower, C. A. (2019), Micro-transfer-printing for heterogeneous integration, *in* '2019 6th International Workshop on Low Temperature Bonding for 3D Integration (LTB-3D)', pp. 34–34.

Corcoran, B., Zhu, C., Schröder, J., Zhuang, L., Foo, B., Burla, M., Beeker, W. P., Leinse, A., Roeloffzen, C. G. & Lowery, A. J. (2016), 'Multipass

performance of a chip-enhanced WSS for Nyquist-WDM sub-band switching', *Journal of Lightwave Technology* **34**(8), 1824–1830.

Corporation, F. (2020), 'WaveShaper Series A Family of Programmable Optical Processors'.
URL:
https://www.finisar.com/sites/default/files/downloads/waveshaper_12page_product_brochure_09_16_1.pdf [Online: Accessed on 27/08/2020].

Cramer, J. M., Scholtz, R. A. & Win, M. Z. (1999), On the analysis of UWB communication channels, *in* 'Proceedings - IEEE Military Communications Conference MILCOM', pp. 1191–1195.

Djordjevic, I. B. (2017), *Advanced optical and wireless communications systems*, 1st edn, Springer Nature.

Doelz, M. L., Heald, E. T. & Martin, D. L. (1957), 'Binary Data Transmission Techniques for Linear Systems', *Proceedings of the IRE* **45**(5), 656–661.

Doi, M., Sugiyama, M., Tanaka, K. & Kawai, M. (2006), 'Advanced LiNbO/sub 3/ optical modulators for broadband optical communications', *IEEE Journal of Selected Topics in Quantum Electronics* **12**(4), 745–750.

Dorf, R. C. (2006), Bandwidth Efficient Modulation (BEM) Concept, *in* 'Broadcasting and Optical Communication Technology', CRC Press, chapter Bandwidth, pp. 10–2, 10–3.

Elganimi, T. Y. (2013), Studying the BER performance, power- and bandwidth- efficiency for FSO communication systems under various modulation schemes, *in* '2013 IEEE Jordan Conference on Applied Electrical Engineering and Computing Technologies, AEECT 2013'.

Ellis, A. D. & Garcia Gunning, F. C. (2005), 'Spectral density enhancement using coherent WDM', *IEEE Photonics Technology Letters* **17**(2), 504–506.

Ellis, A. D. & Gunning, F. C. G. (2005*a*), Achievement of 1 bit/s/Hz information spectral density using coherent WDM, *in* 'Conference on Optical Fiber Communication, Technical Digest Series', pp. 3–3.

Ellis, A. D. & Gunning, F. C. G. (2005*b*), Coherent WDM, toward > 1 bit/s/Hz information spectral density, *in* 'Opto-Ireland 2005: Optoelectronics, Photonic Devices, and Optical Networks', Vol. 5825, International Society for Optics and Photonics, SPIE, pp. 482–490.

Erkilinc, M. S., Kilmurray, S., Maher, R., Paskov, M., Bouziane, R., Pachnicke, S., Griesser, H., Thomsen, B. C., Bayvel, P. & Killey, R. I. (2014), 'Nyquist shaped dispersion precompensated subcarrier modulation with direct detection for spectrally efficient WDM transmission', *Optics Express* **22**, 9420–9431.

Essiambre, R. J., Foschini, G. J., Winzer, P. J., Kramer, G. & Goebel, B. (2010), 'Capacity Limits of Optical Fiber Networks', *Journal of Lightwave Technology* **28**(4), 662–701.

Fabrega, J. M., Svaluto Moreolo, M., Martín, L., Chiadò Piat, A., Riccardi, E., Roccato, D., Sambo, N., Cugini, F., Potì, L., Yan, S., Hugues-Salas, E., Simeonidou, D., Gunkel, M., Palmer, R., Fedderwitz, S., Rafique, D., Rahman, T., de Waardt, H. & Napoli, A. (2016), 'On the Filter Narrowing Issues in Elastic Optical Networks', *Journal of Optical Communications and Networking* **8**(7), A23–A33.

Finisar Corporation (2012), Programmable Narrow-Band Filtering Using the WaveShaper 1000S and WaveShaper 4000S, Technical report, Finisar Corporation.

Finisar Corporation (2014), 'WaveShaper 1000S Programmable Optical Filter'. **URL:** *https://www.finisar.com/sites/default/files/downloads/waveshaper_1000s_product_brief_11_14.pdf [Online: Accessed on 30/08/2020]*.

Finisar Corporation (2016), 'WaveShaper User Manual'. **URL:** *https://www.finisar.com/sites/default/files/resources/waveshaper_user_manual_rev_j.pdf [Online: Accessed on 27/07/2020]*.

Fredrik Ahlbom (2016), Analysis of the Performance of Different DWDM Filter Technologies for Mobile Fronthaul Applications, PhD thesis, KTH Royal Institute of Technology, Stockholm, Sweden.

Frisken, S., Baxter, G., Abakoumov, D., Zhou, H., Clarke, I. & Poole, S. (2011), Flexible and grid-less wavelength selective switch using LCOS technology, *in* 'Optics InfoBase Conference Papers', pp. 1–3.

Fujitsu (2014), 'Fujitsu DAC datasheets'. **URL:** *https://www.fujitsu.com/downloads/MICRO/fsa/formPDF/spbg/dac/SPBG_DAC_MB86065_DS.pdf [Online: Accessed on 27/07/2020]*.

Gavioli, G., Torrengo, E., Bosco, G., Carena, A., Curri, V., Miot, V., Poggiolini,

P., Belmonte, M., Forghieri, F., Muzio, C., Piciaccia, S., Brinciotti, A., Porta, A. L., Lezzi, C., Savory, S. & Abrate, S. (2010), Investigation of the Impact of Ultra-Narrow Carrier Spacing on the Transmission of a 10-Carrier 1Tb/s Superchannel, *in* 'Optical Fiber Communication Conference', Optical Society of America, p. OThD3.

Gentile, K. (2002), 'The care and feeding of digital pulse-shaping filters'.

Ghazisaeidi, A., Tran, P., Brindel, P., Bertran-Pardo, O., Renaudier, J., Charlet, G. & Bigo, S. (2013), Impact of tight optical filtering on the performance of 28 gbaud nyquist-WDM PDM-8QAM over 37.5 GHz grid, *in* 'Optical Fiber Communication Conference, OFC 2013'.

Gnauck, A. H., Winzer, P. J., Chandrasekhar, S., Liu, X., Zhu, B. & Peckham, D. W. (2011), 'Spectrally efficient long-haul wdm transmission using 224-gb/s polarization-multiplexed 16-qam', *Journal of Lightwave Technology* **29**(4), 373–377.

Goh, T., Itoh, M., Yamazaki, H., Saida, T. & Hashimoto, T. (2015), Optical Nyquist-Filtering Multi/Demultiplexer with PLC for 1-Tb/s Class Super-Channel Transceiver, *in* 'Optical Fiber Communication Conference 2015', Los Angeles, p. Tu3A.5.

Gringeri, S., Basch, E. B. & Xia, T. J. (2012), 'Technical considerations for supporting data rates beyond 100 Gb/s', *IEEE Communications Magazine* **50**(2), s21–s30.

Hadkhale, I. (2015), Faster than Nyquist signaling and Analysis of its performance under uncoded/coded transmission systems, Master's thesis, OULU.

Healy, T., Garcia Gunning, F. C., Ellis, A. D. & Bull, J. D. (2007), 'Multi-wavelength source using low drive-voltage amplitude modulators for optical communications', *Optics Express* **15**, 2981–2986.

Heismann, F. (2010), System Requirements for WSS Filter Shape in Cascaded ROADM Networks, *in* 'Optical Fiber Communication Conference', Optical Society of America, p. OThR1.

Hill, K. O., Malo, B., Bilodeau, F., Johnson, D. C. & Albert, J. (1993), 'Bragg gratings fabricated in monomode photosensitive optical fiber by UV exposure through a phase mask', *Applied Physics Letters* **62**(10), 1035–1037.

Hillerkuss, D., Schellinger, T., Jordan, M., Weimann, C., Parmigiani, F., Resan, B., Weingarten, K., Ben-Ezra, S., Nebendahl, B., Koos, C., Freude, W. & Leuthold, J. (2013), 'High-quality optical frequency comb by spectral slicing of spectra broadened by SPM', *IEEE Photonics Journal* **10**(10), 7201011–7201011.

Hillerkuss, D., Schmogrow, R., Schellinger, T., Jordan, M., Winter, M., Huber, G., Vallaitis, T., Bonk, R., Kleinow, P., Frey, F., Roeger, M., Koenig, S., Ludwig, A., Marculescu, A., Li, J., Hoh, M., Dreschmann, M., Meyer, J., Ben Ezra, S., Narkiss, N., Nebendahl, B., Parmigiani, F., Petropoulos, P., Resan, B., Oehler, A., Weingarten, K., Ellermeyer, T., Lutz, J., Moeller, M., Huebner, M., Becker, J., Koos, C., Freude, W. & Leuthold, J. (2011), '26 Tbit s -1 line-rate super-channel transmission utilizing all-optical fast Fourier transform processing', *Nature Photonics* **5**, 364–371.

Hillerkuss, D., Schomogrow, R., Meyer, M., Wolf, S., Jordan, M., Kleinow, P., Lindenmann, N., Schindler, P. C., Melikyan, A., Yang, X., Ben-Ezra, S., Nebendahl, B., Dreschmann, M., Meyer, J., Parmigiani, F., Petropoulos, P., Resan, B., Oehler, A., Weingarten, K., Altenhain, L., Ellermeyer, T., Moeller, M., Huebner, M., Becker, J., Koos, C., Freude, W. & Leuthold, J. (2012), 'Single-Laser 32.5 Tbit/s Nyquist WDM Transmission', *J. Opt. Commun. Netw.* **4**(10), 715–723.

Hillerkuss, D., Winter, M., Teschke, M., Marculescu, A., Li, J., Sigurdsson, G., Worms, K., Ezra, S. B., Narkiss, N., Freude, W. & Leuthold, J. (2010), 'Simple all-optical FFT scheme enabling Tbit/s real-time signal processing', *Opt. Express* **18**(9), 9324–9340.

Huang, Y. K., Qian, D., Saperstein, R. E., Ji, P. N., Cvijetic, N., Xu, L. & Wang, T. (2009), Dual-polarization 2×2 IFFT/FFT optical signal processing for 100-Gb/s QPSK-PDM all-optical OFDM, *in* 'Conference on Optical Fiber Communication, Technical Digest Series'.

Igarashi, K., Mori, Y., Katoh, K. & Kikuchi, K. (2011), Bit-error Rate Performance of Nyquist Wavelength-Division Multiplexed Quadrature Phase-Shift Keying Optical Signals, *in* 'Optical Fiber Communication Conference/National Fiber Optic Engineers Conference 2011', Optical Society of America, p. OMR6.

Imran, M., Anandarajah, P. M., Kaszubowska-Anandarajah, A., Sambo, N. & Poti, L. (2018), 'A Survey of Optical Carrier Generation Techniques for

Terabit Capacity Elastic Optical Networks', *IEEE Communications Surveys and Tutorials* **20**(1), 211–263.

Ip, E., Lau, A. P. T., Barros, D. J. F. & Kahn, J. M. (2008), 'Coherent detection in optical fiber systems', *Optics express* **16**, 753–791.

ITU-T (2003), 'G.694.2:Spectral grids for WDM applications: CWDM wavelength grid'.
URL: *https://www.itu.int/rec/T-REC-G.694.2-200312-I [Online: Accessed on 15/08/2019]*.

ITU-T (2012), 'Spectral grids for WDM applications: DWDM frequency grid'.

Ivan Kaminow, T. L. & Willner, A. (2002), *Optical Fiber Communications*, ivb edn, New York: Elsevier Science.

Kao, K. C. & Hockham, G. A. (1966), 'Dielectric-fibre surface waveguides for optical frequencies', *Proceedings of the Institution of Electrical Engineers* **113**(7), 1151–1158.

Kaur, A. & Garcia Gunning, F. C. (2017*a*), Analogue Pre-filtering Using WSS for spectral efficient transmitters, *in* 'IEEE Photonics Conference', Orlando.

Kaur, A. & Garcia Gunning, F. C. (2017*b*), Spectral Roll-off Reduction using WSS, *in* 'Photonics Ireland Conference', Galway.

Kaur, A. & Garcia Gunning, F. C. (2018), Impact of Analogue Pre-Filtering for Spectral Roll-off Improvement in Spectral Efficient Transmitter, *in* 'International Conference on Transparent Optical Networks'.

Kaushik, S. (2002), *Proceedings of the national conference on advances in contemporary physics and energy*, Allied Publishers.

Kogelnik, H. (1985), 'High-speed lightwave transmission in optical fibers', *Science* **228**(4703), 1043–1048.

Lathi, B. P. (1998), *Modern Digital and Analog Communications Systems*, 3rd edn, Oxford University Press.

Lawrey, E. P. (2001), Adaptive Techniques for Multiuser OFDM, Phd thesis, James Cook University.

Leuthold, J. & Freude, W. (2013), Chapter 9 - Optical OFDM and Nyquist Multiplexing, *in* I. P. Kaminow, T. Li & A. E. Willner, eds, 'Optical Fiber Telecommunications (Sixth Edition)', Academic Press, Boston, pp. 381–432.

Li, Y., Cimini, L. J. & Sollenberger, N. R. (1998), 'Robust channel estimation for OFDM systems with rapid dispersive fading channels', *IEEE Transactions on Communications* **46**(902), 915.

Lin, C.-J., Chi, Y.-C. & Lin, G.-R. (2013), 'The self-started 10 GHz harmonic mode-locking of a hybrid weak-resonant-cavity laser diode and fiber ring link', *Laser Physics Letters* **10**(6), 65801.

Lin, J., Sanferrare1987epehrian, H., Rusch, L. A. & Shi, W. (2019), 'Single-carrier 72 GBaud 32QAM and 84 GBaud 16QAM transmission using a SiP IQ modulator with joint digital-optical pre-compensation', *Optics Express* **27**(4), 5610.

Lin, J., Xi, L., Li, J., Zhang, X., Zhang, X. & Niazi, S. A. (2014), 'Low noise optical multi-carrier generation using optical-FIR filter for ASE noise suppression in re-circulating frequency shifter loop', *Opt. Express* **22**(7), 7852–7864.

Linke, R. A. & Gnauck, A. H. (1988), 'High-capacity coherent lightwave systems', *Journal of Lightwave Technology* **6**(11), 1750–1769.

Lowery, A. J., Xie, Y. & Zhu, C. (2015), 'Systems performance comparison of three all-optical generation schemes for quasi-Nyquist WDM', *Optics Express* **23**, 21706–21718.

Lowery, A. J., Zhuang, L., Corcoran, B., Zhu, C. & Xie, Y. (2017), 'Photonic Circuit Topologies for Optical OFDM and Nyquist WDM', *Journal of Lightwave Technology* **35**(4), 781–791.

Maher, R., Xu, T., Galdino, L., Sato, M., Alvarado, A., Shi, K., Savory, S. J., Thomsen, B. C., Killey, R. I. & Bayvel, P. (2015), 'Spectrally Shaped DP-16QAM Super-Channel Transmission with Multi-Channel Digital Back-Propagation', *Scientific Reports* **5**, 1–8.

Maldonado-Basilio, R., Parra-Cetina, J., Latkowski, S. & Landais, P. (2010), 'Timing-jitter, optical, and mode-beating linewidths analysis on subpicosecond optical pulses generated by a quantum-dash passively mode-locked semiconductor laser', *Optics Letters* **35**, 1184–1186.

Matsui, Y., Mahgerefteh, D., Zheng, X., Liao, C., Fan, Z. F., McCallion, K. & Tayebati, P. (2006), 'Chirp-managed directly modulated laser (CML)', *IEEE Photonics Technology Letters* **18**(2), 385–387.

Mitra, P. P. & Stark, J. B. (2001), 'Nonlinear limits to the information capacity of optical fibre communications', *Nature* **411**, 1027–1030.

Miya, T., Terunuma, Y., Hosaka, T. & Miyashita, T. (1979), 'Ultimate low-loss single-mode fibre at 1.55 μm', *Electronics Letters* **15**(4), 106–108.

Mukherjee, B. (1997), *Optical Communication Networks*, New York: McGraw-Hill.

Nakazawa, M. (2010), *Ultrahigh Spectral Density Coherent Optical Transmission Technologies*, Springer Berlin Heidelberg.

Nyman, B., Farries, M. & Si, C. (2001), 'Technology trends in dense WDM demultiplexers', *Optical Fiber Technology* **7**(4), 255–274.

Nyquist, H. (1928), 'Certain Topics in Telegraph Transmission Theory', *Transactions of the American Institute of Electrical Engineers* .

Pan, J. & Tibuleac, S. (2017), 'Real-time ROADM filtering penalty characterization and generalized precompensation for flexible grid networks', *IEEE Photonics Journal* **9**(3), 1–10.

Payne, D. N. & Laming, R. I. (1991), Optical amplifiers-a telecommunications revolution, *in* 'International Electron Devices Meeting 1991 [Technical Digest]', pp. 3–4.

Peled, A. & Ruiz, A. (1980), 'Frequency Domain Data Transmission Using Reduced Computational Complexity Algorithms', *Record - IEEE International Conference on Acoustics, Speech & Signal Processing* .

Pfau, T., Hoffmann, S. & Noé, R. (2009), 'Hardware-efficient coherent digital receiver concept with feedforward carrier recovery for M-QAM constellations', *Journal of Lightwave Technology* **27**(8), 989–999.

Phabrix (2019), 'Using Pseudo-Random Binary Sequences to Stress Test Serial Digital Interfaces'.
URL: *https://theiabm.org/wp-content/uploads/2019/01/Stress-Whitepaper_January-2019.pdf [Online: Accessed on 24/07/2020].*

Proakis, J. (1989), '(ebook) McGraw Hill - Digital Communications By John Proakis 4th Edition.pdf'.

Puttnam, B. J., Sakaguchi, J., Klaus, W., Awaji, Y., Mendinueta, J. M. D., Wada,

N., Kanno, A. & Kawanishi, T. (2012), Investigating self-homodyne coherent detection in a 19-core spatial-division-multiplexed transmission link, *in* 'European Conference on Optical Communication, ECOC'.

Rafique, D., Napoli, A., Calabro, S. & Spinnler, B. (2014), 'Digital preemphasis in optical communication systems: On the DAC requirements for terabit transmission applications', *Journal of Lightwave Technology* **32**(19), 247–3256.

Rasmussen, C., Pan, Y., Aydinlik, M., Crowley, M., Geyer, J. C., Humblet, P., Liu, F., Mikkelsen, B., Monsen, P., Nadarajah, N., Pendock, G. & Shah, B. (2013), Real-time DSP for 100+ Gb/s, *in* 'Optical Fiber Communication Conference, OFC 2013', p. OW1E.1.

Rhee, J. K. K., Cvijetic, N., Wada, N. & Wang, T. (2013), 'Optical orthogonal frequency division multiplexed transmission using all-optical discrete Fourier transform'.

Roberts, K., Foo, S. H., Moyer, M., Hubbard, M., Sinclair, A., Gaudette, J. & Laperle, C. (2015), 'High capacity transport-100G and beyond', *Journal of Lightwave Technology* .

Roelens, M. A., Frisken, S., Bolger, J. A., Abakoumov, D., Baxter, G., Poole, S. & Eggleton, B. J. (2008), 'Dispersion trimming in a reconfigurable wavelength selective switch', *Journal of Lightwave Technology* **26**(1), 73–78.

S. Chandrasekhar, Xiang Liu, B. Z. & Peckham, D. W. (2009), Transmission of a 1.2-Tb/s 24-carrier no-guard-interval coherent OFDM superchannel over 7200-km of ultra-large-area fiber, *in* '2009 35th European Conference on Optical Communication', Vienna, pp. 1–2.

Sakamoto, T., Kawanishi, T. & Izutsu, M. (2007), 'Asymptotic formalism for ultraflat optical frequency comb generation using a Mach-Zehnder modulator', *Opt. Lett.* **32**(11), 1515–1517.

Sanferrare, R. J. (1987), 'TERRESTRIAL LIGHTWAVE SYSTEMS.', *AT&T Technical Journal* **66**(1), 95–107.

Sanjoh, H., Yamada, E. & Yoshikuni, Y. (2002), Optical orthogonal frequency division multiplexing using frequency/time domain filtering for high spectral efficiency up to 1 bit/s/Hz, *in* 'Optical Fiber Communications Conference', Optical Society of America, p. ThD1.

Sano, A., Yamada, E., Masuda, H., Yamazaki, E., Kobayashi, T., Yoshida, E., Miyamoto, Y., Kudo, R., Ishihara, K. & Takatori, Y. (2009), 'No-Guard-Interval Coherent Optical OFDM for 100-Gb/s Long-Haul WDM Transmission', *Journal of Lightwave Technology* **27**(16), 3705–3713.

Schmogrow, R., Ben-Ezra, S., Schindler, P. C., Nebendahl, B., Koos, C., Freude, W. & Leuthold, J. (2013), 'Pulse-shaping with digital, electrical, and optical filters - A comparison', *Journal of Lightwave Technology* .

Schmogrow, R., Winter, M., Meyer, M., Hillerkuss, D., Wolf, S., Baeuerle, B., Ludwig, A., Nebendahl, B., Ben-Ezra, S., Meyer, J., Dreschmann, M., Huebner, M., Becker, J., Koos, C., Freude, W. & Leuthold, J. (2012), 'Real-time Nyquist pulse generation beyond 100 Gbit/s and its relation to OFDM', *Optics Express* **20**(1), 317.

Schroder, J., Du, L. B., Carpenter, J., Eggleton, B. J. & Lowery, A. J. (2014), 'All-optical OFDM with cyclic prefix insertion using flexible wavelength selective switch optical processing', *Journal of Lightwave Technology* **32**(4), 752–759.

Schröder, J., Roelens, M. A., Du, L. B., Lowery, A. J. & Eggleton, B. J. (2012), LCOS based waveshaper technology for optical signal processing and performance monitoring, *in* 'Technical Digest - 2012 17th Opto-Electronics and Communications Conference, OECC 2012'.

Shalom, H., Zadok, A., Tur, M., Legg, P. J., Cornwell, W. D. & Andonovic, I. (1998), 'On the various time constants of wavelength changes of a DFB laser under direct modulation', *IEEE Journal of Quantum Electronics* **34**(10), 1816–1822.

Shannon, C. E. (1948), 'A Mathematical Theory of Communication', *Bell System Technical Journal* **27**(3), 379–423.

Shieh, W. & Athaudage, C. (2006), 'Coherent optical orthogonal frequency division multiplexing', *Electronics Letters* .

Shieh, W. & Djordjevic, I. (2010), Chapter 12 - Future Research Directions, *in* W. S. Djordjevic, ed., 'OFDM for Optical Communications', Academic Press, Oxford, pp. 413–432.

Simon Haykin (2010), An Introduction to Analog and Digital Communications, *in* 'An Introduction to Analog and Digital Communications', 6th edn, John Wiley & Sons, chapter Inter Symbol Interference and its Cures, pp. 227–236.

Simon Haykin and Bernard Widrow (2003), *Least-Mean-Square Adaptive Filters*, John Wiley and Sons.

Slobodnik, A., Kearns, W. & Noonan, J. (1975), Design, Fabrication and Testing of SAW Butterworth Filters, *in* '1975 IEEE-MTT-S International Microwave Symposium', pp. 353–355.

Song, M., Pincemin, E., Josten, A., Baeuerle, B., Hillerkuss, D., Leuthold, J., Rudnick, R., Marom, D. M., Ezra, S. B., Ferran, J. F., Thouenon, G., Khodashenas, P. S., Rivas-Moscoso, J. M., Betoule, C., Klonidis, D. & Tomkos, I. (2016), 'Flexible optical cross-connects for high bit rate elastic photonic transport networks [invited]', *Journal of Optical Communications and Networking* .

Soto, M. A., Alem, M., Amin Shoaie, M., Vedadi, A., Brès, C.-S., Thévenaz, L. & Schneider, T. (2013), 'Optical sinc-shaped Nyquist pulses of exceptional quality', *Nat Commun* **4**, 1–4.
URL: *http://dx.doi.org/10.1038/ncomms3898*

Stavdas, A. (2010), *Core and Metro Networks*, Wiley.

Takiguchi, K., Oguma, M., Shibata, T. & Takahashi, H. (2009), 'Demultiplexer for optical orthogonal frequency-division multiplexing using an optical fast-Fourier-transform circuit', *Opt. Lett.* **34**(12), 1828–1830.

Technologies, K. (2020), 'Digital Modulation in Communication Systems - An Introduction'.
URL: *https://literature.cdn.keysight.com/litweb/pdf/5965-7160E.pdf.*

Tektronix (2014), 'Tektronix digital oscilloscope datasheets'.
URL: *https://www.tek.com/oscilloscope#all [Online: Accessed on 03/07/2020].*

Teledyne LeCroy (2014), 'Lecroy digital scope datasheets'.
URL: *https://www.testequipmenthq.com/datasheets//*
/LECROY-LT374-Datasheet.pdf[Online: Accessed on 19/03/2019].

Tyndall, J. (1854), 'On some phenomena connected with the motion of liquids.'.

ViaLite Communications (2019), 'Optical Multiplexing'.
URL: *https://www.vialite.com/resources/guides/optical-multiplexing/*
wdm-schematic/ [Online: Accessed on 27/08/2020].

VPIphotonics GmbH (2014), VPItransmissionMaker Optical Systems User's Manual, Technical report, VPIphotonics GmbH.

VPIphotonics GmbH (2015), 'VPItransmissionMaker'.
URL: *http://www.vpiphotonics.com/TMOpticalSystems.php [Online: Accessed on 27/08/2020]*.

Walden, R. H. (1999), 'Analog-to-digital converter survey and analysis', *IEEE Journal on Selected Areas in Communications* **17**(4), 539–550.

Wang, Q., Huo, L., Xing, Y. & Zhou, B. (2014), 'Ultra-flat optical frequency comb generator using a single-driven dual-parallel Mach–Zehnder modulator', *Opt. Lett.* **39**(10), 3050–3053.

Weinstein, S. B. & Ebert, P. M. (1971), 'Data Transmission by Frequency-Division Multiplexing Using the Discrete Fourier Transform', *IEEE Transactions on Communication Technology* **19**(5), 628–634.

Weng, Y., Wang, J., He, X. & Pan, Z. (2018), 'A rigorous analysis of digital pre-emphasis and DAC resolution for interleaved DAC Nyquist-WDM signal generation in high-speed coherent optical transmission systems', *Optics Communications* **409**, 77–85.

Weng, Y., Wang, J. & Pan, Z. (2016), Comparison of advanced DSP techniques for spectrally efficient Nyquist-WDM signal generation using digital FIR filters at transmitters based on higher-order modulation formats, *in* 'Optical Metro Networks and Short-Haul Systems VIII'.

Winzer, P. J., Pfennigbauer, M., Strasser, M. M. & Leeb, W. R. (2001), 'Optimum filter bandwidths for optically preamplified NRZ receivers', *Journal of Lightwave Technology* **19**(9), 1263–1273.

Xiang, M., Tang, H., Fu, S., Tang, M., Shum, P. & Liu, D. (2015), 'Performance Comparison of Offset-16QAM and 16QAM for Nyquist WDM Superchannel with Digital Spectral Shaping', *Journal of Lightwave Technology* **33**(17), 3623–3629.

Xie, X. Z. & Chongjin (2016), *Enabling Technologies for High Spectral-efficiency Coherent Optical Communications Networks*, John Wiley and Sons.

Xie, Y., Geng, Z., Zhuang, L., Burla, M., Taddei, C., Hoekman, M., Leinse, A., Roeloffzen, C. G., Boller, K. J. & Lowery, A. J. (2017), 'Programmable optical

processor chips: Toward photonic RF filters with DSP-level flexibility and MHz-band selectivity', *Nanophotonics* **7**(2), 421–454.

Xie, Y., Zhuang, L., Zhu, C. & Lowery, A. J. (2016), 'Nyquist pulse shaping using arrayed waveguide grating routers', *Optics Express* **24**, 22357–22365.

Yang, H., Robertson, B., Wilkinson, P. & Chu, D. (2016), 'Small phase pattern 2D beam steering and a single LCOS design of 40 1 $\times$ 12 stacked wavelength selective switches', *Optics Express* **24**(11), 12240–12253.

Yang, H., Robertson, B., Wilkinson, P. & Chu, D. (2017), 'Low-Cost CDC ROADM Architecture Based on Stacked Wavelength Selective Switches', *Journal of Optical Communications and Networking* **9**(5), 375–384.

Yichuan Yu, Lewen, R., Irmscher, S., Westergren, U., Thylen, L., Eriksson, U. & Lee, W. S. (2005), 80 Gb/s ETDM transmitter with a traveling-wave electroabsorption modulator, *in* 'OFC/NFOEC Technical Digest. Optical Fiber Communication Conference, 2005.', Vol. 3, pp. 3–3.

Yu, H., Yu, H., Chen, H., Chen, M., Yang, S. & Xie, S. (2016), 'All-optical OFDM demultiplexer based on an integrated silicon-on-insulator technique', *IEEE Photonics Journal* **8**(1), 1–7.

Yu, J. & Zhang, J. (2016), 'Recent progress on high-speed optical transmission'.

Yuanliang Chu, Xiaoping Zheng, Hanyi Zhang, Xueming Liu & Yili Guo (2002), 'The impact of phase errors on arrayed waveguide gratings', *IEEE Journal of Selected Topics in Quantum Electronics* **8**(6), 1122–1129.

Zehnder, L. (1891), 'Ein neuer Interferenzrefraktor', *Zeitschrift für Instrumentenkunde* **11**, 275–285.

Zhalehpour, S., Lin, J., Shi, W. & Rusch, L. A. (2019), 'Reduced-size lookup tables enabling higher-order QAM with all-silicon IQ modulators', *Optics Express* **27**(17), 24243.

Zhang, G., De Leenheer, M., Morea, A. & Mukherjee, B. (2013), 'A survey on OFDM-based elastic core optical networking', *IEEE Communications Surveys and Tutorials* **15**(1), 65–87.

Zhang, J., Chi, N., Yu, J., Shao, Y., Zhu, J., Huang, B. & Tao, L. (2011), 'Generation of coherent and frequency-lock multi-carriers using cascaded phase modulators and recirculating frequency shifter for Tb/s optical communication', *Opt. Express* **19**(14), 12891–12902.

Zhang, J., Chien, H. C., Xia, Y., Chen, Y. & Xiao, J. (2014), A novel adaptive digital pre-equalization scheme for bandwidth limited optical coherent system with DAC for signal generation, *in* 'Optical Fiber Communication Conference, OFC 2014'.

Zhang, J., Yu, J., Chi, N., Shao, Y., Tao, L., Zhu, J. & Wang, Y. (2012), 'Stable Optical Frequency-Locked Multicarriers Generation by Double Recirculating Frequency Shifter Loops for Tb/s Communication', *Journal of Lightwave Technology* **30**(24), 3938–3945.

Zhou, X., Liang, G. & Wang, T. (2011), An optical add-drop multiplexer design based on fiber Bragg gratings, *in* 'ICEOE 2011 - 2011 International Conference on Electronics and Optoelectronics, Proceedings', pp. V2–41–V2–43.